UCID--20622-89-2

DE90 008298

Chemistry & Materials Science Research Report

Weapons-Supporting Research

and

Departmental Institutional Research & Development

January 19, 1990

FOREWORD

The research reported here in summary form was conducted under the auspices of Weapons-Supporting Research (WSR) and Institutional Research and Development (IR&D). The period covered is the second half of FY89.

WSR is the principal source of discretionary funds to support fundamental research in the Chemistry & Materials Science Department (C&MS). The purpose of WSR is to provide the scientific and technical base that is required in the longer term for success of the Weapons Program.

Administratively, WSR is organized into block-funded programs ("thrust areas") and a few smaller projects led by individual investigators. A thrust area is designed to provide a coordinated approach to a focused scientific or technological area and typically involves several senior scientists.

IR&D is intended to broaden the exploratory research base of C&MS. In FY89, IR&D funds have underwritten several single-investigator projects and (in part) relatively large programs such as Spin Polarization and High-Temperature Superconductivity.

In practice, research programs carried out under WSR auspices are similar in spirit and substance to those supported by IR&D. Indeed, some of the work is funded by both sources.

The results reported here are for work in progress; thus, they may be preliminary, fragmentary, or incomplete. Interested readers should consult one of the authors of a report before quoting it or otherwise referring to it.

T. T. Sugihara

CONTENTS

WEAPONS-SUPPORTING RESEARCH

DEPARTMENTAL INSTITUTIONAL RESEARCH & DEVELOPMENT

UCID-20622-89-2

WEAPONS-SUPPORTING RESEARCH

Thrust Areas

FUNDAMENTAL ASPECTS OF METAL PROCESSING

M. E. Kassner (*Thrust Area Leader*)

Overview

Described here is the progress during the second half of FY89 within each of the task areas. Anticipated changes for FY90 are also briefly discussed.

Large-Strain Deformation of Metals and Alloys

M. E. Kassner

Ductility of Aluminum Polycrystals

As discussed in the first-half FY89 progress report for this subtask, we determined the variation of the torsional-ductility of aluminum with temperature and strain rate. These experiments, which provide significant insight into the hot-workability of high-stacking-fault-energy metals and alloys, were analyzed on a fundamental basis. Further tests are being performed on a Reometrics torsion device that is normally used for viscosity measurements of polymers. New, more accurate data have been obtained and are incorporated into the new publication.

Large-Strain Deformation of Al-Mg Alloys

These aluminum-magnesium alloys are in the *5xxx*-series, the major category of commercial and weapons aluminum alloys. Significant controversy exists as to the origin of the microstructure of these alloys when they are deformed to large strains at elevated temperatures (as during metal-forming operations). In particular, a dramatic increase in high-angle boundaries has been observed with large strains. This has been attributed to dynamic recrystallization that accompanies the decrease in stacking-fault energy with Mg additions or, essentially, to continuous dynamic recrystallization. We believe that our earlier "baseline" aluminum results, which proposed the new geometric-dynamic-recrystallization concept, may be relevant with this group of alloys [1]. A review of this subject was written during the second half of this fiscal year. The early tests are currently being performed on the Stanford torsion-testing machine, and microscopic analysis is under way. Early results on a 6 at.% Mg alloy dispute the discontinuous-dynamic-recrystallization concept for these alloys in favor of a geometric-dynamic-recrystallization concept.

Steady-State Flow in Cu and Al at Ambient Temperature

Substantial experimental and theoretical controversy exists as to whether a true mechanical steady state exists with large-strain deformation at ambient temperatures. This has been somewhat intensified by our results for silver, reported during the first half of

FY89 [2]. Several ambient-temperature torsion tests on pure aluminum have been performed on conventional machines during the second half of FY89 with ambiguous results. The Reometrics torsion machine should help with the experimental resolution. Careful activation-energy (and activation-volume) measurements would help with the determination of the steady-state deformation mechanism. These tests have already provided explanations for some of the experimental ambiguities in the literature.

Delayed Failure in Silver-Aided Diffusion Welds

R. S. Rosen *M. E. Kassner* *G. A. Henshall*

Significant new experiments have been performed in this task during the second half of FY89. The effort was principally within the area of direct void growth (DVG) of cavities, the proposed mechanism or theory for delayed failure in thin-interlayer bonds for which the base metals only deform elastically over the relevant range of stresses. Theoretical analysis was completed as well as an extensive microscopic analysis of nucleating voids. Experiments confirming the generality of the conclusions were also performed. The experiments and analyses for this task area are complete and are documented in several new publications.

The following conclusions were substantiated by careful analyses of the stress and temperature dependence of the rupture times, finite-element analysis of the stress state within the interlayer, analysis of the fracture surfaces, conventional light microscopy, and electron microscopy of the interfaces loaded to various fractions of the rupture life:

- For bonds that utilized maraging steel as a base metal (deforming only elastically), the time-to-failure is controlled by the creep rate of silver near the interfaces in the interlayer, which is determined by the effective stress within the interlayer. The plastic deformation causes dislocation pile-ups at interfaces, which cause cavity nucleation. Nucleation continues with creep of the silver interlayer until the concentration of nuclei is sufficiently high to lead to instabilities and eventual failure.
- Delayed failure may be accelerated by base-material creep resulting from the effective stress in the base material. Plastic deformation of the base metal causes corresponding deformation in the interlayer, and cavities nucleate as with elastic base metals.
- These findings appear applicable to silver-interlayer bonds prepared by processes other than physical vapor deposition (brazing, electroplating, solid foils, etc.) and possibly to other interlayer materials.

Funding for this task will be cut by one-half during the next fiscal year. Future studies of the mechanical performance of interlayers will include both gold and our new precipitation-hardened Ag-13.5 at.% Al alloy. Theoretically, the interlayers will increase resistance to delayed failure. Thin-interlayer joints behave anisotropically with respect to in-plane shear stresses and to stresses normal to the bond plane. Multiaxial tests would be phenomenologically very useful and of theoretical value in substantiating the role of shear stresses (plasticity) in delayed failure.

High Strain Rate and Failure of Metals

W. H. Gourdin

As a consequence of the expanding-ring apparatus being moved to the new High-Explosives Applications Facility (HEAF), B191, the experimental program was disrupted for six months. The VISAR was installed with a new beamline in the HEAF north 1-kilogram tank, and new ring hardware was designed and built that is both more stable and more convenient to use. The first testing of the equipment began in mid-August, but continuing problems with critical building systems, including tank-door hardware and control computers, prevented resumption of even an abbreviated schedule of experiments until mid-September.

A paper has been completed in which the results of expanding-ring experiments with 10- to 200-μm grain size oxygen-free electronic (OFE) copper are reported and analyzed in terms of the mechanical threshold stress (MTS) model. Although the emphasis is on the behavior of copper at high rates of tensile strain, model parameters are developed in conjunction with lower rate data obtained on similar material in compression using conventional test techniques. The activation energy for slip and the strain rate pre-exponential were taken from the literature, but other quantities were chosen based on the present data. The athermal stress varies considerably with grain size and can be described with a Hall-Petch type relationship. The magnitude and strain-rate dependence of the initial hardening rate of the mechanical threshold also appear to decrease with increasing grain size. Futhermore, the parameters associated with "recovery" must be altered from those in the literature to reproduce the large drop in the flow stress at high temperatures (400 °C). Overall, however, the model provides an excellent description of the material behavior over a wide range of grain size, strain rate, and temperature. In particular, it successfully reproduces the subtle interplay between temperature and strain rate that occurs during ring expansion.

Measurements were made of the cross-sections of the recovered ring fragments to determine the extent of "uniform" deformation prior to necking and failure. For OFE copper, this uniform strain (0.42±0.08) is noticeably less than the overall failure "strain" (0.49±0.04), but otherwise shows the same decreasing trend with increasing grain size. Electrodeposited copper (UBAC), however, apparently deforms uniformly (0.40) to very near failure (0.42). Similar measurements have been made for tantalum.

During the experimental hiatus, database program dBASE IV was acquired and used as a means of archiving data for each experiment. This will make recovery of the details of individual experiments as well as groups of experiments much more efficient than in the past.

In the coming year, we will study electrodeposited copper at high temperature, looking for possible brittle behavior and a better qualitative correlation with the disintegration of jets of this material. We will also conduct a series of tests on a copper electrodeposited in a cyanide solution that is currently of interest to other programs. Studies of tantalum and shockloaded OFE copper will be completed and a fragmentation study of 4330 steel will be initiated if time and funding permit. As the year progresses, the analytical emphasis will be

shifted to fragmentation. Well validated material models will be inserted into existing computer codes to study the fragmentation of rings and jets. Ring data, obtained under well characterized and controlled conditions, will play a central role in these efforts.

Rapid Solidification of Al-Be Alloys

J. W. Elmer *L. E. Tanner* *M. J. Aziz**

A rapid-solidification model is being developed to describe the formation of ultrafine Be particles that occur in rapidly-solidified Al-Be alloys. These particles form in aluminum-rich alloys (containing ~5 at.% Be) when the alloys are solidified at rates that exceed ~0.1 m/s. The nm-size Be particles have a random crystallographic orientation and a unique modulated appearance, forming in "waves" parallel to the advancing solidification front. These features indicate that the Be particles periodically nucleate and grow from the liquid phase during non-steady-state solidification conditions. Ultrafine dispersions of Be particles are of interest because of the potential technological advantages that these microstructures offer over the rod-like microstructures that form during conventional solidification processing.

A computer program was written in FY89 to analyze the solidification conditions that lead to the development of the ultrafine particles. This program solves the heat-and-mass-transfer equations that govern the solidification process, subject to the kinetic constraints (interface response functions) that the rapidly advancing interface places on the interface temperature and the partition coefficient. These results give the composition of the liquid phase, the partition coefficient, the temperature, and the velocity of the rapidly moving interface as a function of the transient solidification time. These parameters are then used to calculate the propensity for homogeneous nucleation of Be particles from the liquid phase. Preliminary calculations indicate that homogeneous nucleation can be achieved under certain solidification conditions. However, these calculations are particularly sensitive to the material parameters; therefore, accurate values of the data must be collected in order for the model to provide a realistic description of the solidification process.

The computer model will be verified in FY90 using Al-Be as the test system. Verification of this model will be performed by calculating the dependence of the Be particle size and spacing on the solidification-front velocity and comparing these results with experimental observations. Comparison of the model and experiments may require additional rapid-solidification experiments and transmission electron microscopy (TEM) analysis of these rapidly-solidified alloys.

* Harvard University

Incorporation of Advanced Materials Models in FEM Codes

G. A. Henshall *G. L. Goudreau**

The first subtask involved a joint project with the Methods Development Group in NEED of the Mechanical Engineering Department to improve LLNL FEM stress-analysis codes through implementation of advanced material constitutive equations. Specifically, implementation of the MATMOD constitutive equations, developed by a group (including Henshall) at Stanford, was explored. The NIKE, rather than the DYNA, codes were selected for implementation of MATMOD. The "NONSS" explicit time-integration scheme was chosen to numerically integrate the constitutive equations, and a method for sub-incrementing the global NIKE time step using NONSS was developed. Successful results have been obtained for one-element problems, thus demonstrating the viability of the overall method. Numerical problems still exist, however, for multi-element simulations.

The second subtask was to apply the LLNL FEM codes to the stress analysis of the solid-state bonds described in an earlier task review. This was accomplished despite the relative complexity of the bonds. As part of this effort and in support of many other projects at the Laboratory, work began on implementing a primary creep law into the NIKE FEM codes. The primary creep law has been incorporated into the NIKE 2D code for isothermal axisymmetric conditions and has allowed us to analyze diffusion bonds between creeping (stainless steel) base metals. FEM analyses of bonds between elastic (maraging steel) base metals were also performed and have been correlated with various experimental findings. These results have been documented in a recent publication.

Continuation of the MATMOD portion of this project will include:

- Modifying the current implementation as needed to solve the numerical problems
- Adding thermal strains
- Solving several test problems that demonstrate the capabilities added to NIKE by MATMOD

Further work is planned on the primary creep model to:

- Include thermal strains
- Allow for other stress states
- Extend the formulation to three dimensions

Correlation of Electronic Structure with Processing of Advanced Substitutional Alloys

A. Jankowski *P. Turchi*

The objective of this mid-FY89 individual funding and new task area was to examine the origin of phase stability in alloys, both theoretically and experimentally. Attention was directed to the tendency towards ordering as well as to the occurrence of structural transformations in substitutional transition-metal alloys.

---

* Methods Development Group, NEED, Mechanical Engineering Department

Theoretical

Starting from electronic-structure calculations, energetic quantities are incorporated into a statistical model to obtain the alloy phase diagram. Specific features of the electronic density of states will be related to particular atomic configurations. This will be applied for the first time to complex alloys based on the A15 crystalline structure. The A15 structure is one of the building blocks of the σ phase. It is, therefore, of particular interest to study long-range order (LRO) in the σ phase when A15 competes with σ, as noted in a number of experimental phase diagrams including Ga-V and Pd-Ti. A ground-state analysis of the A15 lattice indicated the possible existence of two extra ordered configurations, A_5B_3 and A_7B. The stability of these newly predicted phases were investigated by means of the Cluster Variation Method (CVM) and Monte Carlo (MC) simulations. Typical prototype A15-based order-disorder phase diagrams were calculated and discussed in relation with the experimental situation [3,4].

Experimental

Two approaches to producing an alloy by vapor-deposition are multilayering and co-deposition, from pure elements or composite/compound targets used in the sputter-deposition process. Thin films were sputter-deposited on mica and silicon substrates for x-ray and TEM analysis as well as for transport-property measurement.

$Pd_{0.3}Ti_{0.7}$ thin films have been prepared for study of the short-range ordering (SRO) in the bcc solid solution and for understanding of the existence of an A15 crystalline structure at the composition Ti_4Pd. Hot-stage electron microscopy has been used to study the amorphous-to-crystalline transition of the as-deposited structure. For the first time, an amorphous structure was seen with an apparent phase separation on crystallization and with evidence of diffuse scattering about the high-temperature bcc phase on further annealing. In progress are preparation of $Ga_{0.3}V_{0.7}$ thin films, search for the A_5B_3 structure (newly predicted X-phase), and study of the SRO that develops in the bcc solid solution.

The theoretical effort will be continued on a more quantitative basis with special attention to the Ti-Pd and V-Ga systems. The thin-film approach allows direct creation of a metastable low-temperature structure leading to unusual starting points and paths to an equilibrium structure. The following tasks will be emphasized:

- The bcc-to-A15 transition in alloys and related precursor phenomena, in particular the SRO of DO_3 type in the bcc solid solution above an existing LRO of A15 type.
- The possible existence of the predicted ordered state, the so-called X-phase, at or near the A_5B_3 composition.
- The LRO in the sigma phase over a range of composition where it would compete with the predicted X-phase.

Computer Simulations of Recrystallization Behavior

C. W. Price

The primary objective of this task is development of computer models that will simulate grain growth, formalize grain-impingement geometry, simulate recrystallization kinetics, and isolate the limitations of existing kinetic models. Another important objective is development of improved atomistic models based on correlations among atomistic computer simulations and experimental observations.

The major effort on this task to date has been to properly isolate the various limitations of the kinetic models by using a simplified computer simulation model [5]. This approach has proven to be capable of defining the narrow range of applications to which each model is restricted [6], and it also has been used to resolve the extent to which simultaneous recovery can alter recrystallization kinetics [7]. Additional studies are near completion on limitations that grain-impingement models impose on the existing kinetic models and on how various types of time-dependent relations (other than those used in the existing kinetic models) correlate with experimental kinetic behavior. Two publications for a key conference were prepared during the second half of this fiscal year.

References

1. M. E. Kassner, M. M. Myshlyaev, and H. J. McQueen, "Large-Strain Torsional Deformation in Aluminum at Elevated Temperatures," *Mater. Sci. Eng.* **108A**, 45 (1989).
2. M. E. Kassner, "The Rate-Dependence and Microstructure of High-Purity Silver Deformed to Large Strains between 0.16 and 0.30 T_m," *Metall. Trans.* **20A**, 2001 (1989).
3. P. Turchi and A. Finel, "Possible Ordered States Based On The A15 Crystalline Structure" to be published in *Phys. Rev. Lett.*
4. P. Turchi, G. Treglia, and F. Ducastelle, *J.Phys. F* **13**, 2543 (1983).
5. C. W. Price, "Simulations of Grain Impingement and Recrystallization Kinetics," *Acta Metall.* **35**, 1377 (1987).
6. C. W. Price, "Use of Johnson-Mehl-Avrami Kinetics in Recrystallization of Metals and Crystallization of Metallic Glasses," submitted to *Acta Metall.* (UCRL-99556, 1989).
7. C. W. Price, "Comments on the Extent of Simultaneous Recovery During Recrystallization and Its Effect on Recrystallization Kinetics," *Scripta Metall.*, in press (UCRL-100553, 1989).

Publications and Presentations

Publications

M. E. Kassner, "A Case for Taylor Hardening in Aluminum and Type 304 Stainless Steel at Elevated Temperature," *J. Mater. Sci.*, in press.

M. E. Kassner, "The Rate-Dependence and Microstructure of High-Purity Silver Deformed to Large Strains between 0.16 and 0.30 T_m," *Metall. Trans.* **20A**, 2001 (1989).

M. E. Kassner, "Large-Strain Deformation of Aluminum Single Crystals at Elevated Temperature as a Test of the Geometric-Dynamic-Recrystallization Concept," *Metall. Trans.* **20A**, 2182 (1989).

M. E. Kassner, R. S. Rosen, G. A. Henshall, and W. E. King, "Delayed Failure of Silver-Aided Diffusion Welds Between Steel," in *Proceedings* of the 2nd International Conference on Brazing, High-Temperature Brazing and Diffusion Welding (DVS-Verlag, Düsseldorf, (1989), p. 47.

M. E. Kassner, "Effects of Temperature and Strain-Rate on the Elevated Temperature Ductility of Aluminum in Torsion" (UCRL-101245, 1989).

M. E. Kassner, M. M. Myshlyaev, and H. J. McQueen, "Large-Strain Torsional Deformation in Aluminum at Elevated Temperatures," *Mater. Sci. Eng.* **108A**, 45 (1989).

R. S. Rosen and M. E. Kassner, "Diffusion Welding of Silver Interlayers Coated onto Base Metals Using Planar-Magnetron Sputtering," *J. Vac. Sci. Tech.*, in press (UCRL-101168, 1989).

R. S. Rosen, S. Beitscher, and M. E. Kassner, "Stress Corrosion Cracking of Uranium-Silver Interfaces in Silver-Aided Diffusion Welds," in *Environment-Induced Cracking of Metals* (NACE, Houston, in press), (UCRL-97917 Rev. 1, 1989).

H. J. McQueen, E. Evangelista and M. E. Kassner, "The Classification and Determination of Restorative Mechanisms in the Hot-Working of Al-Alloys," *Z. Metall.*, in press.

M. E. Kassner, R. S. Rosen, G. A. Henshall, and K. D. Challenger, "Time-Dependent Failure of Silver-Interlayer Diffusion Bonds Between Non-Deforming Base Metals," accepted for publication in *Creep and Fracture of Engineering Materials and Structures* (UCRL-102284, 1989).

M. E. Kassner, R. S. Rosen, and G. A. Henshall, "Delayed Mechanical Failure of Silver-Interlayer Diffusion Bonds," to be submitted to *Metall. Trans.* (UCRL-102283, 1989).

M. E. Kassner, P. H. Adler, M. G. Adamson, and D. E. Peterson, "Evaluation and Thermodynamic Analysis of Phase Equilibria in the U-Al System," *J. Nucl. Mater.* **167**, 160 (1989).

G. A. Henshall, R. S. Rosen, M. E. Kassner, and R. G. Whirley, "Tensile Deformation Behavior of Interlayer Bonds Between Elastic and Plastic Base Metals Determined Using Finite-Element Analysis," submitted to *Weld. J.* (UCRL-102280, 1989).

G. A. Henshall and A. K. Miller, "The Influence of Solutes on Flow Stress Plateaus, with Emphasis on Back Stresses and the Development of Unified Constitutive Equations," *Acta Metall.* **37**, 2693 (1989).

J. W. Elmer, S. M. Allen, and T. W. Eagar, "The Influence of Cooling Rate on the Residual Ferrite Content of Stainless Steel Alloys," accepted for publication in the *Proceedings* of the 2nd International Conference on Trends in Welding Research, Gatlinburg, Tenn., Mar. 1989 (UCRL-100776, 1989).

J. W. Elmer, W. Giedt, and T. W. Eagar, "The Transition from Shallow to Deep Penetration During EB Welding," *Weld. J.*, in press (UCRL-101294, 1989).

J. W. Elmer and T. W. Eagar, "Measuring the Ferrite Content of Rapidly-Solidified Stainless Steel Alloys." *Weld. J.*, in press (UCRL-99602, 1989).

J. W. Elmer, S. M. Allen, and T. W. Eagar, "Microstructural Development During Solidification of Stainless Steel Alloys," *Metall. Trans.* **20A**, 2117 (1989).

W. Gourdin and J. W. Dini, "Evaluation of Electroformed Copper for Shaped-Charge Applications," submitted for the *Proceedings* of the Electroforming Symposium, American Society of Electroplaters and Surface Finishers, Las Vegas, Nev., Oct. 25–26, 1989.

W. Gourdin, "VISAR Analysis in the Presence of Large Intensity Changes: Application to the Expanding Ring," *Rev. Sci. Instr.* **60**, 754 (1989).

W. Gourdin, "Constitutive Properties of Copper and Tantalum at High Rates of Tensile Strain: Expanding-Ring Results," in *Proceedings* of the 4th International Conference on the Behavior of Materials at High Rates of Strain, Oxford, U.K., Mar. 19–22, 1989 (UCRL-98812, 1989).

C. W. Price, "Johnson-Mehl-Avrami Kinetics in Recrystallization of Metals and Crystallization of Metallic Glasses," submitted to *Acta Metall.* (UCRL-99556, 1989).
C. W. Price, "Comments on the Extent of Simultaneous Recovery During Recrystallization and Its Effect on Recrystallization Kinetics," *Scripta Metall.*, in press (UCRL-100553, 1989).
C. W. Price, "The Concept of 'Axial-Symmetry Constraint' and Its Significance in Recrystallization," in *Recrystallization '90*, in press (UCRL-100614, 1989).
C. W. Price, "Use of Computer Simulations to Analyze Limitations of Kinetic Models for Recrystallization," in *Recrystallization '90*, in press (UCRL-100615, 1989).
P. Turchi and A. Finel "Possible Ordered States based On The A15 Crystalline Structure" *Phys. Rev. Lett.*, in press.
A. F. Jankowski, M. A. Wall, and P. E. A. Turchi, "Crystallization of Amorphous Ti-Pd," *J. Less Common Met.*, in press.

Presentations

M. E. Kassner, R. S. Rosen, G. A. Henshall, and W. E. King, "Delayed failure of silver-aided diffusion welds between steel," TMS-AIME Fall Meeting, Indianapolis, Ind., Oct. 2–5, 1989.
W. H. Gourdin, presentation on program progress to Technical Coordination Group I, Computational Mechanics and Material Modeling, China Lake, Calif., Apr. 12, 1989.
W. H. Gourdin, presentation on program progress to Technical Coordination Group I, Computational Mechanics and Material Modeling, Los Alamos, N.M., Nov. 9, 1989.
R. S. Rosen, M. E. Kassner, and G. A. Henshall, "Delayed failure of silver-interlayer diffusion welds," Spring IMOG Joining Subgroup Meeting, Livermore, Calif., Apr. 18–20, 1989.
J. W. Elmer and T. W. Eagar, "Variations in the geometric shape of electron-beam welds," American Welding Society Annual Meeting, Washington, D.C., Apr. 1989.
J. W. Elmer, W. Giedt, and T. W. Eagar, "The transition from deep to shallow penetration during EB welding," IMOG Joining Subgroup Meeting, Livermore, Calif., Apr. 1989.
J. W. Elmer, S. M. Allen, and T. W. Eagar, "Microstructural development during rapid solidification of stainless steel alloys," 2nd International Conference on Trends in Welding Research, Gatlinburg, Tenn., May 1989.
M. E. Kassner, R. S. Rosen, G. A. Henshall, and W. E. King, "Delayed failure of silver-aided diffusion welds between steel," 2nd International Conference on Brazing, High-Temperature Brazing and Diffusion Welding, Essen, FRG, Sep. 19–20, 1989.

SYNCHROTRON-RADIATION-BASED MATERIALS SCIENCE

J. Wong (*Thrust Area Leader*)

Overview

The objective of this thrust area is to understand the role of structure (both atomic and electronic) in determining the physicochemical properties of materials and their processing. The tasks defined in this thrust area take advantage of the various unique characteristics of synchrotron radiation such as high intensity, high collimation, high polarization and, broadband tunability from VUV to hard x-ray to probe the structure of matter on an element-selective basis at different levels. The research areas involve both expansion of our existing capabilities in material characterization using these powerful photon sources and development of new capabilities to:

- Probe dilute species in bulk materials.
- Detect submonolayer coverages on surface and interfaces.
- Unravel chemical dynamics of reaction systems *in situ* in real time.

In this report, the technical progress and plans of work in FY90 are described for the following activities:

- Time-resolved diffraction study of solid combustion.
- Thin film and interface structures.
- Advanced microstructural studies using SAXS (small-angle x-ray scattering) and tomography.
- Photocatalysis on doped aerogels.
- Site-specific chemistry.
- YB_{66}: crystal growth and characterization.

Time-Resolved-Diffraction Study of Solid Combustion

J. Wong *E. M. Larson* *J. B. Holt*
P. A. Waide *B. Rupp*

The chemical dynamics and *in situ* phase transformation of a class of fast solid-state reactions at high temperature have thus far been little studied because of a lack of appropriate experimental probes. This class of solid-state reactions is universally accompanied by large negative heats of formation (≥50 kJ/mole). Once ignited, they become self-sustained and propagate to volumetric completion within seconds. These combustion reactions usually consist of a starting powder compact of solid reactants and are characterized by a combustion wavefront and a high self-generated temperature. The mechanism of these novel solid combustion reactions remains largely unknown. The challenge is to determine experimentally the kinetic pathway of these reactions by following the phase transformation of the reactants, via intermediates (if any), to the final products in real time.

In September, we performed a series of proof-of-principle time-resolved (TR) diffraction experiments at Brookhaven NSLS to follow the phase transformation in a number of binary solid combustion systems *in situ* at high temperature. A photodiode array (Princeton Instrument), capable of recording a full scan of 1024 pixels in 4 ms, was used as a reacting specimen situated in a specially designed reaction-chamber diffractometer with a vertical θ-2θ geometry. The system of study consisted of a ceramic system and an intermetallic system:

$$Ti + C = TiC$$
$$Ni + Al = NiAl$$

In the latter reaction, we were able to achieve a time resolution of 50 ms and record the formation of pre-reactive phases, melting of the reactants, reaction intermediates, and final product in a total scan time not longer than two minutes (Fig. SR-1). These experiments open a new route to study the chemical dynamics and phase transformation of reactive systems *in situ*, at high temperature, and under other external perturbations in the time domain of a few milliseconds, a regime not previously accessible.

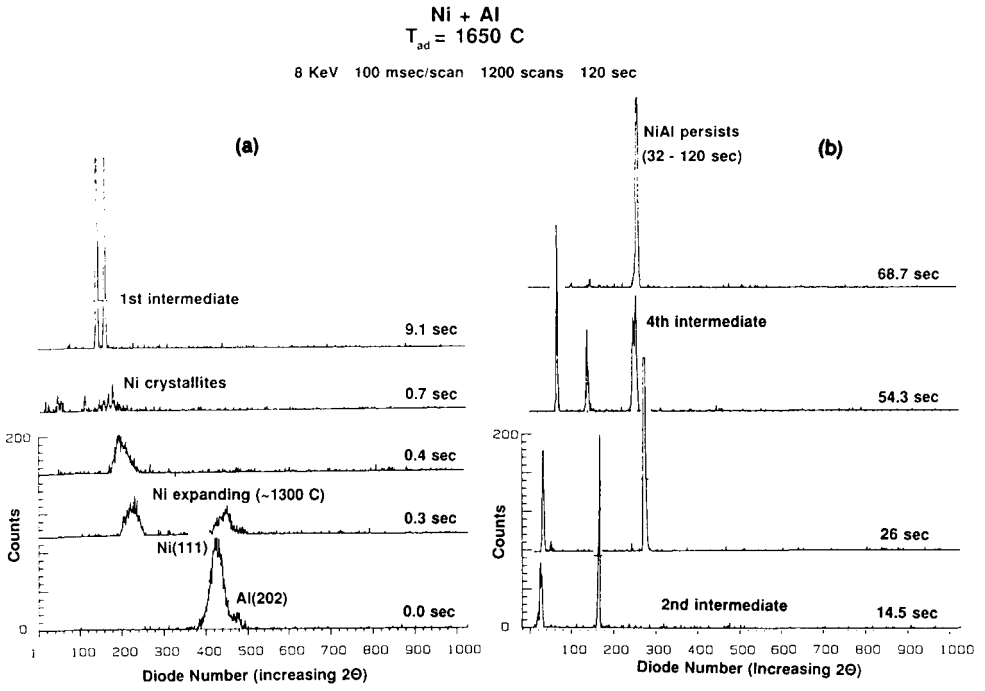

Fig. SR-1. Time-resolved-diffraction scans of the combustion system Ni and Al → NiAl showing the lattice expansion and melting of the Ni reactant appearance, a series of intermediates prior to the formation of the final NiAl product. Each diffraction pattern took 100 ms for a full 1024-pixel scan.

Our FY90 plans include the following:

- Install a second detector head to double the 2θ detection range.
- Stabilize the combusting surface to minimize the error in d-space variation during the TR-XRD (time-resolved x-ray diffraction) measurement.

- Complete a series of systematic TR diffraction measurements on the Ni-Al system as a function of initial composition and correlate the results with the quenching experiments on the 1:1 Ni-Al composition.
- Examine other, more complicated combustion reactions with the TR-XRD technique:
  - ***No liquid phase combustion***
    Example:
    $$Ta + C \rightarrow TaC$$
  - ***Sequential chemical reactions***
    Examples:
    $$WO_3 + 2Al \rightarrow W + Al_2O_3$$
    $$WO_3 + 2Al + C \rightarrow WC + 2Al_2O_3$$
  - ***Gas-solid reactions***
    Example:
    $$Ti + H_2 \rightarrow TiH_2$$
    $$Ti + (1\text{-}x)C + 1/2H_2 \rightarrow TiCH$$
  - ***Oxide reactions (including superconducting oxides)***
    Examples:
    $$PbO + TiO_2 \rightarrow PbTiO_3$$
    $$2BaO_2 + 3\,Cu + 1/2Y_2O_3 \xrightarrow{O_2} YBa_2\,Cu_3O_{7\text{-}x}$$
- Design and implement a high-temperature optical-pyrometer system for high speed and high spatial resolution to measure temperature profile and velocity of the combustion wavefront *in situ* during a TR-XRD experiment.

Two manuscripts reporting our first findings are now under preparation.

Thin-Film and Interface Structure

T. W. Barbee *B. Rupp* *R. Frahm**
J. Wong

Experiments both to demonstrate submonolayer sensitivity and to study interfaces in the copper-tungsten binary have been performed on beamline 10 at Stanford Synchrotron Radiation Laboratory (SSRL). Multilayer-synthesis technology was used to sputter-deposit tungsten-copper films on 3.75 cm × 10 cm × 0.25 cm superpolished fused-silica x-ray optic flats. Tungsten layers 50 nm thick were deposited, then overcoated *in situ* with copper layers designed to give surface copper concentrations of 0.1, 0.5, 1.0, 2.0, and 5.0 monolayers (MLs). Multilayer structures consisting of 5 ML tungsten/5 ML copper and 5 ML tungsten/1 ML copper were also synthesized. All structures were overcoated with 0.7 nm of amorphous carbon to stabilize the film/ambient surfaces against contamination. The operating conditions at SSRL were abnormally poor: 10 kG, <10 mA, 3.3 GeV. Even under such conditions, the copper EXAFS (extended x-ray absorption fine structure) spectra from a 0.1-ML surface concentration film was easily acquired. These results demonstrate that surface coverages of 0.01 ML or less are accessible for study using this technique.

* On sabbatical leave from HASYLAB, West Germany.

In Fig. SR-2, the Fourier transforms of EXAFS signals for bulk copper and for 5 ML, 2 ML, and 1 ML copper coverage on tungsten are given. The copper EXAFS signals at coverages of 2 ML and greater are clearly related to that of the bulk copper. At lower coverages, the EXAFS is significantly changed and appears as expected for an amorphous solid. The interatomic distances derived from these data are consistent with these interpretations. Data indicate that the local environment of the copper in these very thin films is dominated by carbon from the passivating overlayer. Additionally, the near-edge structure appears to change as the copper coverage decreases. This is consistent with evidence for an electronic interfacial bonding state between copper and tungsten that will dominate the low-coverage samples.

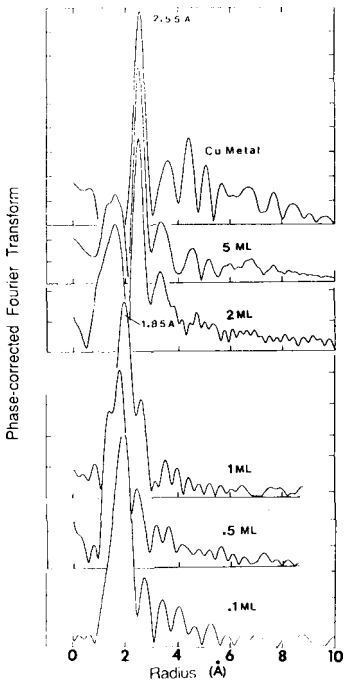

Fig. SR-2. Phase-corrected Fourier transform of Cu K-edge EXAFS from Cu overlayers sputtered in a tungsten substrate at various coverages. A 7-nm protective layer of amorphous C was sputtered on top of the Cu layer.

EXAFS measurements were also obtained from the copper in the multilayer samples. The copper in the 5 ML tungsten/5 ML copper sample was clearly identified as bulk copper. The tungsten in this sample, by contrast, was disordered and appeared amorphous. In the 5 ML tungsten/1 ML copper sample, the copper appeared to be body-centered-cubic, assuming the structure of tungsten.

During FY90, we plan to:

- Perform standing-wave fluorescence EXAFS studies of Pt/Cr, Pd/Ag, Pd/Rh, and Rh/Ag multilayer structures.
- Install a quick-scan procedure (QEXAFS) to obtain EXAFS scans of the order of seconds at beamline 10-2 at SSRL.

- Design and implement a deposition chamber to study *in situ* film growth using a solid-state detector array in vacuum.

Advanced Microstructural Studies

J. H. Kinney *R. A. Saroyan* *U. Bonse**
*S. Stock***

Small-Angle X-ray Scattering (SAXS)

We were awarded two months parasitic time at DESY (the synchrotron in Hamburg, West Germany) to use an ultrahigh-resolution camera to measure small-angle x-ray scattering of resorcinol-formaldehyde aerogels. The data provide interesting comparisons to similar studies of silica aerogels, except no one has been able to observe the large correlation lengths that are possible with this unique Bonse-Hart type geometry.

Magnifying Optics Tomography

Three weeks of dedicated time at DESY testing the x-ray magnifying optics led to the successful measurement of the optical properties of an 8X magnifying geometry. "Magnified" tomography on a 100-μm fiber-aligned composite resulted in a resolution of 2.5 μm. This work leads the way to eventually achieving a spatial resolution equivalent to optical microscopy.

FY90 Plans

- Investigate fatigue crack growth in Ti_3Al composites.
- Identify failure mechanism in SiC/SiC ceramic composites.
- Study Mg/F segregation in dentinal tubules using NSLS fluorescence source.
- Transfer USAXS (ultrasmall-angle x-ray scattering) and SAXS capability to SSRL/PRT beamlines.
- Perform USAXS, especially anomalous scattering in RF aerogels.
- Investigate nucleation and growth in RF foams using SAXS.

Photocatalysis on Doped Aerogels

C. Colmenares *M. Connor* *J. Raymond*
R. Gaver†

The objective of this project is to demonstrate that SiO_2, Al_2O_3, or ThO_2 aerogels doped with photochemically-active ions can be used as heterogeneous catalysts for the production of hydrocarbons from simple gas mixtures ($CO + H_2$, $CO_2 + H_2$, etc.) using sunlight as the energy source. Also, the energy-transfer mechanisms effecting the chemical reactions will be investigated.

---

* On sabbatical leave from University of Dortmund, West Germany.
** Georgia Institute of Technology.
† San Jose State University.

SiO_2 aerogels doped with Ce^{+3}, Eu^{+3}, UO_2^{2+}, and Tb^{+3} have been prepared. The light emission of these four covers most of the visible region: cerium emits in the blue, uranyl and terbium in the green, europium in the red. The first three have been characterized by x-ray spectroscopy, laser-ionization mass analysis (LIMS), and optical spectroscopy. Eu^{+3}- and Ce^{+3}-doped aerogels will be shortly tested for catalytic activity in the fluidized-bed reactor.

Uranyl-doped aerogels show high fluorescence intensity in the 0.5 wt% concentration. This aerogel absorbs at all wavelengths between 250 and 450 nm. The emission consists of a broad, diffuse band that peaks at 518 nm; there is also a much less intense peak at 623 nm. This is quite different from uranyl nitrate crystals, which show five distinct emission lines. The disappearance of these distinct features is due to a decrease in the number of degrees of freedom available to the ion and to the host material being quite amorphous. Fig. SR-3a shows the fluorescence of uranyl nitrate crystals and that of a 0.5% CuO_2^{2+}: SiO_2 aerogel.

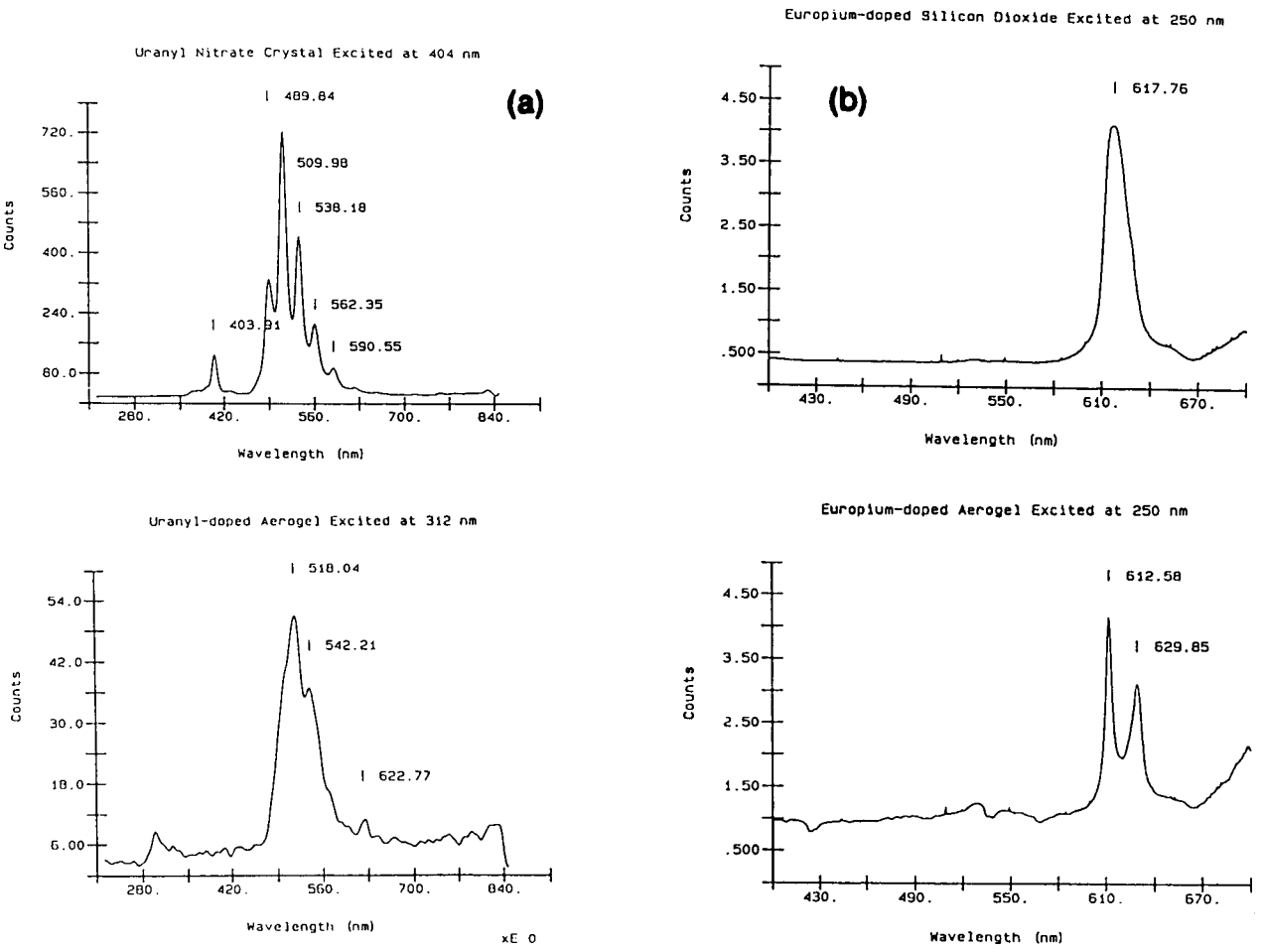

Fig. SR-3. (a) Fluorescence spectra of uranyl nitrate (top) versus that of uranyl-doped aerogel (bottom); (b) fluorescence spectra of Eu-doped SiO_2 glass (top) versus that of Eu-doped aerogel (bottom).

Several different compositions of Eu-doped aerogels have been produced. Only the 1% Eu^{3+} aerogel exhibits the characteristic red emission of the Eu^{3+} ion. The spectrum

shows two distinct peaks, at 612 and 629 nm. Both of these lines have been shown to be induced by absorption at ~280 nm. Both emission and absorption results are quite different from those of other Eu-doped solids. There is a significant difference between the fluorescence of Eu_2O_3: SiO_2 glass and that of a 1% Eu: SiO_2 aerogel (see Fig. SR-3b). The europium in SiO_2 produces a single peak at 617.76 nm, which falls between the two peaks of europium in SiO_2 aerogel (612.58 and 629.85 nm). The data in Figs. SR-2a and SR-2b clearly show the various bonding states that the doping ions assume as a function of the matrix, in particular the uniqueness of the doped aerogels.

In FY90, the aerogel photocatalyst work will include the following:

- Preparing Fe- and Cr-doped aerogels (in which the dopants are expected to have a strong interaction with the SiO_2 matrix) and a Tb-doped aerogel (weak interaction with the matrix).
- Evaluating the Ce- Tb-, Fe-, and Cr-doped aerogels in the fluidized-bed reactor for catalytic activity.
- Performing detailed experiments to elucidate the energy-transfer mechanism in Ce-, Tb-, Eu-, UO_2^{2+}-, Fe-, and Cr-doped SiO_2 aerogels when exposed to sunlight in the presence of gas mixtures.
- Attempting to determine experimentally where and how dopants are located in the SiO_2 aerogel structure, and to measure their valence-band photoemission spectra using synchrotron radiation.

Site-Specific Chemistry: XANES & EXAFS Studies

B. Rupp *E. M. Larson* *M. J. Weber*
J. Wong

We have conducted a series of x-ray absorption spectroscopic (XAS) measurements on the following systems in a recent run at Brookhaven NSLS:

- Cu XANES (x-ray absorption near-edge structure) of $ErBa_2Cu_3O_{6+y}$ as a function of oxygen content in the range $6.1 < y < 7.0$.
- La EXAFS in silicate glasses of geological interest.
- Nd-environment SiO_2 sol gels as intermediates of Nd-doped silicate glasses for laser application.
- Y K-edge EXAFS in YB_{66} as a function of temperature (10–300 K) to study the thermal contribution to the Dekye-Waller factor.
- Systematic study of the $L_{3,2,1}$-edge spectra of rare-earth oxides.

In addition, a multiple-scattering XANES code (Bianconi, University of Rome) is being installed in the CMS1 VAX as is a redesign of code for 80386 work stations.

Our FY90 plans include:

- Completing data analysis of the systems studied above.
- Performing polarization measurements on oriented $ErBa_2Cu_3O_{6+y}$ materials to sort out the various XANES transitions at the Cu-edge.
- Continuing $L_{3,2,1}$-edge spectra of rare-earth trifluoride.
- Studying the effect of co-dopants (Ta) on the Nd local structure in SiO_2 gels.

- Making careful EXAFS measurement of anhydrous CrF_3 to model the environment of Cr^{3+} in fluoride laser crystals.

YB_{66}: A New Soft X-ray Monochromator for SR

J.Wong *G. M. Shimkaveg* *M. J. Eckart*
G. J. Tanaka *Z. Rek*

YB_{66}, a complex binary semiconducting compound, cubic in crystal structure with a cell parameter of 2.344 nm, has been singled out as a potentially useful soft x-ray monochromator for dispersing synchrotron radiation. There is no intrinsic absorption by the constituent elements in the region 1–2 keV (the Y L_3-edge is at 2080 eV). Using the known structure factors for the (400) and (222) reflections (2d values of 1.176 nm and 1.353 nm, respectively), their rocking curves have been calculated and are shown to be comparable to or better than that of beryl ($10\bar{1}0$). In terms of vacuum compatibility, resistance to radiation damage, and thermal and mechanical stability, YB_{66} satisfies all the material requirements for use as a monochromator for synchrotron radiation in the soft x-ray region. Single crystals of this material large enough to intercept 1 mrad of radiation have recently been grown. Rocking-curve measurements, etch-pit density, and x-ray white-beam topography are used to characterize the quality of these large crystals as a function of some critical growth parameters (such as pulling rate and thermal gradient) at the crystal-liquid interface. From this study, it is clear that future work should be directed toward the control and retention of convexity of the crystal-liquid interface during growth, a key factor to achieve high-perfection crystals. Details of this work are described in a recent report (UCRL-102155).

FY90 plans include:

- Controlling experimentally solid-liquid interface convexity during crystal growth.
- Continuing synchrotron-to-topographic characterization.
- Performing rocking-curve measurements in the soft x-ray region.

Publications and Presentations

Publications

F. W. Lytle, R. B. Greegor, J. Wong, and E. M. Larson, "Investigation of the Valence of Pr in $YBa_2Cu_3O_7$," *Phys. Rev. B*, in press.

J. Wong, W. Nixon, J. Mitchell and S. Laderman, "Solute Pairing in fcc Binary and Ternary Cu Alloys," *Physica B* **158**, 25 (1989).

T. W. Barbee and J. Wong, "EXAFS of Near-Monolayer Hf Films," *Physica B* **158**, 670 (1989).

J. Wong and G. A. Slack, "Metals in Beta-Rhombohedral Boron," *Physica B* **158**, 627 (1989).

R. B. Greegor, F. W. Lytle, M. J. Weber, J. Wong, and W. J. Weber, "Application of Various EXAFS Techniques to the Investigation of Structurally Damaged Materials," *Physica B* **158**, 498 (1989).

B. Rupp, P. Allenspach, P. Fischer, and A. Furrer, "On the Correlation of Secondary Structural Effects, Superconductivity and Crystal Field Interaction in $ErBa_2Cu_3O_x$ – New Evidence for a Charge-Transfer Mechanism?" *Physica C*, in press.

A. Furrer, P. Allenspach, B. Rupp, and H. Blank, "Charge Redistribution in the CuO_2 Planes of High-T_c Superconductors $RBa_2Cu_3O_x$ (R: Rare Earth, $6<x<7$) Determined by Neutron Crystal-Field Spectroscopy," *Physica B* invited paper, in press.

H. Lütgemeier, R. A. Brand, Ch. Sauer, B. Rupp, P. M. Meuffels, and W. Zinn, "Magnetic Structure of Cu in Antiferromagnetic $RBa_2Cu_3O_x$," *Physica C*, in press.

H. J. Maier, H. Kaesche, and B. Rupp, "Environmental Effects on the X-ray Line Profiles of Fatigued Low Alloy Steel," submitted to *Scripta Metall.* (1989).

B. Rupp, P. Hotz, and F. Tuppy, "Strengths and Limitations of Physical Methods in Surface Characterization of Bio-Materials," submitted to *Z. Stomatologie* (1989).

J. Wong, G. Shimkaveg, W. Goldstein, M. Eckart, T. Tanaka, Z. Rek, "YB_{66}: A New Soft X-ray Monochromator for Synchrotron Radiation," *Nucl. Instrum. Methods*, in press.

J. Kinney, A. Saroyan, U. Bonse, A. Johnson, and S. Stock, "Nondestructive Investigation of Damage in Composite Materials using XTM," *J. Mater. Res.*, in press.

E. M. Larson, J. Wong, J. B. Holt, P. Waide, and B. Rupp, "Time-Resolved X-ray Diffraction Monitoring the Exothermic High-Temperature Synthesis Reactions of TiC and NiAl Using Synchrotron Radiation," *Science* (1989), in preparation.

E. M. Larson, J. Wong, P. Waide, and J. B. Holt, "Design and Construction of a Diffraction-Reaction Chamber for Time-Resolved Study of High-Temperature Solid-State Combustion Reactions," *Rev. Sci. Instrum.* (1989), in preparation.

U. Bonse, R. Pahl, J. H. Kinney, and R. Pekala, "Ultrasmall-Angle Scattering in Resorcinol Foams," *J. Non-Cryst. Solids*, in press.

S. R. Stock, T. M. Breunig, S. C. Antolovich, J. H. Kinney, Q. C. Johnson, M. C. Nichols, and U. Bonse, "Synchrotron Microtomography of Composites," *Mater. Res. Soc. Symp. Proc.* **113**, 273 (1989).

J. H. Kinney, M. C. Nichols, U. Bonse, Q. C. Johnson, and R. A. Saroyan, "Synchrotron Microtomography on Beamline X-2 at SSRL," *Rev. Sci. Instr.* **60**, 2478 (1989).

U. Bonse, R. Nusshardt, F. Busch, J. H. Kinney, and M. C. Nichols, "Optimization of CCD-based Microtomography," *Rev. Sci. Instr.* **60**, 2471 (1989).

M. C. Nichols, J. H. Kinney, Q. C. Johnson, U. Bonse, R. A. Saroyan, and R. Nusshardt, "Synchrotron Microtomography of Supported Catalysts," *Rev. Sci. Instr.* **60**, 2475 (1989).

U. Bonse, R. Nusshardt, J. H. Kinney, M. C. Nichols, and R. A. Saroyan, "X-ray Tomographic Microscopy of Fiber-Enforced Materials," *J. Mater. Sci.*, in preparation.

Presentations

Invited Talks

J. Wong, "Materials studies using x-ray absorption spectroscopy," Joint AAAS-APT symposium on Synchrotron Radiation, San Francisco, Calif., Jan. 1989.

J. Wong, "Applications of EXAFS and XANES to materials science," Taiwan Synchrotron Radiation Research Center Users Meeting, Taipei, Taiwan, Jul. 1989.

J. Wong, "Principles and applications of XAS to coal and other industrial materials," China Steel Corporation R&D Center, Kaoshiung, Taiwan, Jul. 1989.

B. Holt, "Temperature profiles and *in situ* diffraction studies of SHS reactions," International Symposium on Flame Structure, Alma-Alta., USSR, Sep. 1989.

A. Furrer, P. Allenspach, B. Rupp, and H. Blank, "Change redistribution in the CuO_2 planes of high-T_c superconductors $RBa_2Cu_3O_x$ (R:rare-earth, $6< x <7$) determined by neutron crystal-field spectroscopy," International Conference on Highly Correlated Electron Systems, Santa Fe, N.M., Sep. 1989.

J. H. Kinney, "X-ray tomographic microscopy using synchrotron radiation," 3rd User Meeting of the Advanced Photon Source, Argonne National Laboratory, Argonne, Ill., Oct. 1989.

J. H. Kinney, "X-ray tomographic microscopy," ASNT Topical Meeting on Industrial Computed Tomography, Seattle, Wash., Jul. 25–27, 1989.

Contributing

E. M. Larson, J. Wong, M. Weber, "Coordination of Nd in binary alkali BeF_2 glasses," Annual Meeting of American Crystal. Association, Seattle, Wash., Aug. 1989.

J. Wong et al., "YB_{66}: A new soft x-ray monochromator for synchrotron radiation," 6th International Conference on SR Instrumentation, Berkeley, Calif., Aug. 1989.

T. W. Barbee, Jr., "Interface formation by physical vapor deposition and synchrotron radiation studies," Symposium on Interface Science and Technology, 1989 ACA Meeting, Seattle, Wash., Jul. 23–28, 1989.

B. Rupp et al., "On the correlation of secondary structural effects superconductivity and crystal field interaction in $ErBa_2Cu_3O_x$ new evidence for charge transfer mechanism?" M^2S-HTSC Conference, Stanford, Calif., Jul. 1989.

Patent and Lectures

Patent

C. Colmenares, "Method and apparatus for synthesizing various short chain hydrocarbons," patent application IL-7824, May 2, 1989.

Lectures

J. Wong, "Experimental x-ray absorption spectroscopy using synchrotron radiation," Summer School Lectures (1 week), National Taiwan University, Taipei, Taiwan, Jul. 1989.

J. H. Kinney, "Implementation of x-ray tomographic microscopy for fibers research," Pioneering Research Department, E. I. du Pont de Nemours & Co., Wilmington, Del., Dec. 1, 1989.

Faculty Appointment

J. H. Kinney, Department of Restorative Dentistry, University of California at San Francisco, Oct. 1, 1989.

TRITIUM

P. C. Souers, J. L. Maienschein, G. W. Collins (*Thrust Area Leaders*)

Nuclear-Spin Polarization

The goal is to create a form of solid deuterium-tritium with a longitudinal nuclear relaxation time long enough for a try at nuclear polarization. Ultrapure molecular deuterium-tritide (DT) appears our best current candidate. Our plan is to purify the DT on an adsorption column at 22 K. Creation of the lower temperature infrastructure has taken more time than expected. The 2-mW, 0.5-K Oxford cryostat in a 9-T magnet will arrive in Jan. 1990. A 1.4-K Janis cryostat is almost ready to be tested in a 13-T superconducting magnet. When that is complete, we will have transformed ourselves totally out of the 4-K flow-cryostat mode that characterized the first 15 years of cryogenic D-T in our building.

We have extended our pulsed nuclear magnetic resonance (NMR) measurements from 3.5 K in the flow cryostat to 1.5 K in the Janis ESR cryostat. We found that the longitudinal relaxation time of the triton in regular D-T (D_2-DT-T_2 mixture) was unchanged at the lower temperature, showing that 2 K more of cold had no effect on the molecular rotation.

An unexpected result is shown in Fig. T-1. The triton's NMR signal was expected to decrease about one-third as the J = 1 T_2 converted to J = 0 T_2. The remaining molecular DT signal was expected to be stable. Instead, the triton signal decreased to unexpectedly low values. This decrease was associated with the onset of heat spikes, long attributed by us to mass hydrogen-atom recombination. The reason for this effect is unknown. The NMR frequency was 15 MHz.

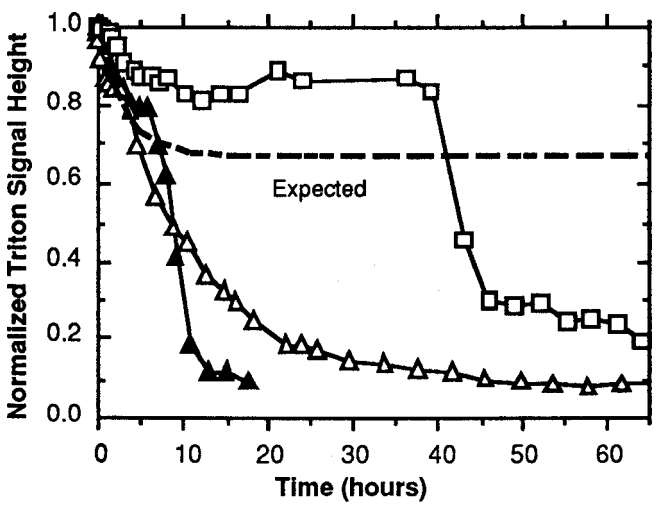

Fig. T-1. Triton longitudinal relaxation time in regular D-T at 1.5 K and 15 MHz. The triton signal height is expected to drop about a third as J=1 T_2 converts to J=0 T_2 and only molecular DT remains. Instead, thermal spikes cause the NMR signal to decline abruptly to low levels. The reason is unknown. Three separate runs are shown.

Both regular D-T and enriched 93% molecular DT were studied at 5 K and 7 MHz, where deuteron NMR was observed. The results are shown in Fig. T-2. The D-in-HD data (taken by A. Honig of Syracuse University) are what we expected for the longitudinal nuclear relaxation time. Our data were markedly different, and the expected long times at low J = 1 concentrations were not seen. The reason for this behavior is unknown. It leaves open the possibility that hydrogen atoms in the solid are interacting with the deuteron by way of its nuclear quadrupole moment. Further work is needed to see if such an unexpected pathway of nuclear relaxation can exist.

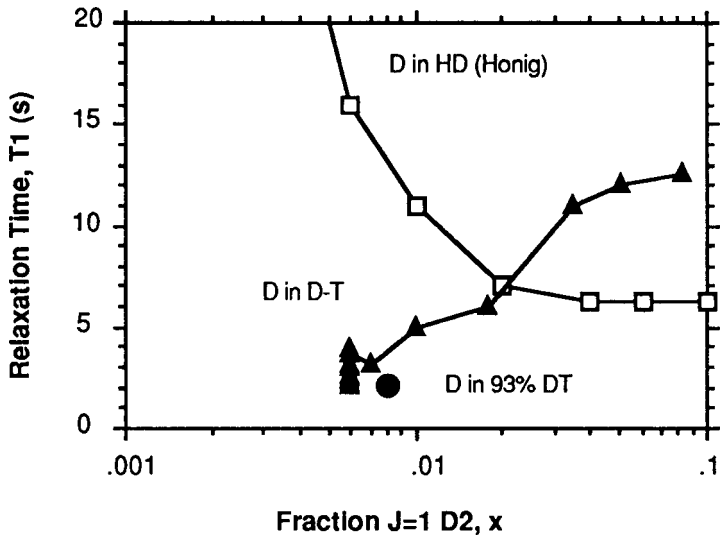

Fig. T-2. Deuteron longitudinal relaxation times in two D-T samples at 5 K. The behavior is quite different from that of the deuteron in the solid-HD data of A. Honig. The reason for the difference is unknown, but it is surely caused by the tritium radioactivity.

Construction of two molecular-DT enrichment columns continues. One will be in a 5-K flow cryostat attached to the Raman spectrometer. The other will go in a new 1.4-K Janis insert in a 13-T superconducting magnet. This will be our first high-field piece of equipment.

Lithium Beryllium Hydride

We have studied the reaction of lithium hydride and beryllium hydride, by using simultaneous differential thermal analysis (DTA) and thermogravimetric analysis (TGA) in conjunction with powder x-ray diffraction (XRD), to try to determine the reaction pathway and to identify the reaction products. We used mixtures of 25% mol LiH + 75% BeH_2, 50% LiH + 50% BeH_2, 67% LiH + 33% BeH_2, and 100% BeH_2. Crystalline BeH_2 was used for these measurements.

Pure BeH_2 decomposes at about 400 °C. However, crystalline BeH_2 has an additional small endotherm at about 175 °C that is not present in amorphous material. XRD measurements on crystalline BeH_2 that has been cycled to 280–290 °C show that the

material is amorphous. Apparently, the endotherm at 175 °C represents a thermally-induced conversion of crystalline BeH_2 to the amorphous form.

Thermal analysis of mixtures of BeH_2 and LiH shows two types of behavior, depending on the composition. Thermal cycling of 67% LiH + 33% BeH_2 to 235 °C shows an endotherm and an exotherm superimposed at about 150–200 °C during the initial heatup, then no thermal features on cooling (Fig. T-3) or in subsequent temperature cycles. There is no mass loss in thermal cycling at this temperature. The DTA patterns at this composition are not seen for other mixtures, so the 67/33 mixture in the first thermal cycle is probably forming Li_2BeH_4, which apparently has no phase changes below 230 °C. Cycling this mixture to 325 °C takes the sample above an apparent phase change, but there is no mass loss in repeated cycling to 325 °C.

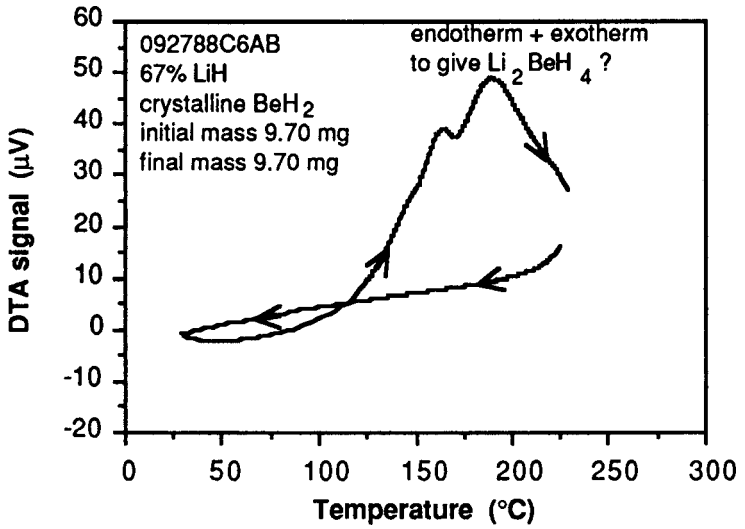

Fig. T-3. Thermal behavior of 67% LiH + 33% BeH_2, first cycle to 230 °C.

Thermal cycling of 50% LiH + 50% BeH_2 shows a different behavior than was observed for the 67/33 composition. A complex endotherm at ~150–200 °C is observed in the first thermal cycle to 230 °C, whereas subsequent thermal cycles show a phase change. These are shown in Figs. T-4 and T-5. A likely product from the first (reaction) endotherm is $LiBeH_3$ since mixtures containing 25% LiH show similar thermal behavior; however, the features are less strong. The subsequent DTA peaks are identified as phase changes because we have observed that the mixture is fluid: It flows readily at first through a 5-µm frit; then it foams when heated to 235 °C as evolved hydrogen and organics blow the fluid phase into a low-density, porous matrix. The product is clearly different from that in the 67/33 mixture since the latter showed no phase changes below 250 °C. There is no mass loss when the thermal cycle is repeated six times, so the product is stable at this maximum temperature.

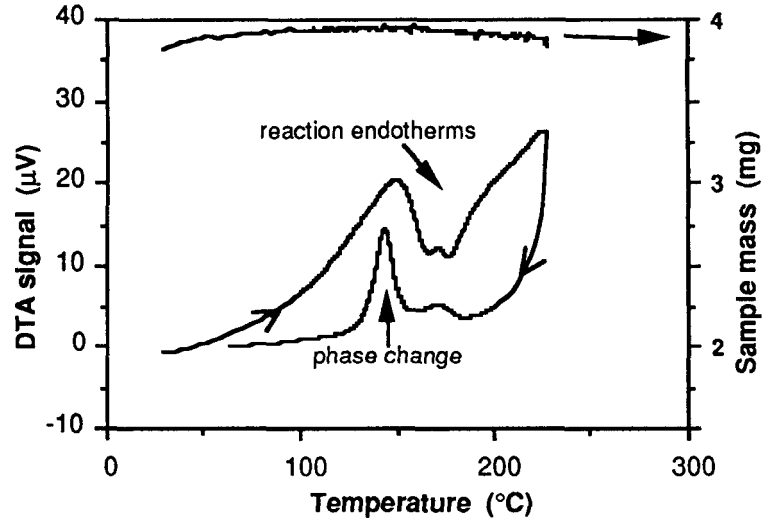

Fig. T-4. Thermal behavior of 50% LiH + 50% BeH_2, first cycle to 230 °C.

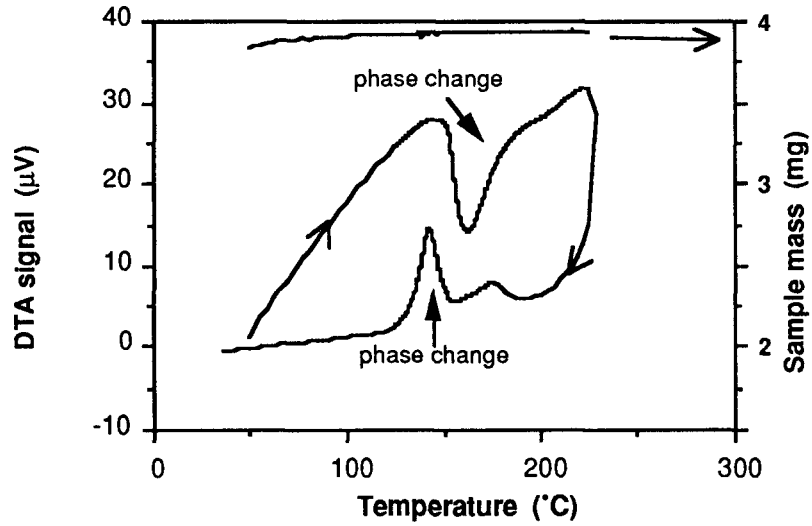

Fig. T-5. Thermal behavior of 50% LiH + 50% BeH_2, second cycle to 230 °C.

When the 50/50 mixture is cycled to 325 °C, we see the reaction to "$LiBeH_3$" at 150–200 °C followed by a subsequent endotherm at 260–280 °C with an accompanying mass loss of 5.6%. This mass loss corresponds to loss of one hydrogen atom. When this hydrogen atom comes off, it blows the material into a super-porous, super-low-density foam that is much bigger than the foam that formed from heating to 235 °C. Additional thermal cycles show an apparent phase change similar to that of Li_2BeH_4. With the loss of one hydrogen atom, Li_2BeH_4 plus Be metal are possible products.

XRD measurements have been made on samples with the above compositions and thermal histories. The results are ambiguous; interpretation is hampered by the lack of good x-ray patterns for the possible products. (Ashby and Prasad [1] and Bell and Coates [2]

report x-ray patterns for several Li-Be hydrides, but the actual identification of their products is uncertain.) All samples in this work were tentatively identified as "Li_3BeH_5"; it was not possible to identify Be metal in any of the samples. From the thermal behavior discussed above, the products are clearly not all the same, so further analysis of XRD data is required.

References

1. E. C. Ashby and H. S. Prasad, *Inorg. Chem.* **14**, 2869 (1975).
2. N. A. Bell and G. E. Coates, *J. Chem. Soc. A*, 628 (1968).

Publications

W. G. Wolfer, C. L. Bisson, P. C. Souers, and R. T. Tsugawa, "The DC Electrical Conductivity of D-T Gas," *Phys. Rev. A*, in press.

P. C. Souers, R. T. Tsugawa, C. L. Bisson, and W. G. Wolfer, "Thomson Space Charge in D-T Gas," *J. Vac. Sci. Tech. A*, in press.

P. C. Souers and P. A. Fedders, "Considerations in the Deuteron Polarization of Solid DT," *Phys. Rev. B*, in press.

J. L. Maienschein, P. E. Barry, F. McMurphy, and J. Bowers, "Synthesis and Properties of a Low-Density, High-Porosity Lithium Hydride-Beryllium Hydride Foam," submitted to *Mater. Sci. Eng.*

PLUTONIUM AND ACTINIDES

G. F. Gallegos (*Thrust Area Leader*)

The plutonium and actinides thrust area continues to focus on three areas:

- Evaluation of plutonium-alloying behavior.
- Thermodynamics of plutonium silicides.
- Liquid-actinide containment.

The experimental part of the plutonium-alloying studies (by sputtering) was wrapped up during this half, and the liquid-actinide containment work was streamlined down to one activity on effects of stress on refractory metals in liquid-actinide environments.

Progress on a new (funded at midyear) proposal, "Reduction of Plutonium-Oxide by Lithium Metal," is also included.

Evaluation of Plutonium-Alloying Behavior

Triode-Sputtering of Pu Alloys

H. F. Rizzo *A. W. Echeverria* *T. B. Massalski*[*]
E. C. McClanahan *M. Stevens*[**] *T. Zocco*[†]

Experimental work was limited to preparing and shipping Pu-Ce, Pu-Sc, and Pu-Yb for TEM and other analysis at Los Alamos National Laboratory; these analyses will be funded by them on this collaborative effort.

In the progress report for the second half of FY88, it was reported that a soft phase of Pu (designated α*) with an α-crystal structure was fabricated by sputtering. The sputtered film had a microhardness of 90–120 H_v rather than the 250 of α-phase Pu. TEM work performed at LANL on this material showed that β-phase Pu was present. This confirms earlier speculation based on differential scanning calorimetry that some of the material in the specimen (~25%) was β-phase Pu. This observation, however, cannot fully account for the low hardness since β-Pu typically has a hardness of ~150 H_v. It still appears that grain-boundary sliding of this extremely fine-grained material is a possible explanation.

The TEM analysis of a sputtered plutonium alloy has verified the existence of mechanical twinning in this alloy. The twinning is the same as that observed in work done to verify crystallographic predictions of the δ-to-α phase change and is not commonly observed in the α-phase structure.

---

[*] Carnegie-Mellon University.
[**] Battelle Pacific Northwest Laboratory.
[†] Los Alamos National Laboratory.

Electronic-Structure Calculations

A. Gonis *P. Wienberger*[*] *M. Boring*[**]
F . Pinski[†]

The long-term objective of this work is calculation of the stable structures that result from alloying Pu with elements such as Al, Ga, Si, Am, Sc, Np, and Ce. We also plan to address the computation of Pu-alloy phase diagrams across the concentration range for these alloy constituents.

The computation of alloy-phase stability of Pu alloys requires the use of computer programs based on the so-called KKR-CPA. Until recently, the KKR-CPA codes that were developed within a relativistic formulation of multiple-scattering theory were not able to take account of charge self-consistency (i.e., rearrangement of electronic charge on alloying). Because this charge transfer effect can be very important in the determination of alloy properties, we decided to expend the effort to incorporate such effects in our codes. A charge-self-consistent total energy KKR-CPA code for non-relativistic systems was developed. We are currently proceeding with the extension of the relativistic code to include the calculation of total energies, a process that will probably be completed in the next 4–5 months.

We also began the computational work outlined in the objectives section and have just completed the electronic-structure calculations for the alloys Pu_xCe_{1-x} (x = 0.90, 0.95). These calculations predicted that Ce tends to stabilize the (monoclinic) α-phase of Pu, which is somewhat in disagreement with earlier points of view and the published Pu-Ce phase diagram. A paper on this part of the work is being submitted to a scientific journal.

Analysis of Pu-Ce System

G. F. Gallegos

Using sputtering results, electronic-structure calculations, and a (phenomenological) model to calculate the binary phase diagram of the Pu-Ce system using F*A*C*T, we observe an interesting correlation as to the role of Ce in Pu. Traditionally, the view of Ce in Pu is a δ-phase stabilizer, similar to gallium in Pu (as seen in their diagrams shown in Figs. PA-1 and PA-2). However, the studies performed showed significant differences.

Experimental evidence, including sputtering results reported previously [1], show that ~20 at.% Ce can be introduced in the α-phase. For Ga, less than 1% can be introduced without stabilizing a non-α-phase. Although sputtering produces non-equilibrium structures, this still suggests that Ce is more soluble than Ga in α-Pu. An additional observation from our technology base work has shown that, in casting dilute Pu alloys of Pu-Ga and Pu-Ce, those of Pu-Ga usually contain mixtures of several phases but those of Pu-Ce do not.

As indicated in the previous section, a case is made that Ce is an α stabilizer. Calculations for Al (or Ga) in an fcc Pu lattice show that decreased f-bonding (hence

[*] Technical University of Vienna.
[**] Los Alamos National Laboratory.
[†] University of Cincinnati.

increased d-bonding) is characteristic of the δ-phase of Pu. For Ce, the same calculations suggest that f-states from the Ce may enhance the f-bonding tendency. Some uncertainty exists due to factors which need to be considered, including the non-self-consistency of the code used.

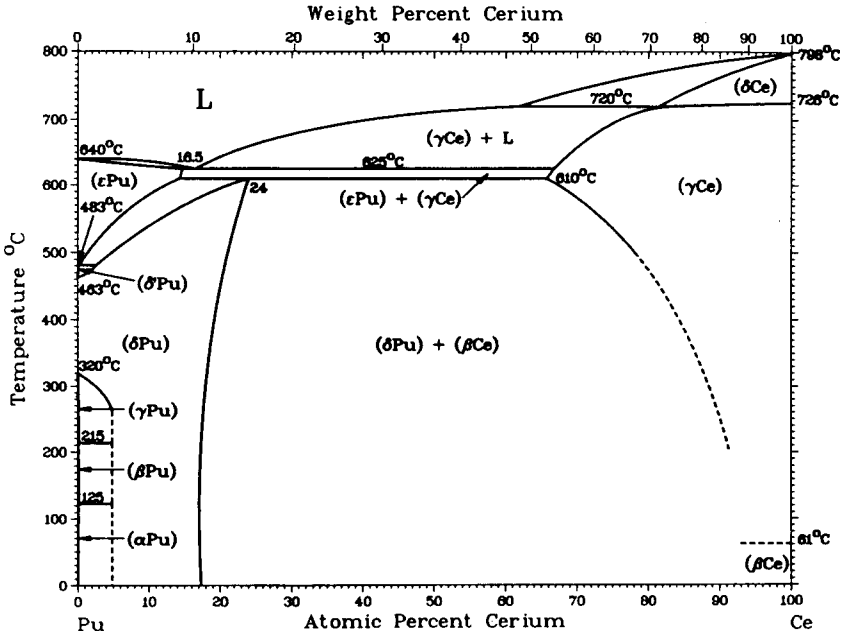

Fig. PA-1. Pu-Ce system published by Ellinger et al.

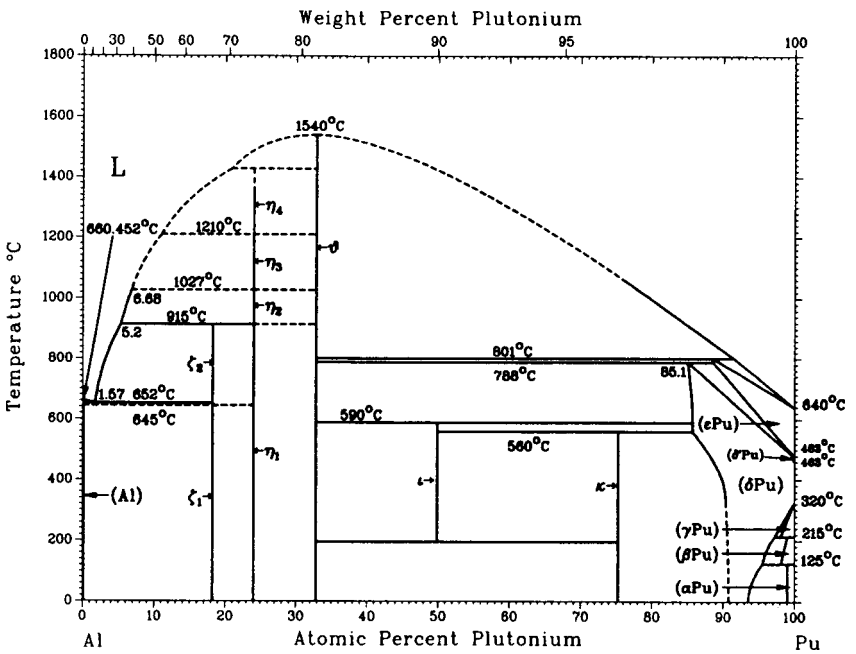

Fig. PA-2. Pu-Al system as reported by Ellinger.

Modeling of the Pu-Ce system using the F*A*C*T program has produced the binary phase diagram in Fig. PA-3, which shows an eutectoid decomposition at 171 °C and contrasts with that in Fig. PA-2. The calculation, based on a regular solution model and minimization of Gibb's free energy, repeatedly showed the same behavior with changes within the experimental error of thermodynamic variables. A similar diagram for the Pu-Al system has been suggested [2]; however, the results using the same computer code are considerably more sensitive to small variations in thermodynamic variables and show a eutectoid at a lower temperature.

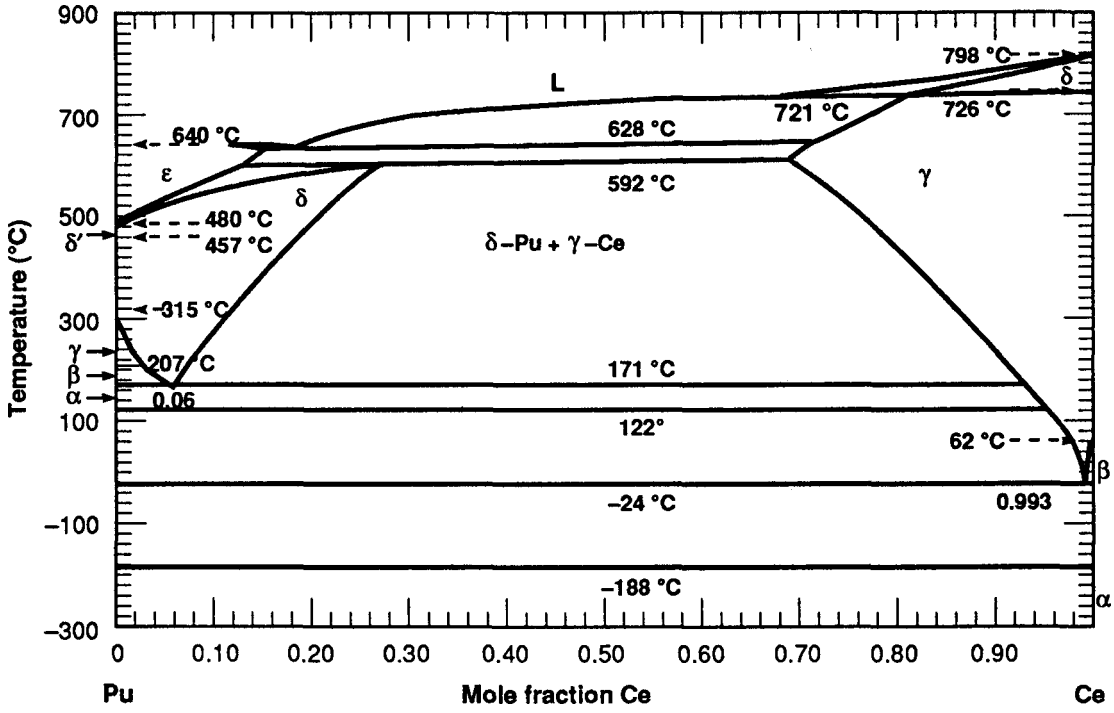

Fig. PA-3. Pu-Ce system as calculated by F*A*C*T.

The evidence presented is not sufficient to classify Ce as an α-stabilizer; however, it is clear that it is not acting simply as a "dilute" Ga or Al. The unusual behavior exhibited by this system may be worthy of further study.

Thermodynamics of Plutonium Silicides

O. H. Krikorian

The objectives and prior work have been reported previously. During this reporting period, considerable progress has been made in the exchange-reaction studies. Arc-meltings have been completed for exchange-reaction mixtures of Pu with Cr_3Si, Mo_3Si, W_3Si_2, and U_3Si_2. This establishes the enthalpy of formation of Pu_5Si_3 as ≤300 kJ/mole, which is considerably more stable than we had anticipated. The Mo-containing sample was not completely melted and will be rerun. Some ambiguities still remain in the analytic interpretations for all the samples as a result of failure to achieve equilibrium and possible

ternary phase formation. Hence, we need to anneal and re-analyze the samples. Also, because of the unexpectedly high stability of Pu_5Si_3, we plan to run some exchange reactions with more stable silicides, such as $Ta_{4.5}Si$, in order to establish an upper limit to the Pu_5Si_3 stability.

The Knudsen-cell effusion studies are awaiting completion of the high-vacuum tungsten furnace. Pure samples of Pu_5Si_3 and Pu_3Si_2 have been prepared by arc-melting for the study.

Installation of a 2000 °C high-vacuum tungsten furnace and glovebox enclosure system is approximately 70% complete. Analytical and calculation efforts to determine free-energy functions and heat capacities are also being pursued in this project.

Free-energy functions are needed for the plutonium-silicide phases in order to evaluate the thermodynamic measurements and to extend the data over the full range of temperature. The basic information required is the heat capacity from absolute zero to the melting point. We are using a theoretical approach to generate the needed functions.

A paper has been completed on methods for calculating the heat capacities of metals. Based on it and the methods that we developed in earlier papers, we are in process of developing methods for calculating the heat capacities of silicides. The methods will be tested on known data on silicides before using them to calculate heat capacity and thermodynamic functions for the plutonium silicides.

Liquid-Actinide Containment

J. Huang *G. F. Gallegos*

Tensile tests have been completed on a series of Ta-Nb alloys. It was found that Ta-10% Nb and Ta-20% Nb were embrittled by liquid U but that the other alloys were not. These results suggest that the embrittlement-susceptible couples have a common type of phase-diagram behavior (such as that of Ta-U or W-U), in which the mutual solubilities between solid and liquid elements are very low (<1–2 at.%) near the temperature at which embrittlement is observed. Furthermore, for polycrystalline materials, embrittlement was associated with penetration of liquid U along grain boundaries. Using a theoretical model by Miedema et al. [3.4], it follows that:

$$\gamma_{SL}^{AB} = (\gamma_{SL}^{I})_A + (\gamma_{SL}^{II})_B + \gamma_{SL}^{III} = 2.5\times10^{-9}\frac{\Delta H_f^A}{(V_m^{2/3})_A} + 0.52\times10^{-7}\frac{T}{(V_m^{2/3})_B} + 2.5\times10^{-9}\frac{\Delta H_{sol}^A}{(V_m^{2/3})_A}$$

where the grain-boundary energy, γ, for Ta, W, Nb, and V and the respective liquid-solid interfacial energies between these metals and liquid U can be calculated. These calculations predicted that:

- Grain-boundary energy is always larger than twice the liquid-solid interfacial energy for all of these metals.
- Grain-boundary penetration of liquid U would occur in all of the elements studied based on the model proposed by Smith [5].

Actual penetration, however, was observed only in Ta and W, not in Nb and V. This discrepancy is attributed partly to the fact that Smith's model, which is based on the minimization of total interfacial energy, cannot be applied to systems (such as Nb-U and V-U) in which solid and liquid have high mutual solubility. For such systems, the mixing between solid and liquid components occurs to such an extent that the minimization of volume free energy in the regions away from the interfaces would also have to be considered. Furthermore, the modification of grain-boundary and solid-liquid interface structures by extensive interdiffusion between liquid and solid elements in these systems could make the calculated grain boundary and interfacial energies inaccurate.

The tensile behavior of single-crystal Ta (4 mm diameter) in liquid U was also studied at a temperature of 1473 K with strain rates of 10^{-4} to 10^{-2} s^{-1}. The stress-strain behavior (Fig. PA-4) shows that embrittlement by liquid U did not occur. A metallographic analysis showed that liquid U did not penetrate the interior of the single crystals except near the surface of the sample where very fine grains had developed due to dynamic recrystallization during tensile testing.

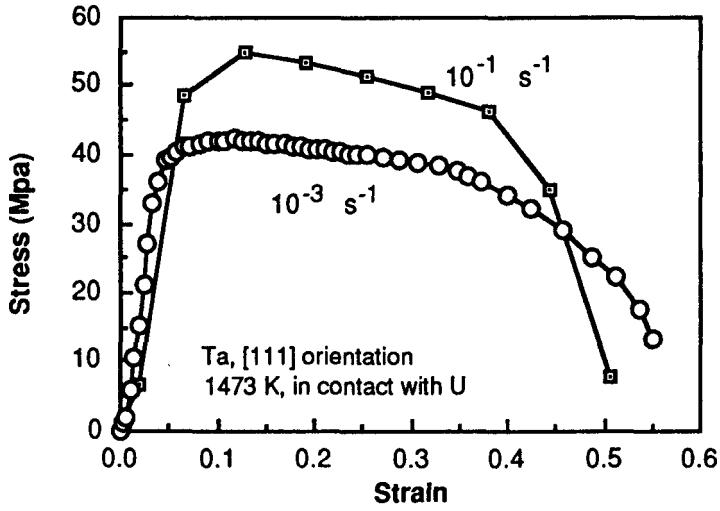

Fig. PA-4. Stress-strain behavior of single-crystal Ta wetted with liquid U, tensile-tested at 1473 K and two different strain rates.

We have also studied the tensile behavior of single crystals of W in liquid U. We conducted two tensile tests of W in the [111] orientation at 1473 K and displacement rates of 0.01 and 1 inch per minute, respectively. Because of an equipment malfunction, we obtained results only at the slower rate test. No embrittlement was observed and the sample necked-down to a sharp tip prior to failure. The results for the tests on single crystals of Ta and W strongly suggest that the embrittlement observed in polycrystals is mainly due to the ease of penetration of liquid U along grain boundaries. The classical LME mechanism, for which the reduction of ductility and strength is due to liquid atom adsorption and resulting surface energy reduction, apparently does not play a significant role in these metals under our tensile-testing conditions. However, a more detailed investigation of the longitudinal cross-sections of the single-crystal Ta and single-crystal W

indicated that many shallow microcracks are actually initiated along certain crystallographic planes of the samples. This evidence suggests that liquid U could actually be moved into the sample by dislocation motion and cause decohesion along the crystallographic planes, a phenomenon similar to that observed in classical LME.

In order to study the tensile behavior of different refractory metals and alloys in liquid Pu, we have been designing and constructing a tensile-testing facility in the Pu building. Most of our work is completed except for an induction power supply that is still being repaired by the vendor. We have prepared several tensile samples of Ta, W, V, Nb, and Cr for future testing. We also started to prepare castings of Pu slugs to fit into our crucibles for liquid-metal tensile testing.

References

1. G. F. Gallegos, "Plutonium and Actinides," in *Chemistry & Materials Science Research Report*, Lawrence Livermore National Laboratory, Livermore, Calif., UCID-20622-88-2 (1988), p. 35.
2. M. G. Adamson and P. H. Adler, "Actinide Thermochemistry," in *Chemistry and Materials Science Quarterly Research Report*, Lawrence Livermore National Laboratory, Livermore, Calif., UCID-20622-87-4 (1987), p. 109.
3. A. R. Miedema and F. J. A. den Broeder, *Z. Metallkd.* **70**, 14 (1979).
4. A. R. Miedema, F. R. de Boer, and R. Boom, *Calphad* **1**, 341 (1977).
5. C. S. Smith, *AIME Trans.* **175**, 15 (1948).

Publications and Presentations

Publications

T. G. Zocco, R. I. Sheldon, M. F. Stevens, and H. F. Rizzo, "Observations of Twinning in Alpha Pu by Transmission Electron Microscopy," *J. Nucl. Mater.*, in press.

H. F. Rizzo, T. B. Massalski, and A. W. Echeverria, "Formation of Metastable Structures and Amorphous Phases in Pu-based Systems using the Sputtering Technique," *Metall. Trans.* **20A**, 813 (1989).

O. H. Krikorian and D. Y. Lai, "Modeling of Heat Capacities of Metals," *J. Nucl. Mater.*, in press (UCRL-98496, 1989)

J. S. Huang and G. F. Gallegos, "Embrittlement by Liquid U in Some Group VB and VIB Metals and Alloys During Tensile Loading at 1473 K," submitted to *Metall. Trans. A* (UCRL-101141, 1989).

Presentations

O. H. Krikorian, "Modeling of heat capacities of metals," ASM Seventh International Symposium on the Thermodynamics of Nuclear Materials, Chicago, Ill., Sep. 26–29, 1989.

J. S. Furr, "Microstructures of arc-cast Pu_5Si_3-Mo, Pu_5Si_3-U, Pu_5Si_3-Cr, and W_5Si_3-Pu buttons" and "Microprobe analysis of the phases present in an arc-cast W_5Si_3 button," (posters) ASM International Metallographic Society Convention, Charlotte, N.C., Jul. 23–26, 1989. ***Received 2nd and 3rd place awards in metallography competition.***

J. S. Huang and G. F. Gallegos, "Tensile behavior of group VB and VIB refractory metals and alloys in liquid U: strain rate effects," Bay Area 26th High Temperature Science and Technology Symposium, Livermore, Calif., May 18, 1989.

HIGH-EXPLOSIVES TECHNOLOGY

J. H. Richardson *(Thrust Area Leader)*

Overview

Development and characterization of energetic materials require a detailed understanding of the hydrodynamics, thermodynamics, and kinetics governing the detonation and explosion regimes. Projects within the high-explosives technology thrust area focus on the following:

- Theoretical description of materials and reactions at high pressures and temperatures.
- Experimental characterization of detonation processes, intermediates, and products.
- Synthesis of new energetic materials.
- Application of synchrotron characterization techniques to determine defects in HE (high-explosive) crystals.

Beginning in FY90, the high-explosives technology WSR thrust area will be synergistically focused on understanding the fundamental issues that control insensitivity in HE. Theory and experiment will be blended in all the projects to yield information on the factors controlling insensitivity at the atomic, microscopic, and macroscopic levels.

Structure and Dynamics of Molecular Fluids Under High-Density Conditions

D. F. Calef *A. L. Nichols, III*

The purpose of this project is theoretical investigation of chemical dynamics under high-pressure conditions. This goal requires the study of both the intramolecular and intermolecular structures and dynamics of mixtures of molecular fluids, especially the role of the high-density dependence environment. Developing reliable, realistic models of mixtures is a prerequisite, as is developing efficient methods for using this information in modeling the dynamics.

The major areas of our effort during the second half of FY89 were developing the molecular-fluid-structure code to perform reaction-barrier calculations and developing methods for generating large-scale models of binary phase separations.

Our molecular-fluid-structure program, MOLECULES, has been improved and tested and is in use. The program solves a set of nonlinear integral equations for the correlations between molecules in a liquid state. This allows thermodynamic properties to be calculated from intermolecular potentials. The improvements include allowing a wider range of potentials and calculating the Helmholtz free energy. A paper describing the method is in preparation. The output from the program, a detailed structural description of a solvent at a given density and temperature, serves as input to a "mixture" code. This code has been completed, and example calculations are being performed.

In order to calculate the environmentally-induced changes in chemical reaction rates, the solvation structure around the molecule must be calculated; this is what the mixture code does. The program calculates the change in free energy along a reaction pathway, a preliminary example being shown in Fig. HE-1. The additional chemical potential multiplied by $\beta = 1/k_B T$ is plotted.

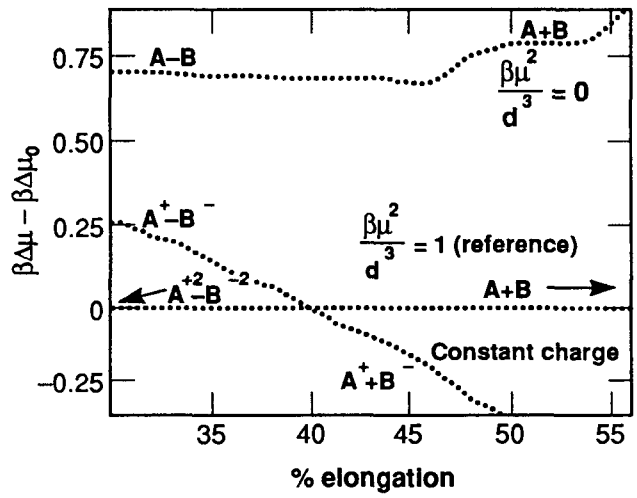

Fig. HE-1. Preliminary example of solvation structure around a molecule, relative chemical potential *vs.* bond length.

The "solvent" for the system shown in Fig. HE-1 corresponds to a linear triatomic with a permanent dipole moment. (For typical molecular scales, the temperature and pressure are approximately those occurring in detonations.) We then calculate the additional free energy it takes to symmetrically stretch another linear triatomic in this solvent. The reference system is a molecule stretching toward neutral fragments in such a way that the reduced dipole moment is constant (the reduced dipole moment is $\beta\mu^2/d^3$, where μ is the dipole moment and d is the diameter of a sphere having the same volume as the triatomic). The upper curve is a neutral molecule; the lower is a dipolar molecule stretching toward ionic fragments. Both curves illustrate the additional solvation given by the polar solvent. In a transition-state theory for the rate constant, the rate would depend exponentially on the chemical potential, so the apparently small effect is greatly magnified.

On a different note, considerable effort was spent developing methods for modeling the *dynamics* of phase separations. This has several applications. For example, in some detonation products, energy is derived from phase separation. The amount and rate of energy release depend on the diffusional formation of large "islands" of material. It is hard to investigate computationally because it would require large numbers of molecules for a straightforward molecular dynamics run. It is also hard to investigate using macroscopic approaches because the geometry of the separating phases can be a complicated random pattern. We are also interested in the structure of the interface between the two phases, which can be used to model foam structure.

The approach we have been developing is based on the discretization scheme of Puri and Oono. Space is modeled as a grid, with each point representing a finite-volume cell. A thermal chemical driving force drives each cell toward being rich in one phase or the other. The dynamics are handled with a discretized version of the diffusion equation. The relatively simple nature of this model allows us to generate reasonably large samples. Examples of this work are available in the LLNL Chemistry Department Annual Report. We are currently exploring three-dimensional versions of the model on a Cray.

High-Pressure-Reaction Chemistry

S. F. Rice

During the second half of FY89, no functioning laboratory was available in which to continue the diamond-anvil-cell experiments that had been so successful the preceding 12 months. The addition of M. F. Foltz to the research project as a postdoctoral research associate has been the most significant event. Foltz' efforts from 6/89–10/89 on computer modelling of high-pressure combustion-front propagation were the most concrete results obtained during this time period.

The data collected during 10/88–3/89 have been analyzed in greater detail. Specifically, results from high-pressure deflagrations on CD_3NO_2 have been shown to be distinctly different from those obtained for CH_3NO_2. Flame-front propagation rates up to 30.0 GPa for the deuterated species are about 50% slower than for ordinary nitromethane. This pronounced deuteration effect is representative of a kinetic isotope effect in the rate-limiting-reaction step in the overall high-pressure combustion of nitromethane. It also clearly demonstrates that the observed variation in the burn rates is due to the chemistry of the reacting material rather than to macroscopic changes in sample geometry as a function of pressure.

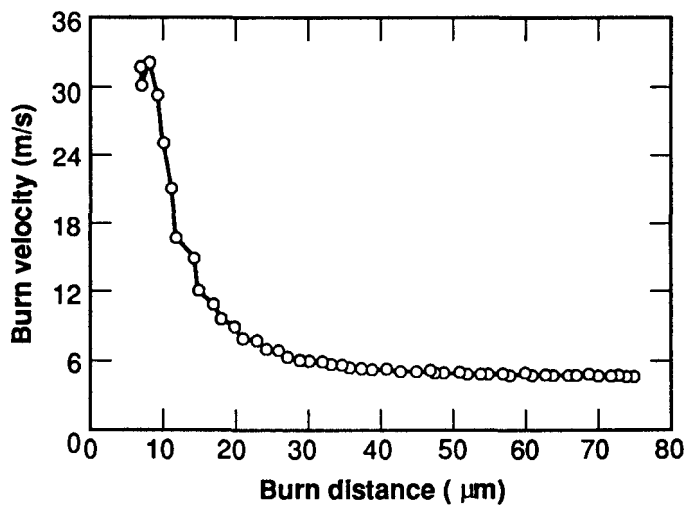

Fig. HE-2. Plot of the calculated wavefront velocity *vs.* distance from the 6-μm-diameter ignition point. The steady-state velocity is about 5.5 m/s. The higher velocity observed initially is due to a high assumed ignition temperature; however, steady state is achieved within 20 μm, a dimension that would be difficult to resolve in many of our experiments.

Figure HE-2 shows some of the results from the modelling effort using TOPAZCHEM, a modified version of a finite-element heat-flow code (TOPAZ) that provides for the presence of up to 40 chemical reactions (modifications done by A. Nichols). A high-velocity flame front is shown to be self-sustaining using a simple reaction scheme and Arrhenius kinetics. Other parameters, such as thermal diffusivities and heats of reaction, are taken from known ambient-condition values. The 5.5 m/s flame front shown in the figure is near the velocity that we measure for propagation of low-pressure (<1.0 GPa) fronts.

Figure HE-3 illustrates the fact that other properties of the flame, such as temperature, are also predicted by the model. We have shown that the steady-state flame temperature is independent of the ignition temperature but depends significantly on a number of parameters in the model. We are currently designing experiments to measure this flame temperature.

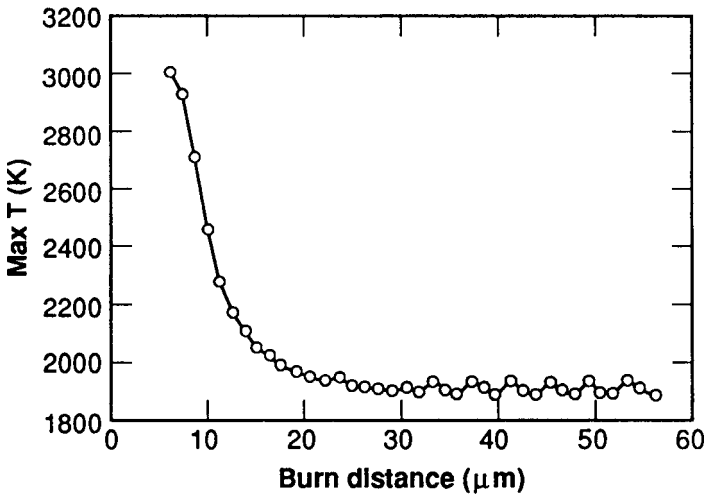

Fig. HE-3. Plot of the flame temperature as a function of distance from the ignition point. With coarse zoning at 1.0 μm, oscillation about the steady-state average of 1900 K occurs; however, reducing the zone size to 0.25 μm serves to smooth out the results.

Radiometric Observation of Detonation Products

R.L. Simpson

Thermodynamic codes used to calculate the states of reactive systems are based on assumed product species and an equation-of-state to describe the physical properties of the system. When applied to explosives, verification of these models is hindered by the extreme environment of detonation. Currently, only pressure-volume behaviors have been determined experimentally. This work attempted to establish the capability to determine the equations-of-state of explosives in a thermodynamically complete fashion. To accomplish this, radiometric techniques were used to examine shockloaded PETN and TNT at known pressure-volume states.

Five experiments were carried out on each of high explosives PETN and TNT. Figure HE-4 shows the experimental configuration used. A tungsten flyer impacts against an aluminum buffer plate at velocity V_{fl}. A shockwave transits the aluminum plate and releases into the explosive sample with a particle velocity that is higher than could be reached by a direct impact of tungsten. This method enables high pressures to be obtained. After the shock enters the sample, it begins to initiate the energetic material. By the time the shock reaches the copper barrier, it is a fully-developed detonation wave. This detonation wave then transits 2.5 mm of sample before impacting a LiF crystal. A fiber-optic radiometer measures the spectral radiance of the 2.5-mm-thick sample cavity. After the detonation wave reaches the LiF crystal, pressure is sustained by the impacting flyer. The actual pressures are calculated using the measured sabot velocity, the known Hugoniots of the inert materials, and the detonation products' PV equation-of-state.

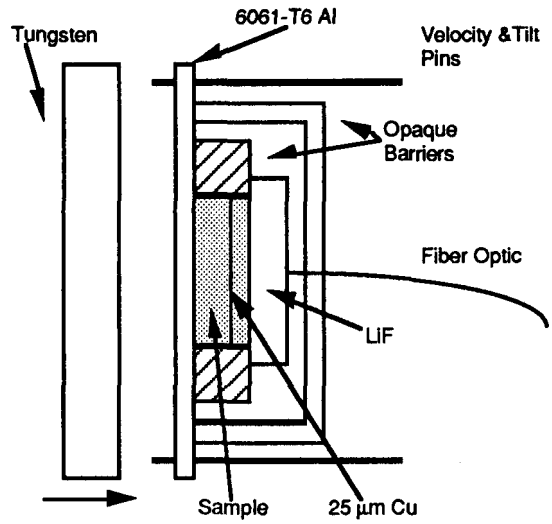

Fig. HE-4. Experimental configuration used for testing PETN and TNT.

With TNT, two experiments were carried out at overdriven detonation conditions: two near the Chapman-Jouguet (CJ) state, one significantly below the CJ pressure. Figure HE-5 shows a radiance trace (λ = 490 nm) at approximately the CJ state. Signal intensity

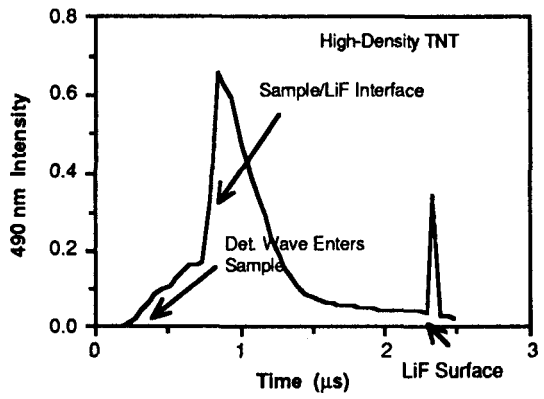

Fig. HE-5. Radiance trace (λ = 490 nm) at approximately the CJ state, for TNT.

gradually increases as the detonation front moves towards the detector. A shock is then reflected back into the sample, and there is a dramatic increase in the signal intensity due to increased pressure and (presumably) further reaction. Determination of temperature from the data is not completed at this time, although indications are that the temperature does not remain constant but increases slightly with time at a given PV state. This is indicative of further reaction (e.g., carbon condensation).

The five PETN experiments were intended to obtain temperature information at known PV states to help complete the equation-of-state information. In addition, two low-density shots were attempted to determine the initial density effects on the final temperature. These last two experiments failed because the sabot broke up at the 2.6 mm/μs velocity required. A 490-nm trace of PETN near the CJ state is shown in Fig. HE-6.

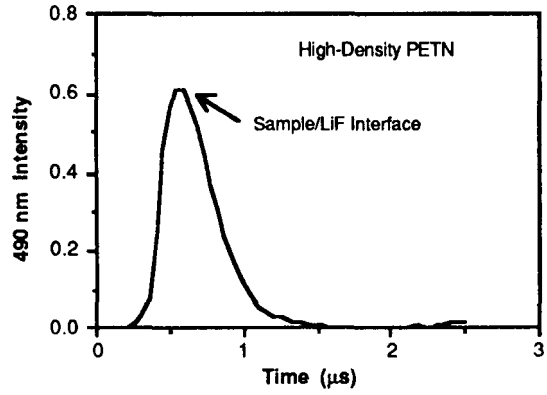

Fig. HE-6. A 490-nm trace of PETN near the CJ state.

The PETN traces are very different from the TNT traces. On reshock, there is not a significant increase in radiant emittance. This is a combination of two effects. First, the detonation products are a better impedance match to LiF. Second, the chemical reaction rates of PETN are much faster than those of TNT. PETN is the only explosive to date in which the reaction zone thickness has not been resolved due to instrument limitations. The time difference between the detonation front and the sonic plane is less than 5 ns, which is beyond the resolution of these radiometric experiments. In addition, PETN is nearly oxygen balanced and only produces trace amounts of condensed products. Hence, unlike the case for TNT, reactions after the sonic plane in PETN probably involve energies that are insignificant relative to the total energy release. Therefore the temperature would not vary in time, and this is what is observed.

Methods to determine the temperature of detonation products at known PV states were established successfully. Time dependent temperature behavior was also observed in the oxygen deficient explosive TNT. The technique should enable future equations of state of detonation products to be resolved in a thermodynamically complete fashion.

Enhanced Insensitivity Study of TATB and Its Analogues

P. F. Pagoria *C. L. Coon* *W. C. Tao*

The objective of this project was to study the sensitivity and physical characteristics of several hydrogen-bonded and deuterated HEs in an attempt to understand the "enhanced insensitivity" of TATB. Appropriate amounts (~50 grams) of the test compounds were synthesized for subsequent sensitivity and physical measurements.

The synthesis and recrystallization of at least 50 grams of picramide, styphnic acid, and trinitrophloroglucinol have been completed [1–6], as shown in Fig. HE-7. In addition, 125 grams of 1,3-diamino-2,4,6-trinitrobenzene (DATB), 1,3,5-triamino-2,4,6-trinitrobenzene (TATB), and Picric acid—denoted by (4), (5), and (6), respectively, in Fig. HE-8—have been obtained from Site 300. The synthesis of the deuterated HEs, ^{2}H-picramide, ^{2}H-DATB, and ^{2}H-TATB is essentially complete. Only their recrystallization remains to be done, at which time all the HEs will be submitted for pressing. The synthesis of the deuterated HEs all followed the same general procedure which involved the treatment of the corresponding chloronitrobenzene derivatives with a 5–10 fold excess of gaseous ND_3 at 10 psi at room temperature overnight. Filtration of the precipitated product and washing with toluene gave the crude product. On recrystallization, the material will be sent for analysis and mass spectroscopy to determine the extent of deuteration.

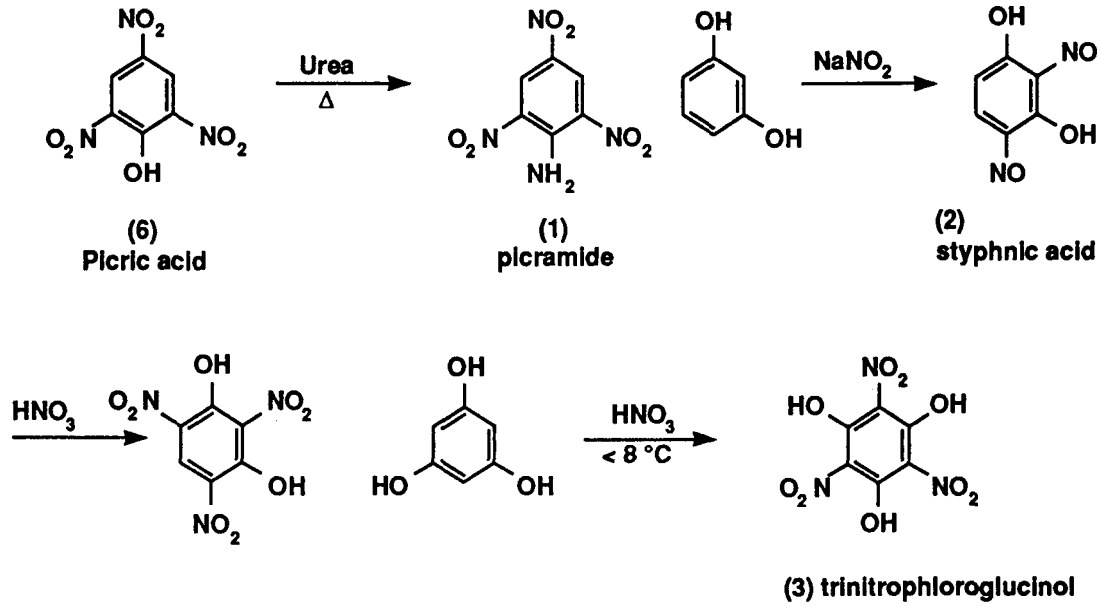

Fig. HE-7. Synthesis of picramide (1), styphnic acid (2), and trinitrophloroglucinol (3).

Each synthesized TATB analog compound will be formulated with ~2 wt% Viton, an inert binder, to facilitate pressing. Several pressing configurations, from individual small pellets to sabot targets, will be fabricated and shipped to Sandia-Albuquerque for dynamic experiments in collaboration with A. Renlund and W. Trott. The experiments consist of measuring the Raman emission from the explosive under shock initiation, with the stimulus

provided by a two-stage gas gun. Previous experiments at Sandia have shown that the pressure-induced shift of the Raman emission at a constant loading pressure are related to the degree of hydrogen-bonding around the chemical bond being examined. It is anticipated that this work will result in two publications after the testing is complete. In addition, some of the synthetic work on the deuterated materials may be publishable.

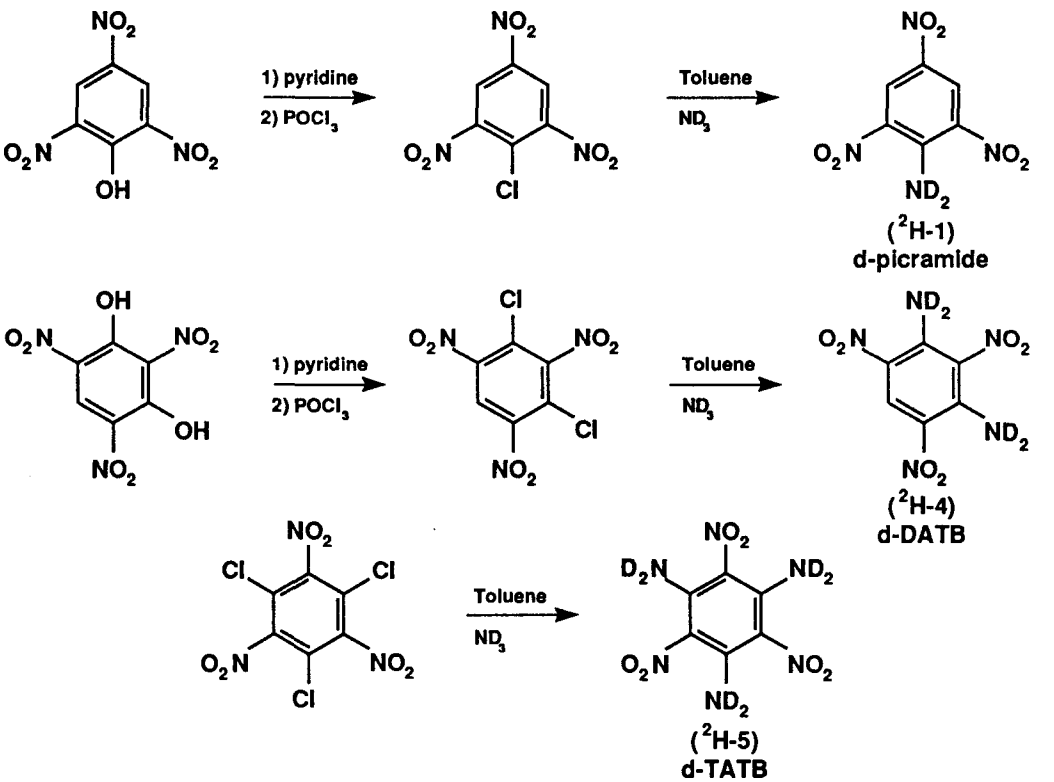

Fig. HE-8. Synthesis of ^{2}H-picramide (^{2}H-1), ^{2}H-DATB (^{2}H-4), and ^{2}H-TATB (^{2}H-5).

Characterization of Solid-State Microstructures in High Explosives by Synchrotron X-ray Tomography

W. C. Tao *J. H. Kinney*

It has been suggested that the microstructural discontinuities in energetic materials serve as sites for local hydrodynamic heating, resulting in the formation of "hot spots." Also, that the rates of coalescence, dissipation, and propagation of these thermal sites are the primary factors determining the initiation sensitivity of condensed energetic formulations. Recent work in this field [7–10] centered on the investigation of shock deformation of large PETN and mechanical deformation of ammonium perchlorate crystals. Their results indicate, on a global scale, that failure modes in the crystal originate along the slip planes and microcracks within the crystal. The objectives of this research are to characterize nondestructively the type and distribution of microstructural defects in HE single crystals and composite formulations and to examine their respective influences on hot-spot generation and propagation.

Since demonstrating the feasibility of using 3D microtomography to study pore distributions in materials having x-ray absorption coefficients similar to those for HEs (polystyrene spheres, coal), we have successfully applied the non-invasive techniques to characterize the detailed microstructures in HMX single crystals and a composite formulation consisting of fuel (RDX, NG/TA), oxidizer ($NaNO_3$), and metallic additives (aluminum). Because of cancellation of two dedicated runs at SSRL, we performed the experiments using a conventional x-ray source coupled with the analytical software and data-acquisition hardware developed for 3D microtomography. Although the exposure time is lengthened and spatial resolution is decreased slightly, we were able to resolve the topographical features of the HMX single crystal illustrated in Fig. HE-9 and the tomographical structure at a depth equal to 25% of the crystal thickness. The inability to probe the bulk of the HMX crystal for microstructural defects is due to beam hardening and penumbral blurring, both inherent technical inefficiencies in a conventional polychromatic x-ray source. With an intense source of monochromatic and a tunable x-ray beam, such as that from a synchrotron facility, we will be able to image the bulk crystal.

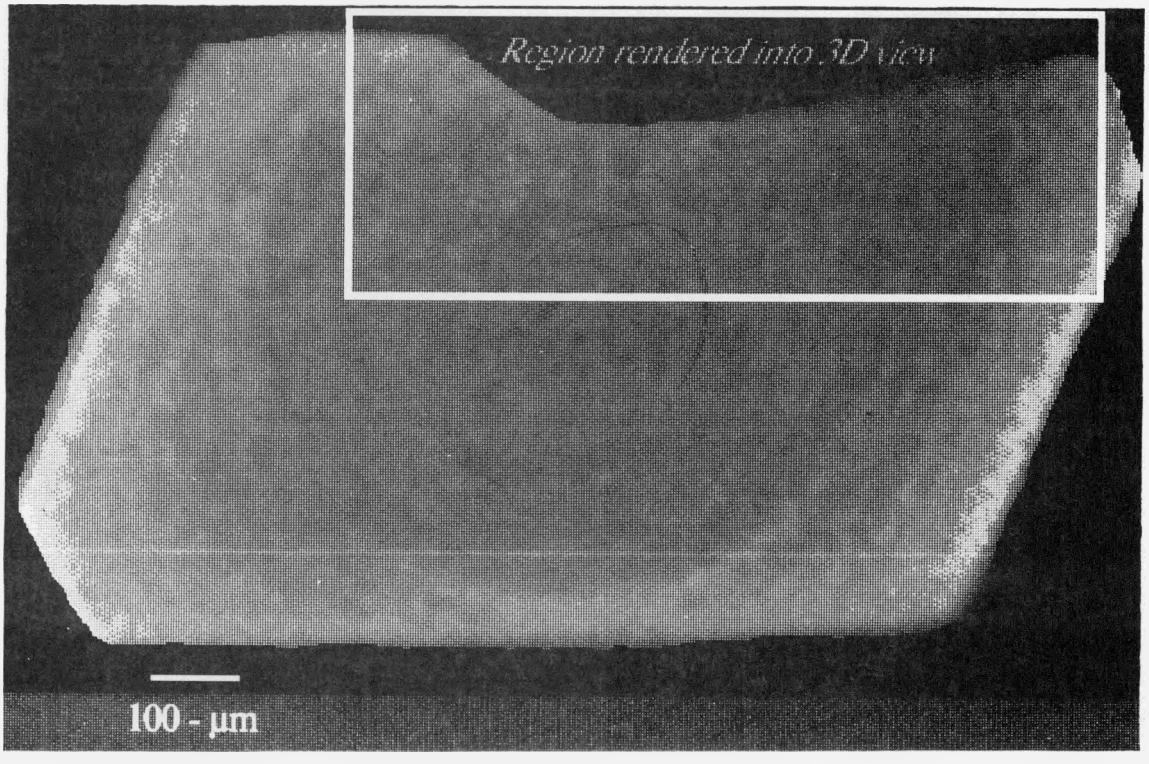

Fig. HE-9. XTM image of single-crystal HMX.

The composite formulation examined was supposedly non-porous, with the 5-μm aluminum dispersed evenly throughout the matrix. From our results, we found that the aluminum was not dispersed below a 50-μm scale and the composition had approximately 5% porosity (Fig. HE-10). This provided insights into the degree of mixing and wetting between components in the composite formulation as related to the formulation methodology. To further test our experimental capability, we designed a phantom matrix using the x-ray absorption coefficients for HMX with a complex integration of defect

structures (pores, aluminum, orthogonal microcracks, density gradients), then subjected this phantom for 3D tomography analysis. Using a well characterized synchrotron beam profile and the radiometric deconvolution techniques of our analytical software, we were able to reproduce the image of the phantom with minimal loss in structural resolution. These results were presented at the 9th Detonation Symposium at Portland, Oregon.

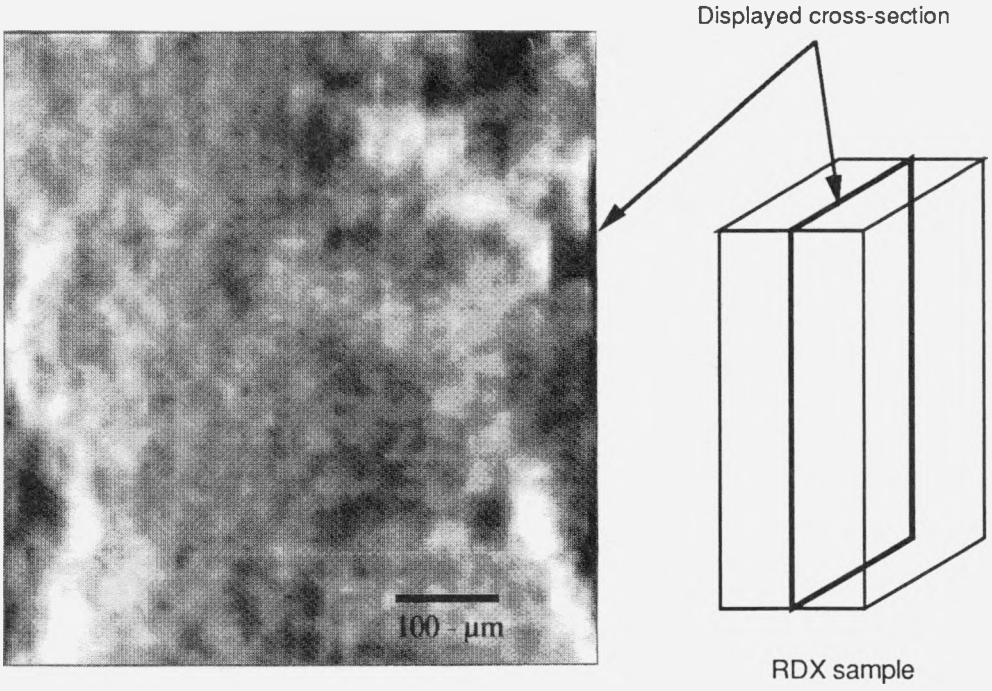

Cross-section of RDX composite showing inhomogeneous distribution of Al particles as well as some noticeable porosity

Fig. HE-10. XTM image of composite RDX.

The next research phase involves studying the correlation between microstructural defects and initiation sensitivity. Two experimental methods will be employed in this phase of the study: microphotography and infrared-emission mapping. Coupled with both streak and frame cameras, ultrafast microphotography allows us to examine a single crystal under shockloading with spatial and temporal resolution of 1 µm and 1 ns, respectively. Measuring the infrared emission *vs.* time yields information on the mechanism of hot-spot formation and dissipation. Using the laser microphotography facility in cooperation with A. Frank from B Division, we have been able to observe the passage of a shockwave, generated by a microslapper against the surface of the crystal, through the defect-mapped region. This microslapper, with a barrel diameter of ~400 µm, can deliver a 50- to 100-µm-thick Mylar flyer at velocities of 2 mm/µs. The optical emission from the collapse of the voids within the defect region as the stress wave passes is measured under cross polarizer. These results are to be presented in the SPIE Conference at San Diego in July 1990.

References

1. E. Y. Spencer and G. F. Wright, "Preparation of Picramide," *Can. J. Res.* **24B**, 204 (1946).
2. B. A. Bydal, "2,4,6-Trinitroresorcinol," *Org. Prep. Proceed. Int.* **5**, 271 (1973).
3. A. A. DeFusco, A. T. Nielsen, and R. L. Atkins, *Org. Prep. Proceed. Int.* **14**, 393 (1982).
4. G. P. Sharnin, B. I. Buzykin, V. V. Nurgatin, and I. E. Moisak, *Zh. Org. Khim.* **3**, 82 (1967).
5. M. Warman and V. J. Siele, *J. Org. Chem.* **26**, 2998 (1961).
6. R. N. Rogers, Los Alamos National Laboratory, Los Alamos, N. M., private communication.
7. M. E. Kipp and R. E. Setchell, "A Shock Initiation Model for Fine-Grained HNS," in *Proceedings* of the 9th International Detonation Symposium, Portland, Ore., Aug. 28–Sep. 1, 1989.
8. H. Moulard, "Particular Aspect of the Explosive Particle Size Effect on Shock Sensitivity of Cast PBX Formulations," in *Proceedings* of the 9th International Detonation Symposium, Portland, Ore., Aug. 28–Sep. 1, 1989.
9. J. E. Field, M. A. Parry, S. J. P. Palmer, and J. M. Huntley, "Deformation and Explosive Properties of HMX Powders and Polymer Bonded Explosives," in *Proceedings* of the 9th International Detonation Symposium, Portland, Ore., Aug. 28–Sep. 1, 1989.
10. W. L. Elban and R. W. Armstrong, "Microhardness Study of RDX to Assess Localized Deformation and its Role in Hot Spot Formation," in *Proceedings* of the 7th International Detonation Symposium, Md., Jun. 16, 1981.

Publications and Presentations

Publications

D. Calef, F. Ree, M. VanThiel, and D. Hamilton, "High-Pressure High-Temperature Phase Changes in Chemically Reactive Mixtures," *High Pressure Sci. Technol.*, 115 (1989).

C. L. Coon, "Synthesis of Dense Energetic Materials," Lawrence Livermore National Laboratory, Livermore, Calif., ONR Annual Progress Report (1989).

C. L. Coon, "Problems of Waste Disposal in Organic Synthesis Laboratories," Oak Ridge National Laboratory, Oak Ridge, Tenn., Report of the Toxic Materials Advisory Committee (1989).

C. L. Coon and E. G. Stewart, "A New Synthesis of 2-Alkylthio-1,3,5-triazines," *J. Syn.* (1989).

C. L. Coon, A. T. Nielsen, R. A. Nissan, D. J. Vanderah, R. D. Gilardi, C. F. George, and J. Flippen-Anderson, "Polyazapolycyclics by Condensation of Aldehydes with Amines. 2. Formation of 2,4,6,8,10,10-Hexabenzyl-2,4,6,8,10,12-hexaazatetracyclo-[5.5.0.05,9.03,11]dodecanes from Blyoxal and Benzylamines1,2," *J. Org. Chem.* (1989).

C. L. Coon, "The Synthesis of Nitrocyanamides," *J. Syn.* (1989).

S. F. Rice, "Single-Pulse, Broad-Band CARS of Nitromethane within a Diamond Anvil Cell.," *J. Phys. Chem.* **93**, 536 (1989).

S. F. Rice, "The A'^2d State of ScO: Analysis of the $A'^2d(v=3) \sim A\ 2p(v=1)$ Perturbation.," *J. Mol. Spectrosc.* **133**, 22 (1989).

R. L. Simpson et al., *High-Performance, Extrusion-Cast Explosives with Low Sensitivity; Interim Report No.2*, Lawrence Livermore National Laboratory, Livermore, Calif., UCRL-53890 (1989).
R. L. Simpson, "Shock-Initiation Studies on Heterogeneous Explosives," in *Combustion & Detonation Phenomena* (ICT, Karlsruhe, 1989).
E. L. Simpson, *The Equation of State of Perfluorododecane to 48 GPa*, Lawrence Livermore National Laboratory, Livermore, Calif., UCID-21710 (1989).
R. L. Simpson, *Model Calculations for the Response of HMX Porous Beds to Deflagration and Shock*, Lawrence Livermore National Laboratory, Livermore, Calif., UCRL-101680 (1989).
W. C. Tao and C. W. Frank, "Energy Migration in Polymeric Blends and Solutions," in *Lasers in Polymer Science and Technology: Applications, Volume I*, J. P. Fouassier and J. F. Rabek, Eds. (CRC Press Inc., Boca Raton, 1989).
W. C. Tao and C. W. Frank, "Excimer Fluorescence as a Molecular Probe of Polymer Blend Miscibility. 9. Effect of Guest Concentration and Annealing in Blends of poly(2-vinylnaphthalene) with poly(cyclohexyl methacrylate)," *Macromolecules*, in press.

Presentations

D. F. Calef and J. D. Bauer, "Electronic state of shock-dissociated molecular fluids," submitted for American Physical Society meeting, Anaheim, Calif., Mar. 1990.
A. L. Nichols and D. F. Calef, "The effect of molecular solvation on bond breaking," submitted for American Physical Society meeting, Anaheim, Calif., Mar. 1990.
S. F. Rice, "Absorption spectroscopy of shocked benzene," 9th Symposium (International) on Detonation, Portland, Ore., Aug. 28–Sep. 1, 1989.
R. L. Simpson, "Reactive-flow measurements and model development for composite explosives," 9th Symposium (International) on Detonation, Portland, Ore., Aug. 28–Sep. 1, 1989.
R. L. Simpson, "Particle size effects in the initiation of explosives containing reactive and non-reactive continuous phases," 9th Symposium (International) on Detonation, Portland, Ore., Aug. 28–Sep. 1, 1989.
W. C. Tao, A. M. Frank, J. E. Shepherd, and R. E. Clements, "The fundamentals of metal combustion in composite explosives revealed by high-speed microphotography," 9th (International) Symposium on Detonation, Portland, Ore., Aug. 28–Sep. 1, 1989.
W. C. Tao and J. H. Kinney, "Characterization of defect microstructures in high explosives using x-ray tomographic microscopy," 9th (International) Symposium on Detonation, Portland, Ore., Aug. 28–Sep. 1, 1989.

INTERFACES, ADHESION, AND BONDING

W. E. King *(Thrust Area Leader)*

Overview

Internal interfaces, like grain boundaries or bimaterial interfaces, play a critical role in performance of materials systems. In conventional materials, the service lifetime of a component may be limited by phenomena such as stress corrosion cracking or cavitation and fracture at interfaces or at a weld or diffusion bond. In next-generation materials such as composites and multilayers, the desired properties of the materials originate at the interfaces engineered into the structure. To address the issues associated with interface science, the interfaces, adhesion, and bonding thrust area treats the four key elements of interface science: *synthesis and processing, structure and composition, properties, and performance.*

The detailed understanding and control of synthesis and processing parameters are critical to the successful production of materials and components to meet design requirements. In the area of synthesis and processing of interfaces, we are probing the fundamental aspects of interface formation using an ultrahigh-vacuum diffusion-bonding machine. In addition to allowing for the fabrication of ideal interfaces, the machine can produce interfaces that simulate those that may be formed in processing environments (i.e., interfaces with impurities, flaws, and inclusions). Atomic and electronic structure and elemental composition of interfaces are being investigated to develop a fundamental understanding of the influence of atomic and electronic structures on the forces that are responsible for bonding of metallic grain boundaries and metal/nonmetal couples. Further, we are investigating the effects of atomic structure, interface chemistry, and interface morphology on macroscopically observable quantities such as deformation, damage accumulation, fracture resistance, and bond strength. In order to predict performance of interfaces, we couple atomistic theory with computational mechanics. Results of these predictions will be validated by experiment.

This report describes the technical activities and progress of the interfaces, adhesion, and bonding thrust area during the period 4/1/89–9/30/89. We describe recent results on the effect of atomic relaxations on the density of electronic states at twist and tilt grain boundaries in Cu. We also describe experimental results on the $\Sigma 5(310)$ symmetric-tilt boundary in Nb.

Electronic-Structure Calculations of Grain Boundaries in Cu

A. Gonis *E. Sowa* *S. Foiles*[*]

We have developed a first-principles method, the real-space multiple-scattering theory (RSMST), for calculating the electronic structure of systems with extended defects such as

[*] Sandia National Laboratories–Livermore.

surfaces and interfaces [1,2]. Motivated by the desire to gain insight into bonding mechanisms at metallic interfaces, we have applied it to selected grain boundaries in Cu [3]. These calculations help bridge the gap between existing *ab initio* electronic-structure methods and calculations based on empirical interatomic potentials, such as the embedded-atom method (EAM).

The RSMST provides an exact treatment of the Schrödinger equation for semi-infinite (surfaces) and doubly semi-infinite (interfaces, grain boundaries) systems within the Born-Oppenheimer approximation and the local-density approximation to density-functional theory. The new approach treats properly the boundary conditions of such systems. Bloch's theorem, which requires translational invariance, is the basis of most current first-principles electronic-structure methods. In order to use these methods to treat a surface or interface where translational invariance is broken, it is necessary to approximate the properties of an isolated interface by those of a set of periodically-repeating slabs of finite thickness. This is only possible for interfaces with special symmetry properties; even then, one must ensure that the slabs are thick enough to avoid interactions between interfaces. The RSMST avoids these problems by replacing full translational invariance with the concept of semi-infinite periodicity and by replacing Bloch's theorem with the more general principle of removal invariance. This allows one to solve the Schrödinger equation in real space, takes advantage of the remaining symmetry of an interface system, and allows the study of complex systems, including grain boundaries, that have impurities and bimaterial interfaces.

The current implementation of the RSMST solves for the electronic structure of a system with fixed atomic positions and fixed electronic potentials. The effects of EAM-predicted relaxations on the electronic structure at $\Sigma 5$ twist and tilt grain boundaries in Cu have been determined with this code. This work is described below. Recently, we made improvements in the implementation of removal invariance, which will allow us to treat these grain boundaries with smaller clusters. This reduces both memory and CPU time requirements and has enabled us to begin extending the real-space computer code to include charge self-consistency and total-energy capabilities. In the meantime, a hybrid code that is applicable to systems with coherent interfaces has been developed. It uses periodic boundary conditions parallel to the interface and removal invariance perpendicular to the interface and is fully self-consistent.

In the calculations reported here, we used the self-consistent potentials for bulk Cu given by Moruzzi, Janak, and Williams (MJW). The atomic coordinates of the unrelaxed grain boundaries are easily found through an appropriate twisting or tilting of one half of the underlying lattice. We used unpublished EAM calculations of Foiles to obtain the atomic coordinates of relaxed twist and tilt grain boundaries in Cu. The results for the tilt boundary were reported previously [4].

Figure IA-1 displays the local electronic density-of-states (DOS) corresponding to a coincidence site (a site common to the lattices on both sides of an interface) at both an unrelaxed and a relaxed $\Sigma 5(100)$ 36.9°-twist grain boundaries in Cu. The bulk Cu DOS, calculated with the RSMST, is also displayed for comparison. (This bulk DOS reproduces the main features of the MJW calculation; small differences may be attributed to our use of

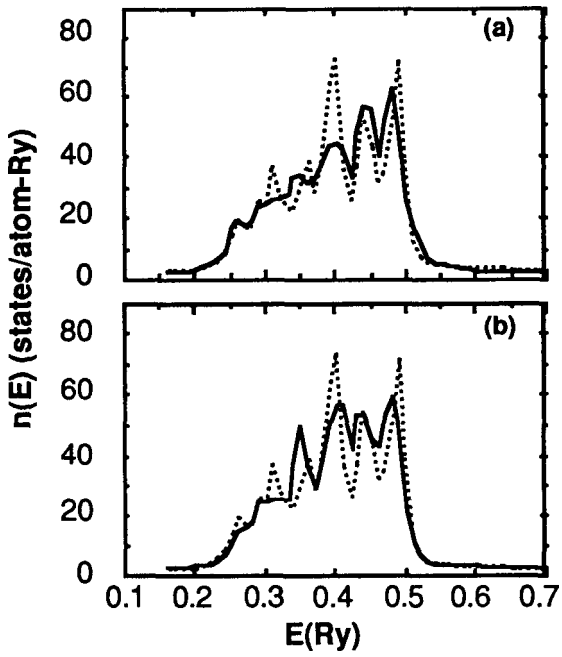

Fig. IA-1. DOS calculated at a coincidence lattice site of a Σ5-twist grain boundary in Cu.

a coarser energy grid and a small imaginary component of the energy.) The DOS of the unrelaxed grain boundary exhibits considerable smearing of structure compared to the bulk DOS because of the loss of periodicity and the associated destruction of the Van Hove singularities. The grain-boundary DOS is slightly broader than that of the bulk material due to the decreased distance between some of the Cu atoms across the interface. (In fact, simply twisting one half of the crystal with respect to the other results in some of the atoms overlapping across the boundary).

Both the atomistic and electronic characteristics change noticeably in the case of the relaxed grain boundary. The EAM calculations indicate that the interplanar spacing increases by about 20% across the interface from its bulk value, decreases by 2% in the next set of layers, and remains essentially unchanged in layers deeper inside the material. The increase is the result of relieving the overlap conditions across the interface mentioned above, and its effects on the electronic structure are similar to those associated with decreased coordination. In these first calculations, we included only the 20% expansion at the boundary layer, which is the dominant effect. It is seen that the DOS at the grain boundary is indeed narrower than that of bulk Cu. It is also seen that the relaxed-grain-boundary DOS is shifted slightly toward lower energies (compared with that of bulk Cu and that of the unrelaxed configuration) and that it possesses somewhat sharper structure than the DOS at an unrelaxed grain boundary. Although the present, non-charge-self-consistent calculation cannot provide reliable information about the relative energies of the various configurations, both of these effects are consistent with the lower energy of the EAM-relaxed configuration with respect to the unrelaxed one.

Σ5(310) Tilt Grain Boundary in Nb

W. E. King *A. Coombs* *S. Fadeff*
*B. Gibbesch** *G. Smith* *A. Connor*

We have established the capability for routine fabrication of well-oriented, flat single crystals. These crystals are intended to be diffusion bonded to form bicrystals. We report on the fabrication of two bicrystals. The interfaces were Σ5(310)-tilt grain boundaries. This interface was selected based on a recent EAM investigation in V. The grain-boundary energy *vs.* orientation curve for symmetric-tilt grain boundaries was calculated. The tilt axis was <100>. The result is shown in Fig. IA-2a. The boundary that was selected for investigation exhibited a cusp in the energy *vs.* tilt angle curve. The Σ5(310)-tilt grain boundary in the bcc structure is shown in Fig. IA-2b. The boundary is a symmetric pure-tilt boundary. It is equivalent to a 180°-twist boundary on the (310) plane.

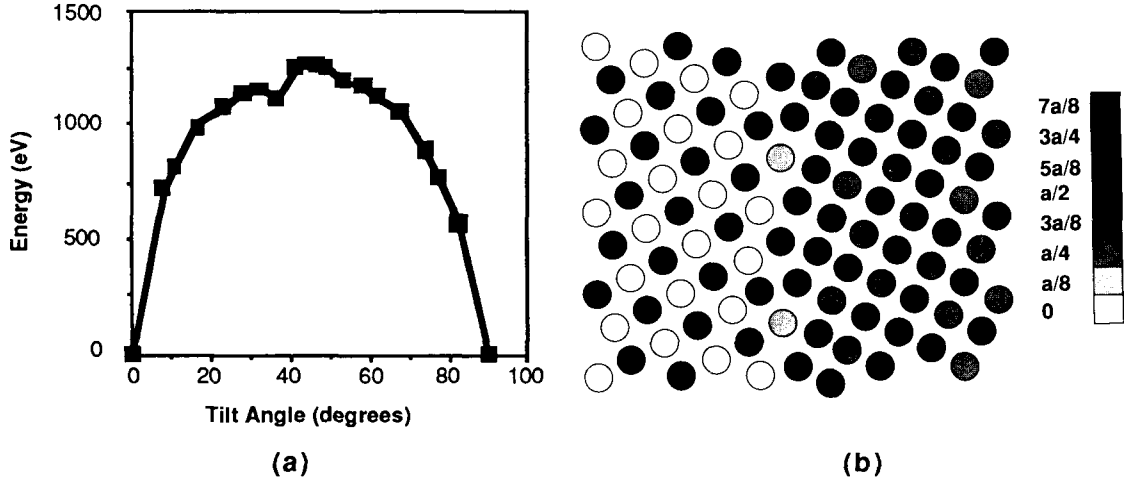

Fig. IA-2. (a) Energy *vs.* orientation curve for <100> symmetric-tilt grain boundaries calculated using an EAM potential for V. (b) The relaxed, lowest-energy structure of the Σ5(310)-tilt grain boundary deduced by Foiles using an EAM potential for V.

The Experiment

Two Nb single-crystal boules were obtained from the Materials Processing Center at Ames National Laboratory. These crystals were prepared from high-purity Nb rod using the arc-zone refining method. Since no seed crystal is used, this method yields randomly-oriented single crystals. In this case, however, the resultant single-crystal bars both had their long axis within 2° of <310>.

The single-crystal boules were oriented to within 1° of <310> using Laue back-reflection XRD patterns. The oriented rods were cut into 3-mm-thick slabs using electro-discharge machining. Each slab was mounted on a special goniometer and polished to remove surface damage. The direction of the surface normal of the slab was measured using Laue back-reflection XRD patterns. The sample was tilted so the <310> direction

* MPI.

was parallel to the x-ray beam. The specimen was repolished so the surface normal was then parallel to <310>. The direction of the surface normal was checked using Laue patterns, and the tilt/polish procedure was repeated until the sample surface normal was parallel to <310> to within 0.2°.

An example of the <310> Laue pattern is shown in Fig. IA-3a. The samples were then removed from the goniometer, inverted, and mounted on a parallel polisher. The exposed surface was ground and polished until the surface normal was parallel to <-3-10>. The flatness of the sample, measured using a surface profilometer, is illustrated in Fig. IA-3b. The variation in the surface profile is ±200 nm over a 5-mm region in the center of the sample. We expect to make major improvements in surface flatness, particularly near the edge of the sample.

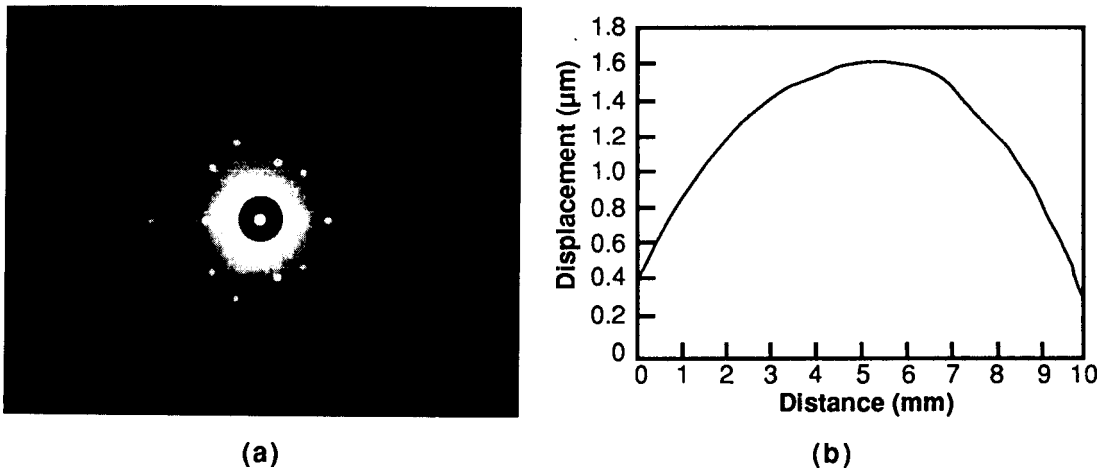

Fig. IA-3. (a) Laue pattern from (310) surface of single crystal. (b) Surface profilometer trace across polished sample.

The samples were demounted and cleaned. At this point, it was necessary to establish and indicate the relative orientation of the two crystals about <310> such that the <001> directions of the crystals were antiparallel. This was accomplished by attaching each crystal to a single-rotation goniometer with the surface normal of the sample parallel to the rotation axis. In this way, only the twist orientation of the crystals about their surface normals was adjustable. The goniometers were then mounted opposing one another on the x-ray track with the x-ray beam perpendicular to <310>, and the Laue back-reflection method was used to set the twist orientation of each sample independently by successively driving each crystal into the x-ray beam. One sample was set with <001> parallel to the x-ray beam and the other with <00-1> parallel to the x-ray beam.

Laue patterns are shown in Fig. IA-4. After the desired orientation was established, the crystals were driven together and fastened with a solvent-soluble epoxy. On removal of the bicrystal, an optical flat was polished along the outer edge, parallel to the twist axis of the bicrystal. This optical flat was used for alignment of the samples in the ultrahigh-vacuum diffusion-bonding machine. The epoxy was then dissolved from the crystals, and the crystals were cleaned before being introduced into the UHV diffusion-bonding machine

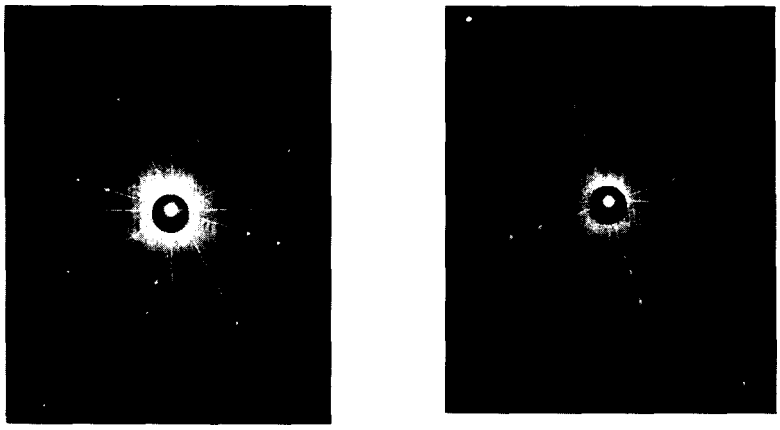

Fig. IA-4. Laue patterns from the aligned single crystals showing the symmetric tilt of the grain boundary, taken parallel to the tilt axis prior to bonding.

at the Max Planck Institut in Stuttgart, West Germany. Samples were sputtered using 4×10^{18} cm^{-2}, 5-kV Ar^{+} ions. The sputtering-time evolution of the Auger electron spectra (AES) from the samples is shown in Figs. IA-5a and IA-5b. After each sample was cleaned, it was transported to the bonding chamber.

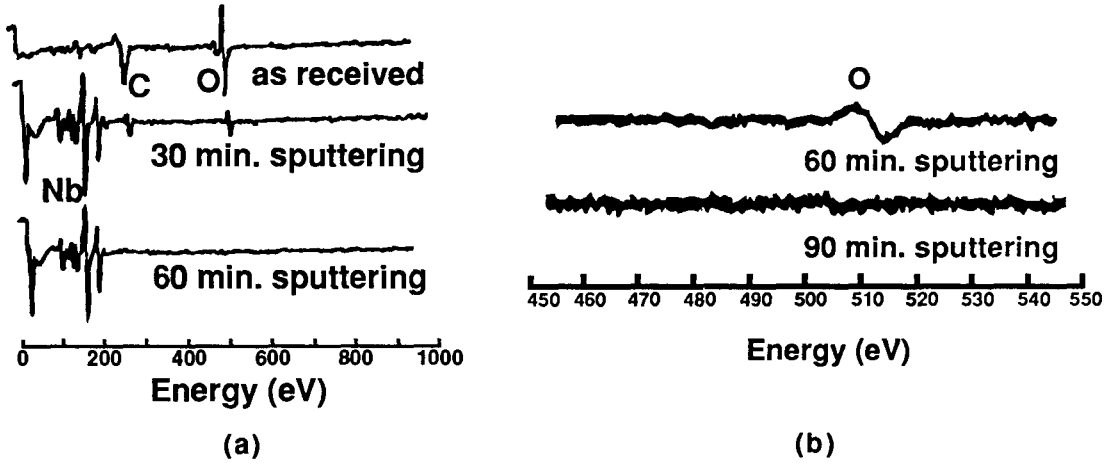

Fig. IA-5. (a) AES spectra as a function of sputtering time. (b) AES scan taken with higher sensitivity showing the elimination of the O peak.

Two alumina blanks and the Nb samples were stacked on an alumina anvil that is part of the crystal-bonding press. The precision crystal-orientation device surrounded the sample stack. The fingers of the precision crystal-orientation device were rotatable, which facilitated setting of the twist orientation of the samples. This was accomplished using a laser-beam reflection off the optical flats that had been polished onto the sides of the samples in the final stages of preparation. At this point, a second alumina anvil was brought to rest on top of the stack, and the fingers were withdrawn. A static load was

added to the stack using a novel hydraulic system. The entire sample stack was then raised into an RF heating coil with Mo susceptor. The temperature of the sample was raised to 1500 °C over a 1-hour period. A 100-kg load was added, and the temperature and pressure were held for 2 hours. After annealing, the furnace was cooled for 3 hours and the sample was removed from the bonding machine.

Optical Observations of Bonded Samples

Two views of the as-bonded sample are shown in Fig. IA-6. The sample is composed of two polycrystalline alumina blocks on either end, sandwiching two Nb single crystals. The comparison between the straight-edge and the sample shows that the sample was not under uniaxial compression during bonding. The alumina blocks were observed to have a gray deposit on the surfaces that were parallel to the axis of compression.

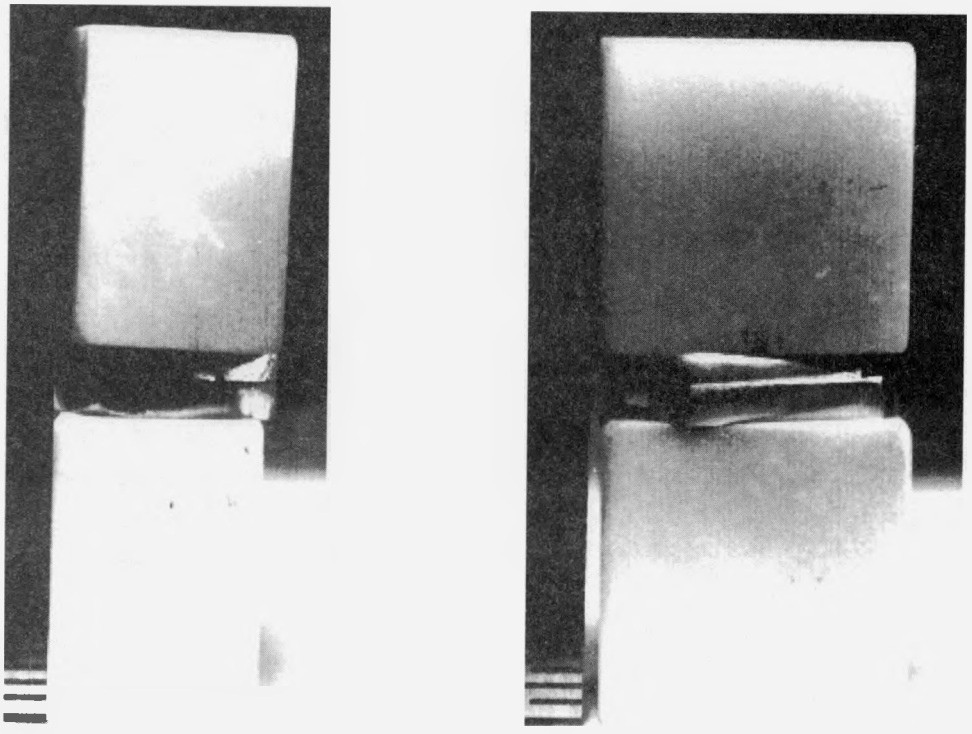

Fig. IA-6. Two views of an as-bonded sample showing the extent of deformation that occurred during the bonding process. Each mark on the scales at left is 1/32 inch.

XPS Investigation of Deposit

The gray deposit on the alumina was first surveyed using XPS (x-ray photoelectron spectroscopy) to determine what elements were present on the surface. Higher-resolution scans of the individual elements were then taken to determine concentrations and oxidation states. Eight elements were found on the surface of the alumina: carbon, oxygen, sodium, aluminum, calcium, copper, molybdenum, and chlorine. Two species of molybdenum were present. Twenty percent of the molybdenum peak was present as metal with a

binding energy of 227.7 eV. The remaining 80% was oxidized and had a binding energy of 232.0 eV; however, the exact species was not identified.

Conclusions

We attribute the black appearance of the polycrystalline alumina to the presence of Mo. More significant deposits of the black material can be observed on the anvil in the bonding machine. The susceptor of the RF furnace is made from Mo. We believe that, during the bonding process, the polycrystalline alumina outgasses oxygen that can oxidize the susceptor. Such oxides of Mo are volatile and can redeposit on the sample. The deformation of the sample can be due to two cause: improper sample geometry and non-uniaxial compression during bonding. If the sample geometry is not correct, the sample stack can become tilted and introduce an additional tilt in the interface. If the plungers of the bonding machine are unstable, it is possible that the compression is not uniaxial. These phenomena will be investigated further to determine the cause of the deformation.

References

1. X.–G. Zhang, A. Gonis, and J. M. MacLaren, *Phys. Rev. B.* **40**, 3694 (1989).
2. X.–G. Zhang and A. Gonis, *Phys. Rev. Lett.* **62**, 1161 (1989).
3. E. C. Sowa, A. Gonis, X. –G. Zhang, and S. M. Foiles, *Phys. Rev. B, Rapid Communications*, in press.
4. W. E. King, "Interfaces, Adhesion, and Bonding," in *Chemistry & Materials Science Research Report, First Half FY89*, Lawrence Livermore National Laboratory, Livermore, Calif., UCID-20622-89-1 (1989), p. 24.

Publications and Presentations

Publications

S. A. Bradley, W. E. King, and C. W. Allen, Eds., "Surfaces and Interfaces," in *Ultramicroscopy*, Proceedings of the Second Conference on Frontiers of Electron Microscopy in Materials Science, Vol. 29, (North-Holland, Amsterdam, 1989).

A. Dominguez-Rodriguez, A. R. De Arellano-Lopez, K. C. Goretta, W. E. King, J.-H. Park, and J. L. Routbort, "Creep of Cr_2O_3 and Yttrium-Doped Cr_2O_3," *Mater. Sci. Technol.* **5**, 499 (1989).

M. C. Kim, M. J. McNallan, C. C. Cheng, and W. E. King, "The Effects of Crystallization on the Microhardness of *Fe-22.5Al-10Zr* Metallic Ribbons," *J. Mater. Sci. Lett.* **8**, 793 (1989).

W. E. King, Ed., *Fifty Years of the Reactive Element Effect*, Vol. 39 (Trans Tech Publications, Aedermann, 1989).

W. E. King, *UHV Bonding*, Lawrence Livermore National Laboratory, Livermore, Calif., UCID-21494-89-1 (1989).

W. E. King, "Interfaces, Adhesion, and Bonding," in *Chemistry & Materials Science Research Report, First Half FY89*, Lawrence Livermore National Laboratory, Livermore, Calif., UCID-20622-89-1 (1989).

G. L. Nutt, W. Lai, K. E. Froeschner, and W. E. King, "Direct Measurement of Interface Bond Strength," *Scripta Metall.*, in press.

X.–G. Zhang, E. C. Sowa, and A. Gonis, "A First-Principles Method for the Determination of the Electronic Structure of Grain Boundaries," *Scripta Metall.*, in press.

X.–G. Zhang, A. Gonis, and J. MacLaren, "Real-Space Multiple-Scattering Theory and the Electronic Structure of Systems with Full or Reduced Symmetry," *Phys. Rev. B*, in press.

X.–G. Zhang and A. Gonis, "A New Real-Space Multiple-Scattering Theory Method for the Determination of Electronic Structure," *Phys. Rev. Lett.* **62**, 1161 (1989).

Presentations

W. E. King, "Use of shock waves to assess the bond strength at metal/ceramic interfaces," Max Planck Institut für Metallforschung, Institut für Werkstoffwissenschaft, Stuttgart, West Germany, Sep. 13, 1989.

E. C. Sowa, "Electronic structure calculations at metal grain boundaries," Max Planck Institut für Metallforschung, Institut für Werkstoffwissenschaft, Stuttgart, West Germany, Sep. 12, 1989.

M. E. Kassner, R. S. Rosen, G. A. Henshall, and W. E. King, "Delayed failure of silver-aided diffusion welds between steel," 2nd International Conference on Brazing, High Temperature Brazing, and Diffusion Welding, Essen, West Germany, 1989.

W. E. King and J. H.Park, "The effect of impurity segregation on grain boundary diffusion in Cr_2O_3," Session 2: *Dynamical Properties* of the International Congress on Intergranular and Interphase Boundaries in Materials: IIB89, Ecole des Mines des Paris, Paris, France, Sep. 4–8, 1989,

W. E. King, "Effect of impurities, flaws, and inclusions on adhesion and bonding at internal interfaces," Sandia National Laboratories–Livermore, Livermore, Calif., 1989.

G. L. Nutt, W. Lai, K. E. Froeschner, and W. E. King, "Direct measurement of the bond strength of metal/ceramic interfaces," Session 3: *Heterophase Interfaces* of the International Congress on Intergranular and Interphase Boundaries in Materials: IIB89, Ecole des Mines des Paris, France, Sep. 4–8, 1989,

G. L. Nutt, W. Lai, and K. E. Froschner, "Use of shock-waves to assess the adhesion of metal/ceramic interfaces," 1989 spring meeting of the Materials Research Society, San Diego, Calif., 1989.

G. Nutt, W. Lai, and K. E. Froschner, "Influence of plasticity in adhesive bond strength measurements," Materials Research Society, Boston, Mass., Nov. 27–Dec. 2, 1989,

G. Nutt, W. Lai, K. Froeschner, and W. E. King, "Measurement of the bond strength at metal/ceramic interfaces," Materials Research Society, San Diego, Calif., 1989.

R. S. Rosen, M. E. Kassner, G. A. Henshall, and W. E. King, "Delayed failure of silver-aided diffusion welds between steel," 1989 TMS Fall Meeting, Indianapolis, Ind., Oct. 2–5, 1989,

E. C. Sowa, A. Gonis, and X.–G. Zhang, "First-principles calculations of the electronic structure of grain boundaries," International Congress on Intergranular and Interphase Boundaries in Materials: IIB89, Ecole des Mines de Paris, Paris, France, Sep. 4–8, 1989,

E. C. Sowa, A. Gonis, and X.–G. Zhang, "First-principles calculations of the electronic structure of grain boundaries," 49th Annual Physical Electronics Conference, Seattle, Wash., Jun. 26–28, 1989,

E. C. Sowa, A. Gonis, X.-G. Zhang, and S. M. Foiles, "The electronic structure of $\Sigma 5$ grain boundaries in Cu," Materials Research Society, Boston, Mass., Nov. 27–Dec. 2, 1989.

HIGH-TRANSITION-TEMPERATURE SUPERCONDUCTIVITY*

M. Fluss (*Thrust Area Leader*)

Background

A program to study high-transition-temperature superconducting oxides is under way. The main focus of the activities in the high-T_c program has been on phenomena related to the basic understanding of superconductivity. These efforts are guided by a wide-ranging theoretical effort in band theory, ligand field theory, and basic considerations of the superconducting pairing mechanism. Our present experimental tasks consist of electronic-structure measurements, materials synthesis and physical properties, and thin-film production. The continuing discovery of new high-T_c superconducting systems and the accompanying body of data and calculations have provided guideposts for the direction of future work. However, there are significant open questions in both the technology and the physical properties of these materials. The source of the superconducting mechanism has not yet been confirmed, and the methods for making useful varieties of these materials are still in development.

Electronic Structure

R. H. Howell
J. Tobin
R. West[**]
Z. Z. Wang[††]
A. Wachs
P. Turchi
J. Kaiser[**]
F. Solal
P. Sterne
J. Jean[†]

A detailed understanding of the electronic structure of high-T_c oxides is a necessary part of both determining the source of the superconducting interaction and defining the directions for the discovery of new materials and processing techniques. Our experimental effort to determine the electronic structure uses a combination of positron-annihilation analysis and photoemission using both laboratory and synchrotron photon sources.

LLNL is a leader in positron-annihilation analysis, and all established experimental tools are available for use in the high-T_c program. These measurements are a standard source of electron momentum and electron-density distribution data. We have completed a collaborative experiment with West and Kaiser and with Wang [1]. In this experiment, exceptionally high-quality single crystals of $YBa_2Cu_3O_{7-y}$ were measured in the annihilation-radiation angular-correlation (ACAR) technique providing electron-momentum distribution data.

We have obtained the highest quality data available to date on the $YBa_2Cu_3O_{7-y}$ system with counts an order of magnitude higher than those in other published data. The objective

---

* This report summarizes technical progress achieved under both WSR and IR&D support during the second half of FY89.

** University of Texas at Arlington.
† University of Missouri.
†† Princeton University.

of these experiments is to identify the features of the electronic structure of the material, with particular emphasis on the shape of the Fermi surface; highly accurate statistics are a necessary requirement. We have identified several features that are unambiguously related to the crystalline structure of the sample in all methods of data analysis, including differentiation of the data as collected. These same features can be reproduced by a calculation of the ACAR spectrum that contains no electrons in the Fermi sea. These calculations were performed at LLNL in an atomic-orbital, molecular-orbital formalism. The results of calculations performed in this formalism have been well tested in previous studies of NiO- and $La_{1.85}Sr_{0.15}CuO_4$-insulating systems, in which it was found to reproduce all of the identifiable features. We conclude that the features identified in our data are derived from the covalent bonds between the Cu(d) and O(p) orbitals and that a measurement with a higher statistical accuracy will be necessary to allow confirmed identification of features related to the Fermi surface.

We have completed an upgrade of our apparatus to obtain higher counting rates and have begun experiments on a new series of samples. We have synthesized samples of untwinned $YBa_2Cu_3O_{7-y}$ and are obtaining premeasurement values for transport and crystalline properties [2]. Measurement of these samples will allow the first unique identification of electronic-structure features identified with the CuO planes and those of the chains. The initial data from these measurements are expected early in 1990. A second series of measurements has begun on high-quality samples of $La_{1.85}Sr_{0.15}CuO_4$ obtained from Dr. K. Kitazawa of the University of Tokyo. Due to the relative simplicity of the La-based system, these measurements offer the best chance of relating the details of the measured electronic structure with complete calculations of the system.

Synchrotron x-ray induced photoemission is a new activity at LLNL. Photoemission data have produced strong indications of a distinct Fermi edge in the electron-energy distributions. Using angle-resolved detection of the photoelectrons and light from the Alladin storage ring at the University of Wisconsin, we have completed initial experiments to measure the core and valence-band features from samples of untwinned $YBa_2Cu_3O_{7-y}$ crystals. We were unable to identify directionally-dependent features of the bands near the Fermi surface in these preliminary data; however, improved data to be taken later this year should show these features if they exist. Based on published data, we can also expect to directly observe the relationship of the superconducting gap and the crystal symmetry.

The source of changes in the lifetime of positrons in samples cooled below the superconducting transition remains unidentified. Initial measurements on the $YBa_2Cu_3O_{7-y}$ system have shown strong sample dependence, but some systematics were suggested in the original data [3]. We have completed a series of coordinated measurements on Zn-doped $YBa_2Cu_3O_{7-y}$ materials in collaboration with Jean [4]. The results of this study suggest that the sample dependence of measurements in the $YBa_2Cu_3O_{7-y}$ system is due to small amounts of sample contamination. In other measurements performed at LLNL and Missouri on negative-charge carrier systems ($Nd_{1.85}Ce_{0.15}CuO_4$ and $Ba_{0.6}K_{0.4}BiO_3$), we found no change in the positron lifetime. These results are consistent with a model based on pairing of the positive-charge carriers proposed to explain the observed data.

Theory

P. E. A. Turchi *P. Sterne* *A. McMahan*
B. Grant

The overall theoretical efforts at LLNL cover a broad scope. Besides new suggestions about the form of the superconducting state, problems in calculating the details of the electronic levels and internal electric fields have been solved by several techniques. Also, the phase stability of the oxide systems has been studied and several detailed connections between specific calculations and experimental data have been made.

Special techniques must be developed to perform electronic-structure calculations due to the strong correlation and dispersion effects found in high-T_c oxides. These materials exhibit both itinerant electron dispersion and localized electron correlations. Our strategy to reduce the number of configurations required to properly treat the full problem is to reduce the number of degrees of freedom to an extended Hubbard model. Our model contains only the crucial Cu(3d) and O(2p) states obtainable from simpler Hubbard and t-J models. Approximate solutions of these models are beginning to link high-T_c superconductivity to quantum spin-liquid states.

To test these techniques, we have compared the results of our calculations for La_2CuO_4 (which can be doped to become a high-T_c superconductor) and three isostructural compounds (La_2NiO_4, K_2CuF_4 and K_2NiF_4) [5]. We have now obtained results for all of these systems, which (by comparison) are validating our extended Hubbard model. The details of the symmetry and other properties of the calculated states can be compared to point out features that may correlate with superconductivity (e.g., only La_2CuO_4 has a spin 1/2, antiferromagnetic, x^2-y^2 symmetric-spin system).

We have made a first-principles calculation of the phase diagram for $YBa_2Cu_3O_{7-y}$ that is in excellent agreement with experiment. With these calculations, we can address questions about the stability of the oxygen in the $YBa_2Cu_3O_{7-y}$ system and crystallographic phase change from tetragonal to orthorhombic controlled by the oxygen content [6]. This is an important question since oxygen content is strongly correlated with superconductivity in $YBa_2Cu_3O_{7-y}$. The calculations were performed in an Ising model using pair interactions obtained from a parameterization of several density-functional theory calculations on systems with specific, ordered oxygen content. The phase is then obtained by minimizing the total energy of the oxygen interactions.

In these calculations, we have predicted both the correct oxygen-temperature profile for the orthorhombic-to-tetragonal phase transition and the double-cell phase having every other oxygen chain missing.

There are large changes in the positron lifetime values in samples cooled below T_c [3]. To better understand the systematics surrounding lifetime values, we have integrated lifetime calculations into our *ab initio* band-structure programs based on a linear muffin-tin orbital (LMTO) potential. Effects of polarization induced by the positron charge are included from electron gas calculations, and the positron spatial distribution is part of our calculated result. We have tested our method by calculating metallic lifetimes and found very good agreement.

We are now using our LMTO-derived lifetime calculation to calculate the $B_{1-x}K_xBO_3$ system for several K concentrations. The results of these calculations are being compared to measured lifetimes at similar concentrations of K to help understand the measured lifetime variations.

Materials Synthesis and Measurements

H. Radousky *R. Glass* *M. Costantino*
P. Hahn *J. O'Brien* *K. McCarty*[*]
R. Shelton[**] *J.Z. Liu*[**] *J.L. Peng*[**]

We are preparing superconducting-oxide materials for physical studies including high-quality single crystals and special polycrystalline samples. Untwinned crystals of $YBa_2Cu_3O_{7-y}$ have been prepared for electronic-structure and transport studies. Elemental substitutions in high-T_c materials have been introduced to induce changes in physical properties to identify properties related to the high-T_c mechanism. These experiments, being performed at Davis, have focused on four systems that have specific and unusual features: $Y_{1-x}Pr_xBa_2Cu_3O_7$, $YBa_2Cu_3O_{6.2}Br_y$, $Nd_{2-x}Ce_xCuO_{4-y}$, and $Ba_{1-x}K_xBiO_3$. The Y-Pr substitution is of interest because Pr is the only rare-earth substitution that destroys superconductivity. The Nd-Ce and Ba-K systems both have properties that are significantly different from those of the original high-T_c systems; the Br substitution offers both a new way to study the hole doping and a new, technologically-important, low-temperature processing technique.

There is general agreement that part of the function of the oxygen in $YBa_2Cu_3O_{7-y}$ superconductors is to dope holes onto particular CuO planes where the superconductivity occurs. We have successfully substituted Br in oxygen-deficient $YBa_2Cu_3O_{7-y}$ and obtained a superconductor with $T_c = 90$ K [7]. Since the Br diffusion is four orders of magnitude faster than that of oxygen, the bromination process can be carried out at low temperatures (260 °C) and times of a few minutes. We have performed initial studies of the properties of the resulting compound to determine the crystal structure, microscopic phase purity, thermal stability, oxygen content, and superconducting transport properties (Fig. S-1).

We have determined that an amount of Br roughly equal to the oxygen deficit is uniformly distributed in the material we produce, with some formation of second-phase Br-rich regions after saturation intake of Br into the primary material. The Br is much more stable to heating than is the oxygen remaining in the material after oxygen has been released. Reitveld analysis of x-ray data shows little modification of the crystal parameters by the introduction of Br but fails to identify a lattice site for the Br, suggesting that the Br is in some interstitial position. These data suggest that the Br is displacing some oxygen atoms from lattice sites but that the bromine uptake is a diffusion-limited process.

Since bromine uptake at low temperatures is controlled by the temperature dependence of the diffusion rate, it is possible to extend the exposure time and lower the temperature in

[*] Sandia, Livermore.
[**] University of California, Davis.

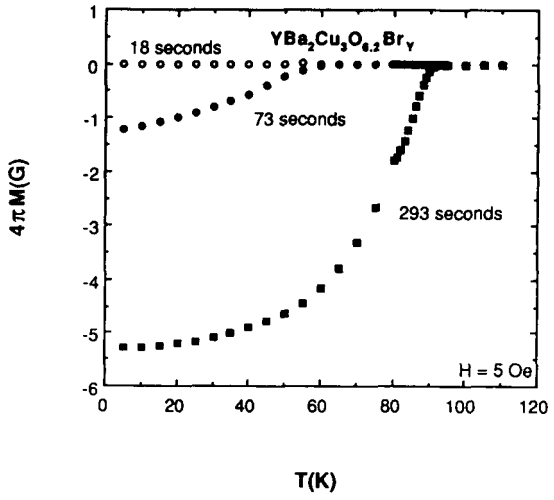

Fig. S-1. Magnetization data for several Br concentrations, achieved by exposures of 0.3, 1.2, and 4.9 minutes at 260 °C. Further bromination does not increase the zero-field-cooled fraction. Applied field was 5 Oe.

the process. We have achieved 90-K superconductors with 15-minute exposure at 200 °C. At this processing temperature, it is possible for the first time to consider integrating high-T_c materials into conventional electronics-processing applications.

As-grown single crystals of $YBa_2Cu_3O_{7-y}$ always have a heavily twinned structure that provides a serious complication in most experiments. We have made untwinned single crystals from twinned stock by uniaxial compression. We have used these crystals in initial transport measurements and have initiated studies of their electronic structure through use of photoemission, positron annihilation and Raman spectroscopy.

Preliminary measurements of DC magnetization and magnetically-determined critical current have been performed [2]. In these measurements, we found that the Meissner fraction was increased for every direction of the untwinned samples and that there was no obvious asymmetry between the a- and b-axis directions. We also measured the remanent magnetization in a strong (1.5-T) magnetic field. From these data and a simple model (the Bean model), critical currents can be estimated in the untwinned crystals. If the twin boundaries dominate as pinning sites, there would be a significant drop in the critical-current value in the untwinned samples compared to similar twinned crystals. Our data indicate that the critical current, as determined from magnetic data, is minimally changed by the detwinning process. This strongly suggests that the twin sites are not the dominant flux-pinning centers in these samples.

In our continuing work, investigations of the $Nd_{2-x}Ce_xCuO_4$ and $Ba_{1-x}K_xBiO_3$ materials have continued with high-quality samples of both materials routinely available for experiments. In the Nd-Ce system, we have found that the normal-state resistivity of $Ce_{0.15}$ compounds increases as ln(T) up to 400 K [8]. This dependence is typical of the Kondo effect, in which charge carriers scatter from magnetic ions. In the $Ba_{1-x}K_xBiO_3$ system, we have measured Raman spectra in collaboration with Sandia. We have found evidence of coupling between high-frequency optical phonons and the electronic states in

superconducting $Ba_{0.6}K_{0.4}BiO_3$ (T_c = 24 K) but not in non-superconducting $Ba_{0.8}K_{0.2}BiO_3$.

We have continued our work in the Y-Pr substitution system. It is a test ground for studying interactions between the substitute and the superconducting carriers. We believe, based on our previous measurements of the critical magnetic fields and initial oxidation-state data, that the Pr introduces pair breaking through magnetic interactions. There is now substantial evidence that the Pr is in a 3+ oxidation state from x-ray absorption and photoemission. These data are consistent with resistivity measurements in the normal state, in which no change to the insulating states was seen when the Pr concentration was increased and superconductivity was destroyed.

If the addition of Pr was modifying the hole distribution, then adding oxygen might reverse this process. Extra oxygen can donate additional holes to the CuO planes to compensate for the presence of any Pr^{+4}. We have found that increasing the oxygen content of the samples to 7.1±0.04 did not restore the T_c of the Pr-doped samples. These are new data in support of our belief that Pr introduces pair breaking through magnetic interactions.

Thin-Film Production

M. Balooch *F. Mitlitsky* *F. Magnotta*
T. Barbee *B. Olsen* *R. Russo**

Thin-film samples of high-T_c superconductors have great value as experimental samples and as the source material for the development of superconducting devices. Experiments on the properties of superconducting junction, tunneling, and flux pinning are often best performed on thin-film samples with high critical currents. Also thin films of high-T_c superconductors deposited on flexible substrates are a leading candidate for early production of superconducting wire.

We are routinely producing high-quality thin films at LLNL in collaboration with Lawrence Berkeley Laboratory. Films of $YBa_2Cu_3O_{7-y}$ with good superconducting properties are produced using laser ablation. A single $YBa_2Cu_3O_{7-y}$ target is illuminated by a 1-mJ/pulse KrF excimer laser. Ablated material is deposited in a narrow spot onto substrates of MgO. The process is performed in a partial oxygen atmosphere. The parameters required to produce superconducting films have been identified, but problems of non-uniform film thickness and cluster formation remain. We are currently studying the details of the ablative process at the source to gain farther understanding of these issues.

To use thin films in experiments and to eventually build devices from them, it is necessary to be able to deposit them on a variety of substrates and to form necessary patterns for the path of the superconducting circuit. This is especially required in electronic-device production. We have recently been successful in drawing μm-scale circuit paths using laser-pantography techniques. Laser-etching techniques have many applications in the processing of conventional semiconductor-based electronics and may be

* Lawrence Berkeley Laboratory.

particularly valuable in superconductor-device processing due to the high packing density available with superconductor circuits.

References

1. H. Haghighi, J. H. Kaiser, S. Rayner, R. N. West, Al. L. Wachs, R. H. Howell, P. E. A. Turchi, M. J. Fluss, Y. C. Jean, and Z. Z. Wang, "A Positron Study of the Electronic Structure of $YBa_2Cu_3O_{7-\delta}$," *J. Phys.: Condensed Matter*, in press.
2. J.Z. Liu, M.D. Lan, P. Klavins and R.N. Shelton, "Meissner Effect and Magnetic Critical Current Density in Detwinned $YBa_2Cu_3O_{7-x}$ Single Crystals," submitted to *Phys. Rev. Lett.*
3. Y. C. Jean, J. Kyle, H. Nakanishi, P. E. A. Turchi, R. H. Howell, A. L. Wachs, M. J. Fluss, R. L. Meng, H. P. Hor, J. Z. Huang, and C. W. Chu, "Evidence for a Common High Temperature Superconducting Mechanism in $La_{1.85}Sr_{0.15}CuO_4$ and $YBa_2Cu_3O_7$, *Phys. Rev. Lett.* **60**, 1069 (1988).
4. Y. C. Jean, C. S. Sundar, a. Bharathi, J. Kyle, H. Nakanishi, P. K. Tseng, P. H. Hor, R. L. Meng, Z. J. Huang, C. W. Chu, Z. Z. Wang, P. E. A. Turchi, R. H. Howell, A. L. Wachs, and M. J. Fluss, "Local Charge Density Change and Superconductivity: A Positron Study," submitted to *Phys. Rev. Lett.*
5. J. F. Annett, R. M. Martin, A. K. McMahan, and S. Satpathy, "The Electronic Hamiltonian and Antiferromagnetic Interactions in La_2CuO_4," *Phys. Rev. B* **40**, 2620, (1989)
6. P. A. Sterne and L. T. Wille, "Oxygen Vacancy Ordering in $YBa_2Cu_3O_{7-y}$," presented at International M^2S-HTSC, Stanford, Calif. (1989).
7. H. B. Radousky, R. S. Glass, P. A. Hahn, M. J. Fluss, R. G. Meisenheimer, B. P. Bonner, C. I. Merzbacher, E. M. Larson, K. D. McKeegan, J. C. O'Brien, J. L. Peng, R. N. Shelton, and K. F. McCarty, "Metallization and Superconducting Properties of $YBa_2Cu_3O_{6.2}Br_y$," submitted to *Phys. Rev. B.*
8. J. L. Peng, R. N. Shelton, and H. B. Radousky, "Preparation and Magnetic Scattering in $Nd_{2-x}Ce_xCuO_{4-d}$," *Solid State Commun.*, in press.

WEAPONS-SUPPORTING RESEARCH

Individual Projects

ENZYME MIMICS FOR METHANE CONVERSION

M. Droege

Overview

The purpose of this research is the development of new catalyst materials to facilitate reactions that convert methane to liquid fuels. The general rationale and the background for the biomimetic approach were presented in the progress report for the first half of FY89.

Experimental Progress

Summary of Research Progress for the First Half of FY89

Our research goals during the first half of FY89 were to develop the synthetic methodology needed to build potential biomimetic complexes and to demonstrate the feasibility of this overall approach, at least from the synthetic chemistry aspect. We have been successful in preparing low-molecular-weight complexes in which a metal of interest (Fe, Cu, etc.) is coordinated to atoms or molecules that may resemble components of the enzyme. To do this, we prepared symmetrical chelating structures that bind two metal ions in a fashion thought to be similar to that found in the native enzyme. The organic structures have been characterized by ^{1}H and ^{13}C NMR spectroscopy, IR spectroscopy, and elemental analysis. Metal-containing complexes of Co, Cu, and Fe have been synthesized and isolated as crystalline complexes using the chelating structures with benzimidazole coordinating groups. These complexes were synthesized by stoichiometric reactions in methanol using hydrated metal salts with either ClO_4^- or BF_4^- counterions. The colored metal-containing complexes are formed rapidly and are isolated by vapor diffusion using diethyl ether. The complexes have been characterized by IR spectroscopy and elemental analysis. Additional characterization studies including single-crystal x-rays are planned.

Research Progress for the Last Half of FY89

For the remainder of the fiscal year, our work has focused on the synthesis of more elaborate unsymmetrical structures. These ligands are important since they force reaction at one metal site (as the enzyme does) in contrast to the symmetrical ligands described above. This is in keeping with a closer structural analogy between the native enzyme site and a potential biomimetic complex. We have relied on much of the synthetic methodology we developed during the first half of FY89. The initial synthetic route to a new ligand is summarized in the illustration at the top of the next page:

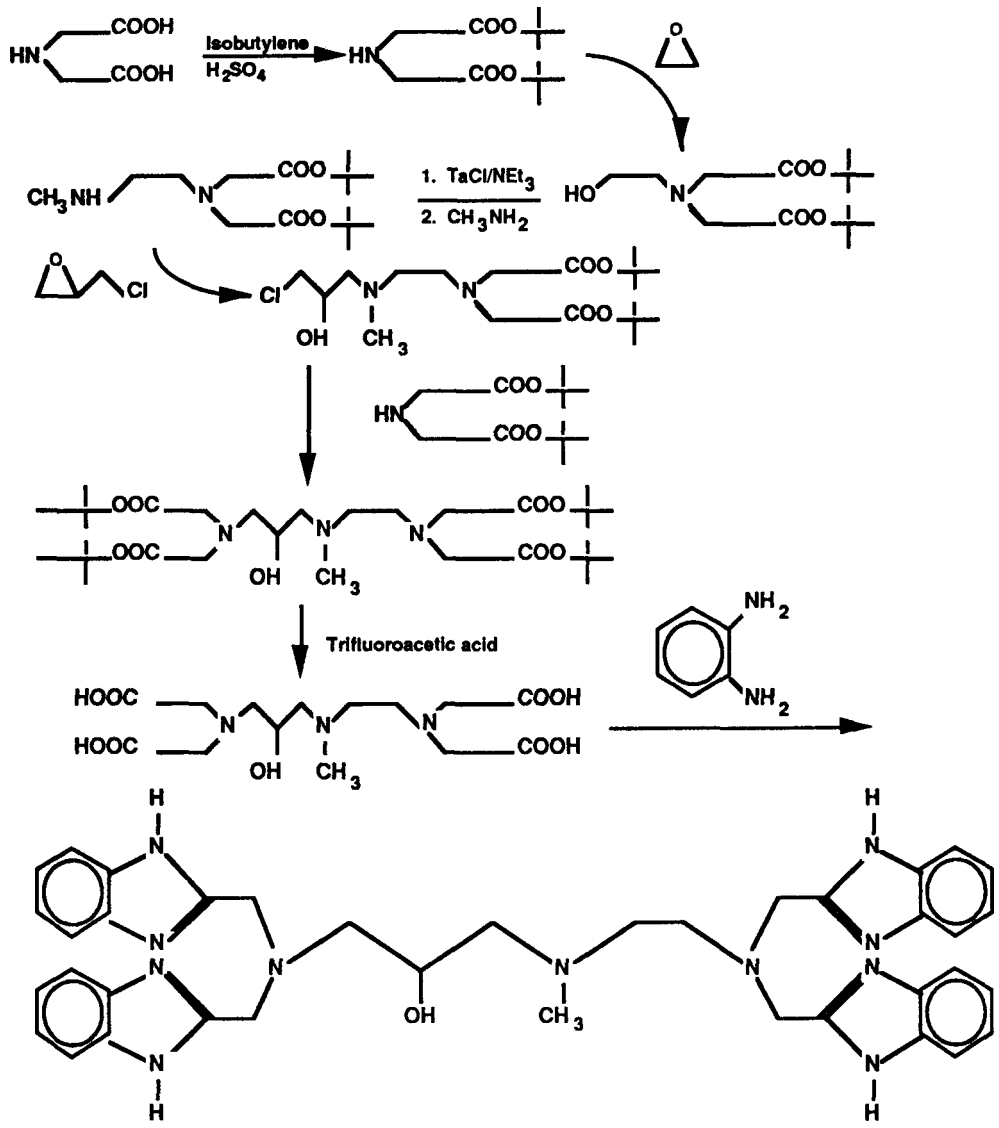

The preparation of this ligand is much more complex than is that of the symmetrical ligand and requires a greater degree of synthetic control at each reaction step. For example, we have been successful in preparing the amine-hydroxy chloride complex:

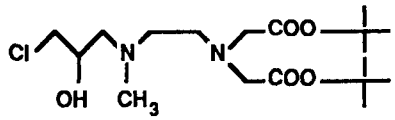

However, this is a reactive species under our reaction conditions and undergoes side reactions involving attack of the methylamine on the chloride position forming a four-member nitrogen heterocycle or reacts further by initially re-forming the epoxide

functionality. As a result, we have spent considerable time exploring alternative routes. One route has been to react iminodiacetic acid with epichlorohydrin forming the hydroxy-chloride followed by reaction with N-methylamineethylenebromide:

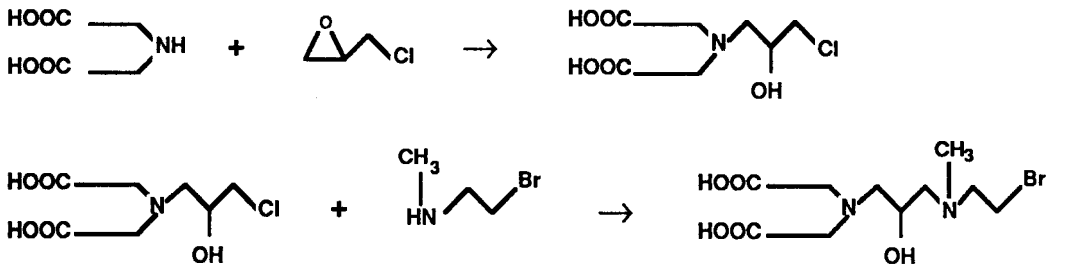

A subsequent reaction with aqueous ammonia and chloroacetic acid should result in 1 (free acid). This route is of interest since there is no leaving group (Cl^-) needed for unwanted side reactions. We are now working to complete this synthesis and isolate the pure ligand. Using the procedure described earlier, metal incorporation will then be performed resulting in the following complex:

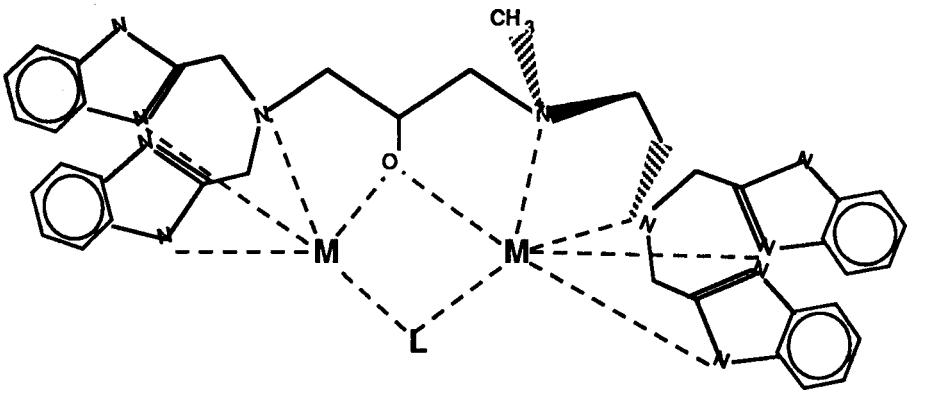

Future work includes full characterization on models including spectral (UV/VIS, ESR, IR/Raman), magnetic, and redox properties (electrochemistry). These properties will be compared with those generated by study of the native MMO enzyme. The comparison of the physical properties will be used to suggest modification to the ligand system in order to better model the active site of MMO. Binding studies of methane and oxygen with the isolated complexes and/or new complexes will begin. Initial studies will focus on the addition of oxygen to the binuclear complexes. In particular, we are seeking complexes that irreversibly bind oxygen and activate it for further reaction. For an iron-containing complex, oxygen substrate can be introduced either as dioxygen to the fully-reduced complex [Fe(II)-Fe(II)] or as peroxide to the fully-oxidized complex [Fe(III)-Fe(III)]. These studies will probe both the structural requirements and the reaction pathways that are important for catalysts that convert methane to methanol.

STRUCTURAL CHARACTERIZATION AND MODELING OF ORGANIC AEROGELS

R. W. Pekala *S. A. Letts* *R. C. Cook*

Overview

The structure and properties of organic aerogels are largely controlled by the concentration of catalyst (e.g., sodium carbonate) used in the sol-gel polymerization. This study utilizes small-angle scattering, TEM, and computer modeling to examine the microstructure of organic aerogels as a function of polymerization conditions (viz., resorcinol-to-catalyst ratio).

Scattering Measurements

Small-angle neutron scattering (SANS) measurements were conducted at the Los Alamos Neutron-Scattering Center on organic aerogels synthesized with different resorcinol/catalyst ratios. The scattering vector (q) ranged from 0.02 nm^{-1} to 1.5 nm^{-1} on this instrument, which permitted the examination of structural features in the aerogels with correlation lengths of 0.5–50 nm.

In contrast to silica aerogels [1,2], mass fractal behavior was not observed for organic aerogels at densities of 0.05–0.10 g/cm^3. This finding was quite surprising since TEM photos of the organic aerogels show an interconnected bead/particle structure similar to that of silica aerogels. Nevertheless, the SANS data corroborate mechanical-property data that show differences in the power-law relationship between compressive modulus and density for these materials [3].

Guinier plots of the SANS data indicate that the radius of gyration (R_g) for the aerogels is a function of polymerization conditions. Figure SC-1 shows the relationship between R_g and the resorcinol-to-catalyst ratio. As the catalyst concentration increases, the radius of gyration is observed to decrease in the same fashion as particle size. Nevertheless, the measured radii of gyration are too large to represent the individual particles within an aerogel. The radius of gyration is probably better equated with cell/pore size. If individual cells/pores could be modeled as spheres, the R_g would have to be multiplied by 2.5 to obtain the diameter of the cell. As a result, cell sizes of 15–40 nm would be observed for the aerogels. These figures are similar to those derived from high-resolution scanning electron microscopy (SEM) and TEM photos.

Microscopy

Two electron microscopy techniques were used to characterize the morphology of resorcinol-formaldehyde (RF) gels and aerogels: field-emission scanning electron microscopy (FESEM) and freeze-fracture transmission electron microscopy (FFTEM). Each technique probes a different aspect of the RF microstructure.

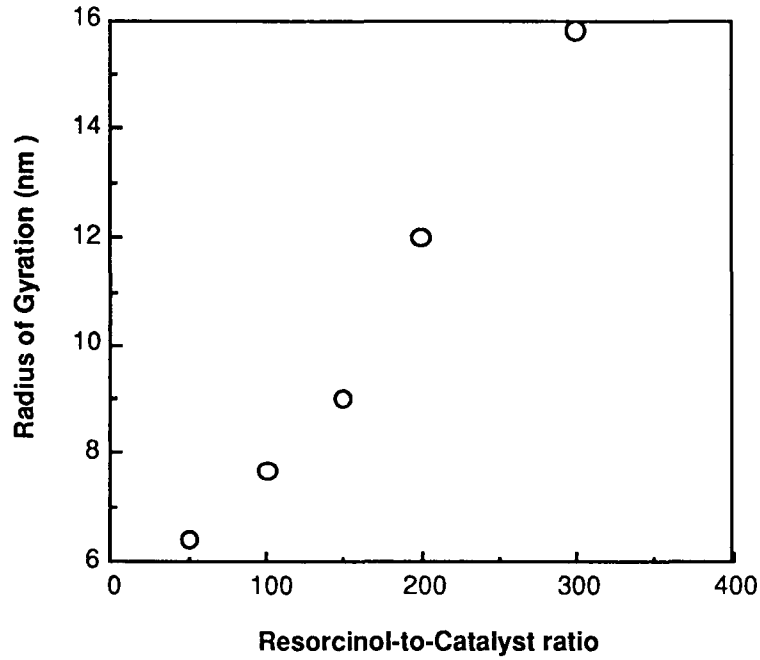

Fig. SC-1. Radius of gyration determined from SANS data as a function of polymerization conditions.

Recent advances in FESEM have resulted in dramatically improved image quality for carbonized RF foams. The high conductivity of the carbonized foam has reduced charging effects. Use of an accelerating voltage of 25 kV with a very thin (~5 nm) carbon coating has also helped to increase resolution and reduce charging. At 100,000X magnification, a "string-of-pearls" structure is observed in the aerogels. The diameter of a CRF cluster is typically 20–40 nm. These values are higher than previously reported TEM values because of the 5-nm carbon coating applied to the specimen.

Freeze-fracture replicas were obtained from an RF gel. Micrographs show individual clusters and chains of clusters having a diameter of approximately 20 nm. Comparing freeze-fracture and FESEM micrographs at the same magnification shows both have approximately the same morphology. This result indicates that the RF gel morphology is preserved during hypercritical drying and even after carbonization.

Computer Modeling

In order to examine the details of the various RF structures, we have calculated the radial-distribution function (RDF) from the positions of the spheres in our computer model. For the system without a bond-angle potential, the clusters appear to be forming hexagonal close-packed structures. By contrast, the RDF for the system with the minimum in the bond-angle potential set at 180° shows the formation of an open extended structure, characterized by crosslinked branch points at which only three chains come together. This open structure is more characteristic of what is seen experimentally; the simulations suggest that this formation of extended linear chains is essential for gelation, particularly at lower densities.

The origin of this string-of-pearls structure may lie with this system's electrical double-layer properties, which depend on both solution ionic strength and bead size. Pierre [4] has shown that agglomeration into dense particles will occur if either the primary particles are very small or the ionic strength is high, so the range of the potential is very short. However, if the particles are larger, the particle-particle repulsion resulting from the electrical double layer will be stronger in midchain than at the chain ends, thus promoting linear growth.

References

1. D. W. Schaefer and K. D. Keefer, *Phys. Rev. Lett.* **56**, 2199 (1986).
2. R. Vacher, T. Woignier, J. Pelous, and E. Courtens, *Phys. Rev. B* **37**, 6500 (1988).
3. J. D. LeMay, Lawrence Livermore National Laboratory, private communication.
4 A. C. Pierre, *J. Non-Cryst. Solids*, in press.

Presentations

R. W. Pekala, "Synthetic control of molecular structure in organic aerogels," submitted for MRS Meeting, Boston, Mass., Nov. 24–Dec. 2, 1989.

S. A. Letts, "Morphological and rheological characterization of resorcinol-formaldehyde gels," submitted for MRS Meeting, Boston, Mass., Nov. 24–Dec. 2, 1989.

LASER-INDUCED CHEMISTRY

C. G. Stevens *W. E. Conaway*

Overview

A full understanding of the properties and behavior of highly-energized molecules is of importance to a number of significant industrial processes and technologies. These include research into improvements in combustion of fossil fuels and in the formulation of high explosives. To this end, we are developing and applying new laser techniques that stimulate and interrogate these high-energy transformations.

The objectives of this project are to characterize the excited-state behavior of isolated molecular systems and to identify optical excitation schemes that generate bond- or mode-selective chemistry. Our approach has been to use overtone-pumping of local mode X–H stretches followed by excitation to a directly-dissociative electronic state. The candidate systems we have chosen to study are H_2O and its deuterated analog HOD. To date, we have successfully demonstrated the ability to photodissociate from single rovibrational states of H_2O (see Fig. LI-1) and to detect quantum-state selectively the OH(X, v = 0) product fragments (Fig. LI-2).

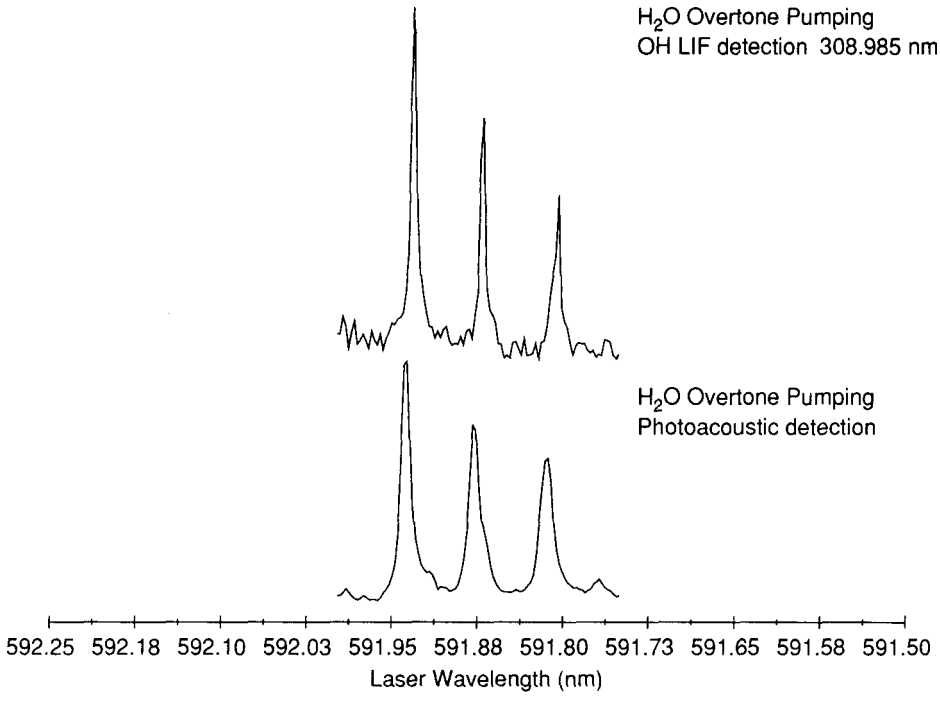

Fig. LI-1. Laser-induced-fluorescence action spectrum compared to photoacoustic absorption spectrum for H_2O.

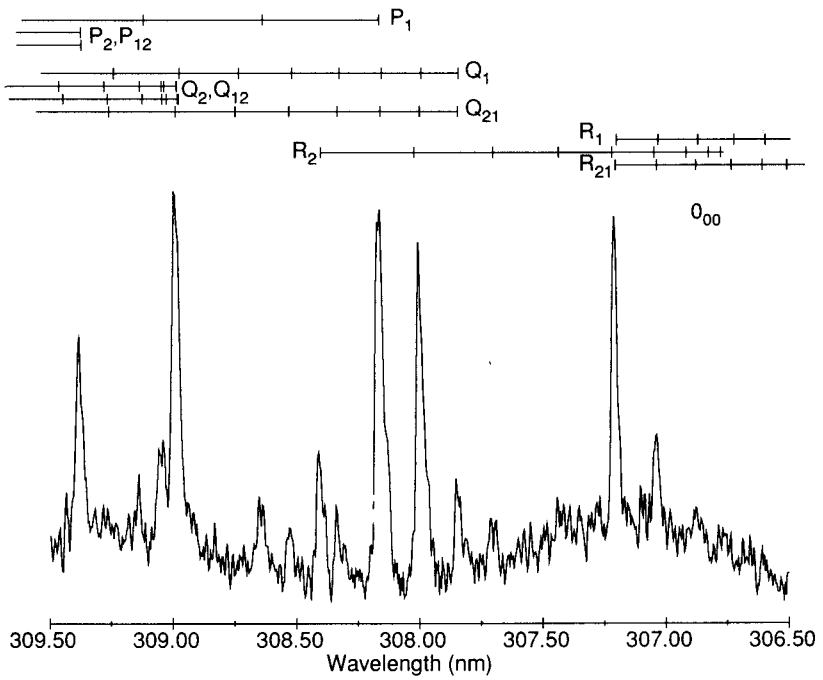

Fig. LI-2. Nascent LiF spectrum observed for photodissociation from H_2O (0,5)$^-0_{00}$.

Technical Progress During Second Half FY89

Technical progress for this period was significantly delayed by a three-month period in which we were without laboratory space. Among the improvements associated with the subsequent move are a doubling of laboratory floor area and a significant increase in the amount of optical table space. In addition, equipment ordered during the delay included a capacitance manometer and servo valve to provide closed-loop control of the gas pressure in the sample cell, polarization optics to measure the laser-power dependence of and alignment effects in the OH laser-induced fluorescence spectra, and laser optics to increase the flexibility of the 532-nm distribution system for the Nd:YAG laser.

During the move into and equipment setup in our new location, we have made detailed measurements of the $5\nu_{OH}$ overtone region in both H_2O and HOD by photoacoustic absorption spectroscopy. A comparison between H_2O and HOD in this region is shown in Fig. LI-3. Rotational and vibrational assignments for H_2O are from Camy-Peret et al. [1]. Similar assignments for HOD are not yet available. The photoacoustic spectra give an indication of what transitions should be considered for overtone pumping, an important milestone on the way to two-step photodissociation in the HOD system.

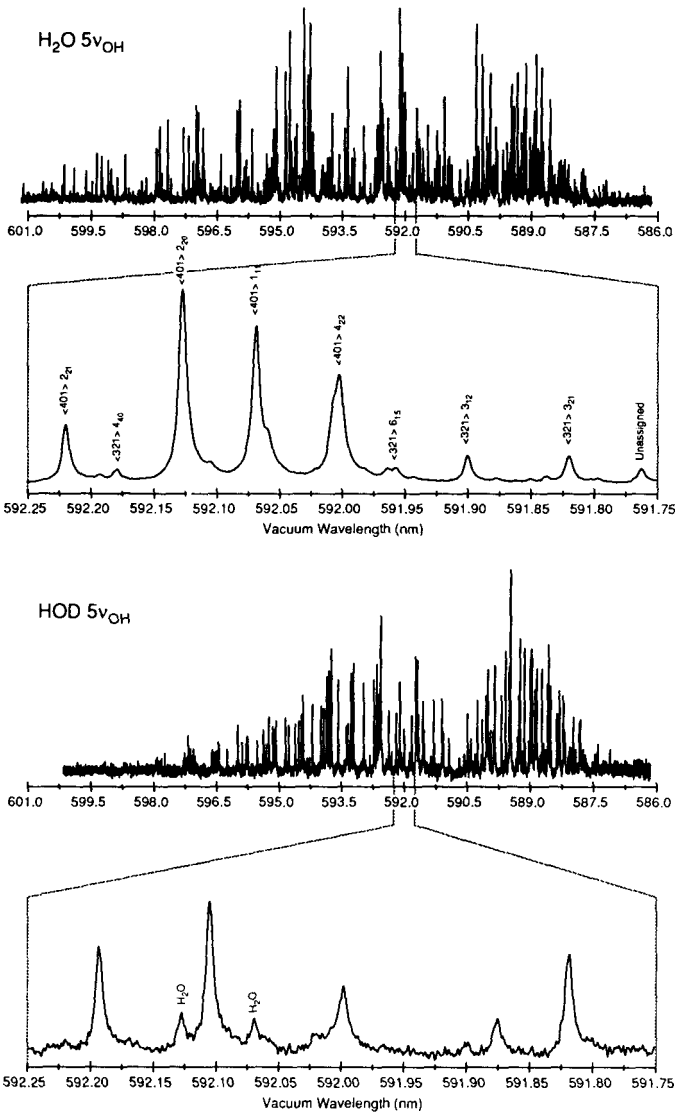

Fig. LI-3. Photoacoustic absorption spectra for H_2O (top) and HOD (bottom).

References

1. C. Camy-Peret, J.-M. Flaud, J.-Y. Mandin, J.-P. Chevillard, J. W. Brault, D. A. Ramsay, M. Vervloet, and J. Chauville, "The High-Resolution Spectrum of Water Vapor between 16,500 cm^{-1} and 25,250 cm^{-1}," *J. Mol. Spectrosc.* **113**, 208 (1985).

Publications and Presentations

Publications

M. W. Crofton, C. G. Stevens, D. Klenerman, J. H. Gutow, and R. N. Zare, "Overtone Spectra of C–H Oscillators in Cold Molecules," *J. Chem. Phys.* **89**, 7100 (1988).

W. E. Conaway, D. S. Leonard, and C. G. Stevens, *State-to-State Photodissociation from Highly Excited Vibrational States of H_2O*, Lawrence Livermore National Laboratory, Livermore, Calif., UCRL-100041 (1989).

Presentations

W. E. Conaway, "State-to-state photodissociation from highly excited vibrational states of H_2O," XVIIIth Informal Photochemistry Conference, Santa Monica, Calif., Jan. 1989.

C. G. Stevens, "Two-step photodissociation of molecules via overtone states: a route to bond-selective chemistry," Department of Chemistry, University of Southern California, Los Angeles, Calif., Mar. 1989.

W. E. Conaway, "State-to-state photodissociation dynamics of highly excited vibrational states of H_2O," Molecular Science Research Center, Battelle Pacific Northwest Laboratory, Richland, Wash., Jul. 1989.

DEPARTMENTAL
INSTITUTIONAL RESEARCH & DEVELOPMENT

Individual Projects

SITE-SPECIFIC CHEMISTRY USING SYNCHROTRON RADIATION

J. Wong (Principal Investigator)
E. M. Larson, M. J. Weber, F. W. Lytle, R. B. Greegor** (Co-investigators)

Overview

This IR&D project is in its third and final year. The approach of this experimental program is to employ x-ray absorption spectroscopy (XAS) utilizing intense synchrotron radiation as a light source to probe the local atomic and electronic structure (chemical bonding) of materials with a view of gaining a better understanding of their physicochemical properties. A number of materials have been investigated in the preceding two years:

- Metal-doped beta boron thermoelectric materials [1].
- Rare-earth metal ions substituted into $YBa_2Cu_3O_7$ (YBC) [2].
- Site-selective detection with optical EXAFS [3].
- Interface structure of near-monolayer Hf on a Pt/C layer [4].
- Solute pairing in solution-hardened fcc Cu alloys [5].
- Lanthanide ions in borosilicate glasses [6].

Those studies together with the ones reported here serve to establish a new experimental capability at LLNL to enhance our basic understanding of materials and their processing from the point of view of site-specific chemistry in terms of bond distance, central atom coordination, valence, site symmetry, and coordination geometry.

3d Metals Substitution in $YBa_2Cu_3O_7$

We have investigated the local atomic structure and coordination geometry of 3d transition metals from Ti to Zn substituted for 10% Cu in YBC using a combination of EXAFS and XANES [7]. The samples are represented by $YBa_2(CuO_{.9}M_{.1})_3O_7$, where M = Ti, V, Cr, Mn, Fe, Co, Ni, or Zn. These samples have been investigated previously by Xiao et al. [8] using x-ray diffraction (XRD), resistance, magnetization, and magnetic susceptibility (above T_c) measurements. These measurements showed that T_c was depressed for all 3d metals, particularly Zn, Co, and Fe. Preliminary XRD revealed that all samples were single phase, with the same perovskite-like structure as undoped YBC.

The ionic sizes of the 3d metals are comparable to that of Cu, so it is expected that some fraction of the added elements will occupy either the Cu(1) or Cu(2) sites. Indeed, the effect on T_c indicates that some degree of some kind of substitution occurred although this could not be quantified in previous work by Xiao et al. To examine the extent and nature of this substitution, we have used XAS to examine the Y, Cu, and 3d metal local electronic and structural environment. In addition to analyzing the XAS of each 3d element to determine its lattice sites and valences, which are averaged over all sites it occupies, we used the EXAFS-derived radial structure function of Y and Cu in each sample to sense the

* The Boeing Company.

degree of substitution from the perspective of their lattice positions. We believe this approach to be particularly useful when a major fraction of the added element does not substitute into a normal lattice site but forms a separate phase. As long as this phase is not commensurate with the lattice, it will be essentially invisible from the perspective of the Y and Cu sites because of the averaging that would occur with a randomly-dispersed impurity phase. This Y/Cu radial structure function analysis was also sensitive to the varying degree of Y/Cu anti-site disorder induced by the 3d metals substitution.The results indicate that Ti, Mn, Fe, and Co are incorporated into the YBC planar, fourfold-coordinated Cu(1) site. The V goes into the Cu(2) site while Ni appears to be substituting for Cu in both the Cu(1) and Cu(2) sites. The added 3d elements also affect the degree of anti-site Cu/Y disorder. At a 10% level of substitution (with respect to the total Cu content in the YBC structure), there appears to be an additional segregated oxide phase for each of the above 3d metals with most of the Cr in a chromate phase and the Ni in a NiO-like phase.

Optical absorption and emission spectra and L-edge extended x-ray absorption fine structure were measured for Nd^{3+}-doped SiO_2 that had been prepared by various techniques including melting, hot pressing, chemical vapor deposition, and sol gel. Spectral properties can vary with the processing technique used and with the introduction of additives. Although optical spectra are similar at low Nd concentrations (~0.1 cation%), large differences in band shapes and intensities are observed at higher concentrations and in the presence of codopants (Li^+, Al^{3+}, La^{3+}, P^{5+}, Ta^{5+}) and residual OH^-. These differences are related to ion clustering and to changes in the strength and symmetry of the local field at the Nd^{3+} site. These in turn affect the lasing characteristics.

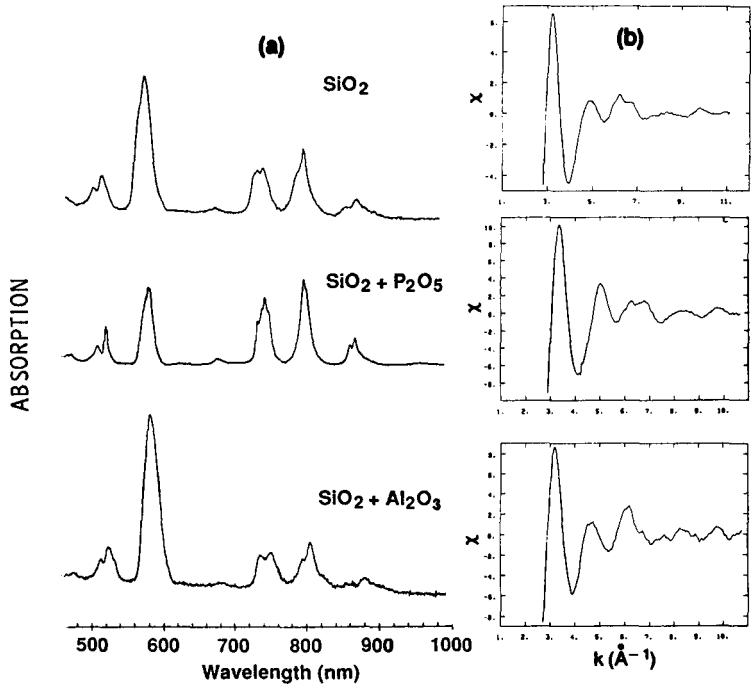

Fig. SS-1. (a) Optical absorption spectrum and (b) L_3-edge EXAFS of Nd^{3+} in pure SiO_2, SiO_2 doped with P_2O_5, and Al_2O_3.

In Fig. SS-1, absorption spectra are shown at the left and the EXAFS signals at the right for simple SiO_2 and for SiO_2 codoped with P_2O_5 and Al_2O_3 (~1 mol%). Note the large differences in the relative intensities of the Nd^{3+} absorption bands. These differences are analyzed in terms of the Judd-Ofelt intensity parameter and associated changes in the symmetry and bonding at the Nd^{3+} site. EXAFS spectra are being used to model the changes in the Nd coordination environment.

References

1. J. Wong and G. A. Slack, "EXAFS and XANES studies of the bonding and structure of metals in beta boron," *Proceedings* of the 9th International Symposium on Boron and Borides, H. Werheit, Ed. (Universität Duisburg Gesamthochschule, Duisburg, 1987), p. 268.
2. F. W. Lytle, G. van der Laan, R. B. Greegor, E. M. Larson, and J. Wong, "Determination of the Valence of Pr, Gd and Ho in YBC," *SSRL Activity Report*, Stanford, Calif. (1988) and *Phys. Rev. B*, in press.
3. R. B. Greegor, F. W. Lytle, D. R. Sandstrom, M. J. Weber, and J. Wong, "Site selectivity in Mn glass using optical XANES," *SSRL Activity Report*, Stanford, Calif. (1987).
4. T. Barbee and J. Wong, "EXAFS of near monolayer Hf layer," *SSRL Activity Report*, Stanford, Calif. (1987) and *Physica B* **158**, 670 (1989).
5. J. Wong, W. E. Nixon, J. W. Mitchell and S. Laderman, "Solute pairing in solution hardened binary and ternary Fcc alloys," *SSRL Activity Report*, Stanford, Calif. (1988) and *Physica B* **158**, 25 (1989).
6. E. M. Larson, F. W. Lytle, P. G. Eller, R. B. Greegor, M. P. Eastman, "XAS Study of Lanthanide Ion Speciation in Borosilicate Glasses," *J. Non-Cryst. Solids*, in press.
7. R. B. Greegor, F. W. Lytle, J. Wong, and E. M. Larson, "XAS absorption spectroscopic investigation of 3d metals substitution in high temperature superconductors," *SSRL Activity Report*, Stanford, Calif. (1988) and *Phys. Rev. B*, in preparation.
8 Xiao et al., *Phys. Rev. B* **36**, 8782 (1987).

Presentations

1. M. J. Weber, "Science and technology of laser glasses," invited survey lecture XV International Congress on Glass, Leningrad, USSR, Jul. 2–7, 1989.
2. E. M. Larson, J. Wong, and M. J. Weber, "The determination of the near-neighbor environment of Nd^{3+} in a series of BeF_2 laser glasses using X-ray absorption spectroscopy," American Crystallographic Association Annual Meeting on Interface Science and Technology, Seattle, Wash., Jul. 23–29, 1989.

ELECTRONIC STRUCTURE OF SYSTEMS WITH REDUCED SYMMETRY

A. Gonis

Overview

The main goal of this research project is the development of formal and computational methods for the calculation of the electronic structure of surfaces and interfaces. Such new methods are needed because existing first-principles approaches to the study of electronic structure are unable to treat rigorously the semi-infinite extent of surface and interface systems.

During the last two years, we have introduced a new approach to the implementation of Green's-function-based multiple-scattering theory (MST) that allows for an exact treatment, within a single-particle picture, of reduced-symmetry systems (surfaces, interfaces, and grain boundaries).

This approach is formulated in real space, rather than reciprocal space, and allows study of the electronic structure and related properties as functions of the distance from a surface or interface region.

Initial applications of this new method were made to model systems for the purpose of comparing the models with systems that are amenable to treatment by conventional methods. More recently, applications to realistic materials have been made.

Progress

During the last half of FY 89, we succeeded in coding a version of the formalism that drastically reduces the sizes of the matrices used in the calculation of the electronic Green's function. This version yields much more precise results than the previous one and leads to accelerated convergence rates. In addition, a version of the code was extended to include charge self-consistency and total energy and was further improved in terms of its convergence properties.

In addition to these developments, we have also incorporated the ideas underlying our real-space method to the analysis of low-energy-electron-diffraction (LEED) spectra. This work is being carried out in collaboration with Dr. Van Hove's group at LBL. Original calculations for a (100) free surface of Cu have been carried out and compared successfully with those obtained by a method known as layer doubling. We are now studying high-Miller-index surfaces, for which layer doubling may be inapplicable but for which the new approach is expected to converge.

Publications

X.-G. Zhang and A. Gonis, "New Real-Space Multiple-Scattering Theory Method for the Determination of Electronic Structure," *Phys. Rev. Lett.* **62**, 1161 (1989).

A. Gonis, X.-G. Zhang, and D. M. Nicholson, "Multiple-Scattering Green's-Function Method for Space-Filling Cell Potentials," *Phys. Rev. B* **40**, 947 (1989).

X.-G. Zhang, A. Gonis and James M. MacLaren, "Real-Space Multiple-Scattering Theory and the Electronic Structure of Systems with Full or Reduced Symmetry," *Phys. Rev. B* **40**, 3694 (1989).

THE STRUCTURE-PROPERTY LINK IN SUB-NANOMETER MATERIALS

A.F. Jankowski (Principal Investigator)
S. R. Nutt[*] and *W. D. Nix*[**] (Co-Investigators)

The structure-property link in materials with sub-nanometer dimensions is of increasing scientific interest. In particular, the elastic moduli of alloy systems can be changed by two orders of magnitude using multilayer structures. The origin of such changes, unobtainable using conventional processing, is investigated using x-ray diffraction (XRD), transmission electron microscopy (TEM), and microindentation.

Multilayers are thin-film structures in which the composition is modulated in one dimension. When multilayers consist of noble metal-transition metal layer pairs, the elastic properties differ significantly from a bulk averaging of the components. The techniques of microindentation (to determine hardness and elastic moduli) and microbeam deflection (to determine yield strength and elastic moduli) are used to facilitate physical property measurements without tedious substrate removal.

The metallic-multilayer system chosen was synthesized using magnetron sputter deposition. The thin-film samples are composed of several hundred layer pairs with unique repeat periodicities ranging from 0.6 to 9 nm.

The samples produced are metastable by definition. The artificial introduction of a composition modulation places each constituent atom in a non-equilibrium position. The effects of subsequent lattice distortions on the physical properties are accentuated with the magnitude of the atomic displacements. This is the case for symmetrically similar crystal systems with a large lattice misfit. The Au/Ni-layered system, with a 15% misfit, was therefore chosen for study.

Characterization of the Au/Ni multilayers was pursued using x-ray diffraction and high-resolution electron microscopy. Kinematical diffraction modeling of lattice distortions in the Au and Ni layers indicated maximum strain at the Au/Ni interface (compressive for Au and tensile for Ni) with relaxation into the intralayer region [1]. The accompanying changes in the average d-spacing in the modulation direction with layer-pair spacing are shown in Figs. SP-1 and SP-2. The maximum in-plane compressive strains found near a 2-nm repeat period have produced an expansion in the average lattice spacing in the modulation direction. Imaging of the distorted lattice structure was accomplished using transmission electron microscopy of multilayer samples viewed in cross-section. Interface-dominated Au/Ni structures (with layer pairs less than 2–3 nm thick) were found to be a single-phase distorted lattice, whereas multilayer structures with long repeat periods (layer pairs >3 nm thick) had additional Au and Ni bulk components [2]. This confirms the XRD modeling result of strain relaxation into the intralayer regions from coherently-strained Au-Ni interfaces.

---

[*] Brown University.
[**] Stanford University.

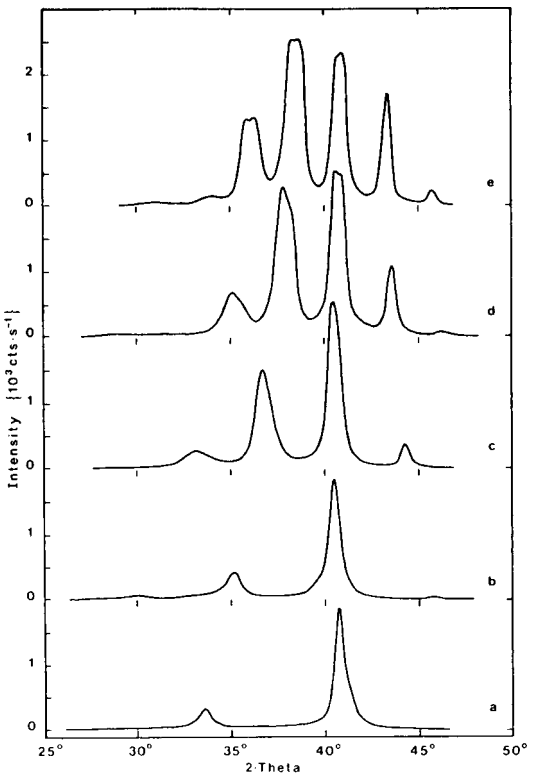

Fig. SP-1. θ/2θ scans, using CuK_α radiation, are shown of Au/Ni superlattices with repeat periodicities of (a) 1.30 (b) 1.77 (c) 2.48 (d) 3.35 and (e) 3.98 nm.

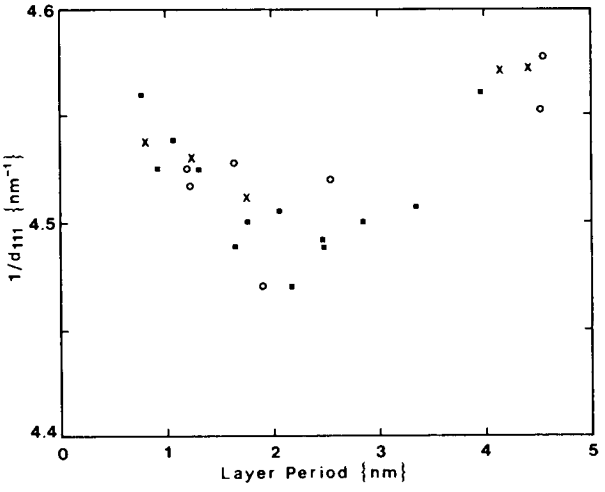

Fig. SP-2. The reciprocal of the lattice spacing in the Au/Ni superlattice growth direction, $(d_{111})^{-1}$, is plotted as it varies with periodicity, $d_{Au/Ni}$, for individual samples synthesized using magnetron sputter deposition.

A microindenter was used to initially quantify the mechanical properties of the Au/Ni multilayers. Films 450 nm thick were indented with a pyramid-shaped stylus to a depth less than 30 nm. Hardness measurements indicate a maximum near a 2-nm repeat period [3]. Data-reduction methods recently developed will enable the determination of elastic properties from the elastic-plastic response of the indentation load-displacement curves.

The link between the atomic displacements of the multilayer structure and the physical property measurements is made through the coherency strain model (CSM). A periodic distortion of the superlattice, a "strain wave," is considered in modeling the multilayer elastic behavior [4–9]. Relaxation from coherently strained interfaces is used in an ion-core-based energy formulation of the elastic moduli with respect to a second-order differentiation of lattice strain. In agreement with the microindentation results, a maximum in the biaxial elastic modulus is found for multilayers with repeat periodicities near 2 nm. The interference effect between the interfaces on the equilibrium lattice structure have been recently addressed utilizing Kanzaki forces [10]. The interface created by the composition discontinuity between layers is accounted for in a modeling approach which predicts relaxation of the lattice from coherently strained interfaces. Consistency is found between the newly developed interface-interference approach, the CSM, and results obtained from the reported XRD and TEM analysis.

In the coming year, continuing efforts will emphasize improving multilayer microstructure through synthesis and characterization, separating the elastic component from microindentation load-displacement curves, and using microdeflection of multilayer cantilever beams to determine elastic moduli and yield strength. In addition, the magnetic corollaries to elastic modulus trends will be analyzed using a SQUID magnetometer. Specifically, magnetic anisotropy as a function of layer-pair spacings will be investigated.

References

1. J. Chaudhuri, S. Shah, and A. F. Jankowski, "X-Ray Diffraction Analysis of Au/Ni Multilayers," *Mater. Res. Soc. Symp. Proc.* **132**, 231 (1989).
2. S. R. Nutt, K. Green, W. D. Nix, S. Baker, and A. F. Jankowski, "Gold-Nickel Multilayer Films: Structure-Property Correlations," *Mater. Res. Soc. Symp. Proc.* **130,** 129 (1989).
3. S. Baker, W. D. Nix, and A. Jankowski, private communication.
4. A. F. Jankowski, "The Strain Wave Approach to Modulus Enhancement and Stability of Metallic Multilayers," *J. Phys. Chem. Solids* **50**, 641 (1989).
5. A. F. Jankowski, "Origin of the Supermodulus Effect: Artificial Ordering Considerations," *Mater. Sci. Eng. A* **114**, L17 (1989).
6. A. F. Jankowski, "Comment on 'Lattice expansions and contractions in metallic superlattices'," *Phys. Rev. Lett.* **63**, 1892 (1989).
7. A. F. Jankowski, "Lattice Spacing Variations in Gold-Nickel Superlattices," *Superlattices & Microstructures* **6**, 427 (1989).
8. A. F. Jankowski, "Short Period Multilayers: Interface Dominated Structures," *Mater. Sci. Eng.*, in press.
9. M. A. Wall and A. F. Jankowski, "Atomic Imaging of Au/Ni Multilayers," *Thin Solid Films*, in press.
10. T. Tsakalakos and A. Jankowski, "Interface Phenomena in Multilayers," *Mater. Sci. Eng.*, in press.

Invited Presentations

M. A. Wall and A. F. Jankowski, "Atomic imaging of Au/Ni multilayers," 16th International Conference on Metallurgical Coatings, San Diego, Calif., Apr. 17–21, 1989.

A. F. Jankowski, "Short-period multilayers: interface-dominated structures," American Crystallographic Association Annual Meeting on Interface Science and Technology, Seattle, Wash., Jul. 23–28, 1989.

LASER-PRODUCED MOLECULAR PLASMAS

C. Stevens *A. Droege* *G. Haugen*
W. Conaway *S. Steward* *R. Pekala*

Overview

The study of dense, complex plasmas in the temperature range of 3,000 K to 10,000 K is a relatively unexplored area of chemical physics and material science. This "molecular-plasma" regime is important to many technical areas of interest, including materials production and analysis by plasma techniques. A fundamental understanding of materials heated to these temperatures is also central to confident prediction of the performance of materials in nuclear-weapons research and development. It is the objective of this project to determine experimentally the thermodynamic properties of materials heated to these temperatures.

Experimental studies of material properties at these temperatures and densities are complicated by the need to establish local thermodynamic equilibrium (LTE) through even heating of the materials and to diagnose the resulting high-density, optically thick plasma. We have overcome these difficulties in our experimental approach by investigating the laser heating of thin free-standing polymeric films ranging in thickness from 100 nm to 1 μm. By restricting the thickness of the film, we can hold the laser fluence requirements to uniformly heat the materials below nonlinear-absorption thresholds. The absorptivity and other properties can be tailored by selection of specific polymer mixtures. The free-standing films are optically thin, which allows use of optical absorption and emission to diagnose the species development in the evolving plasma. Temperature measurements are made by viewing light emitted along the optically thick dimension.

Technical Activities and Results

The films we are investigating are designed by polymer blending of polystyrene and polyphenylene oxide to absorb 10% of the incident 266-nm laser light. Our first concern is whether this design allows us to deposit energy uniformly into the film, creating a thermally homogeneous plasma in the temperature range of interest. We have obtained evidence for uniform heating by photographing the film edge-on, using self-luminosity to image the plasma. The photographed plume shows a forward-back emission symmetry and cosine intensity distribution expected of a simple vaporization process. This contrasts to the plume jetting seen in non-uniform ablation processes.

We have demonstrated our ability to collect 20-ns wavelength-dispersed exposures of the plasma under optically thin conditions. These spectra, an example of which is illustrated in Fig. LP-1, are dominated by emission from molecular fragment species, primarily C_2 and CO. Recently, we have worked to increase our laser energy and spot size to obtain optically thick column emission for temperature determination of the blackbody spectral profile.

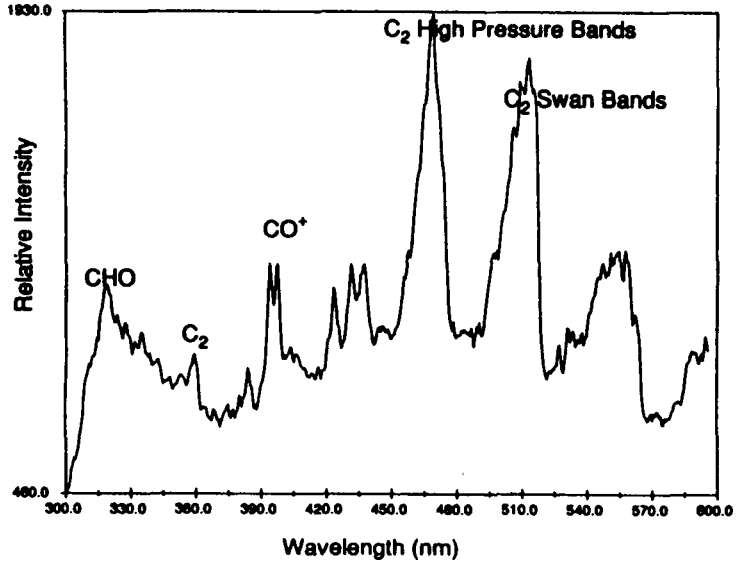

Fig. LP-1. Spectrum of a laser-produced plasma under optically thin conditions.

Measuring pressure inside the laser-generated plasmas is a major challenge. We have identified an approach that can yield internal pressures accurate to within 10% by measuring the velocity of a shock wave launched into a surrounding rare gas, such as argon [1]. A quantitative relationship has been developed between the measured shock velocity in the gas and the initial material driving pressure. Figure LP-2 illustrates the relationship between the log of the ratio of the initial plasma pressure P_p to the surrounding

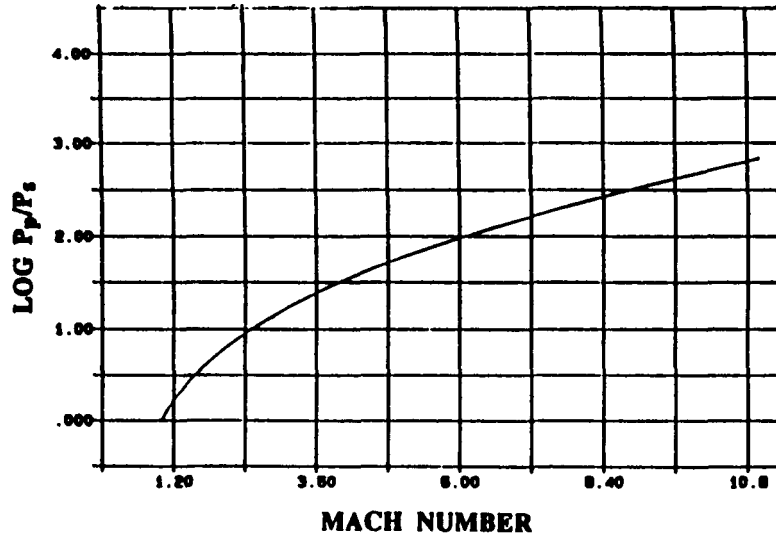

Fig. LP-2. Dependence of the Mach number of a developing shock wave in a 300-K argon buffer gas on the ratio of the plasma driving pressure to the surrounding buffer gas pressure.

rare-gas pressure P_s and the Mach number of the developing shock wave for the case of a 10,000-K carbon-atom plasma in a 300-K argon-buffer gas. Preliminary experiments have been conducted in which we have measured shock fronts traveling through the films. A

laser backlight and streak camera are used to record a Schlieren-like image created by the passage of a shockwave-initiated density gradient. This technique is being adapted to measure shock velocities in surrounding argon gas, providing a determination of plasma pressure.

We have developed [2] and demonstrated the feasibility of methods for measuring temperature, pressure, and speciation in dense "molecular" plasmas. In the upcoming year, we will apply these techniques to actual measurements and will be developing calorimetric and spectral scattering techniques for quantifying the amount of laser energy actually deposited into the film.

References

1. G. Haugen, C. Stevens, A. Droege, and W. Conaway, *Laser Vaporization of Free-Standing Thin Films: 1. Analysis of Pressure Measurement Techniques*, in preparation.
2. F.J.D. Serduke, C. G. Stevens, M. Friedman, and G. Grutmann, "Evaluation of a Proposed Electron Density Diagnostic for NOVA X-ray Transmission Experiments," abstract prepared for 1989 Topical Conference on Physics of Radiatively Driven ICF Targets, Livermore, Calif., UCRL-99835.(1989).